

## Response to Anonymous Referee #1's Comments

First of all we thank the reviewer for his valuable suggestion on our study and sincerely appreciate the reviewer's insightful and helpful comments.

Below we explicitly respond to each of the items raised in the comments by anonymous referee #1. These comments are indicated in **bold**, whereas the author's response is presented in **blue** and revisions in **red** in revised manuscript.

### R1C1:

**The authors present an analysis of atmospheric ammonia over South and East Asia based on the MOZART-4 model that is driven by the HTAP-v2 emission inventory. Model results are compared against IASI satellite observations (total column), as well as surface observations of CPCB (India) and NNDMN (China) for the year 2010. This topic is very important, since ammonia partitions into the only ubiquitous volatile cation, i.e., ammonium ( $\text{NH}_4^+$ ).  $\text{NH}_4^+$  plays a crucial role in air quality and visibility due to its volatility and ability to neutralize acidic air pollutants, which are often of anthropogenic origin. And despite the various air pollution abatement efforts, ammonia concentrations are increasing in many regions of the world and are thus still of concern, not only in Asia. Despite some fundamental weakness in the modelling approach (which is unfortunately common to most such modeling studies and therefore is not a reason for rejection), this study is overall sufficiently sound. I would therefore recommend publication, if the authors take the following comments and discussion points into account.**

**We thank the reviewer for carefully reading the manuscript. We agree that the suggested discussion will improve the quality of the manuscript.**

### R1C2:

**The study reveals that spatial differences (total column) between MOZART-4 and IASI are generally largest during local autumn/winter season, with an overestimation compared to IASI observations. This overestimation is most pronounced for IGP South Asia ( $20^\circ\text{N}$ - $32^\circ\text{N}$ ,  $70^\circ\text{E}$ - $95^\circ\text{E}$ ), while rather an underestimation is found for NCP East Asia ( $30^\circ\text{N}$ - $40^\circ\text{N}$ ,  $110^\circ\text{E}$ - $120^\circ\text{E}$ ), especially during the summer months. On the other hand, the comparison of surface concentrations reveals that the model underestimates the ammonia observations over South and East Asia throughout the year. This is shown by monthly mean (time series) and annual averages (scatter plot), and these results are in contrast to the total column case (model burden w.r.t. IASI observations).**

**Yes, we agree with the reviewer's observations that the difference between is most pronounced for IGP South Asia. The following Fig. 1 below shows the time-height distribution of  $\text{NH}_3$  and mean planetary boundary layer height (PBLH) averaged over the IGP region, respectively. It can be seen that during winter months, higher**

atmospheric stability prevents the mixing of boundary layer  $\text{NH}_3$  to the free troposphere over IGP, which is reflected in the higher winter-time values of MOZART-4  $\text{NH}_3$  columns. Similarly, a higher  $\text{NH}_3/\text{NH}_4^+$  ratio (Fig. S3 in the revised Supplement) and lower dry and wet deposition (Fig. S4 and S5 in the revised Supplement) of  $\text{NH}_3$  over IGP in winter months enhances the accumulation of  $\text{NH}_3$  in the boundary layer compared to summer months. On the other hand, very little  $\text{NH}_3$  gets detected by the satellite at the higher altitudes, where the satellite's detection sensitivity is more than that at the surface (Clarisson et al., 2010). IASI measurements' limited sensitivity to detect boundary layer  $\text{NH}_3$  (Van Damme et al., 2014) could be one of the reasons for large differences between MOZART-4 and IASI in winter seasons. Also, the wheat crop sowing over IGP involves a higher fertilizer application rate during peak winter months that releases a significant quantity of  $\text{NH}_3$  into the atmosphere. However, this seasonality is largely missing in the emissions (Fig. 2 (top, left in the revised manuscript)), indicating that the winter-time meteorology largely drives higher MOZART-4  $\text{NH}_3$  over this region.

Also, the emission fluxes of  $\text{SO}_2$  and  $\text{NO}_x$  over IGP are only one-fourth of that over NCP (Wang et al., 2020). Therefore, relatively low  $\text{SO}_2$  and  $\text{NO}_x$  concentration could be an important factor for Higher  $\text{NH}_3$  columns over IGP during winter.

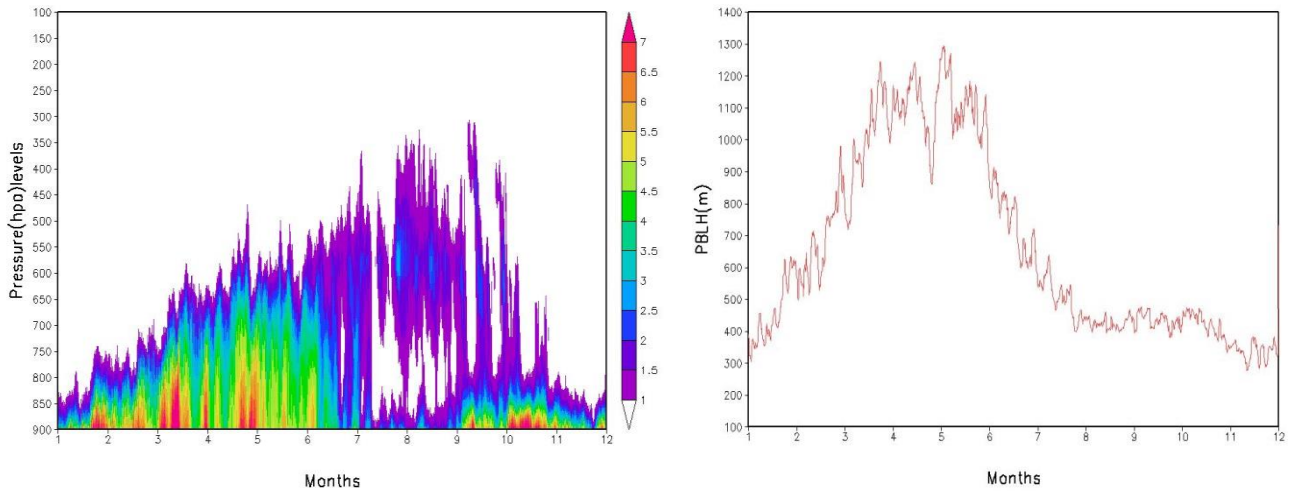


Figure 1: Daily vertical distribution of distribution of  $\text{NH}_3$  (ppb) averaged over IGP South Asia ( $20^\circ\text{N}$ - $32^\circ\text{N}$ ,  $70^\circ\text{E}$ - $95^\circ\text{E}$ ) (left) and daily mean Planetary Boundary Layer height (PBLH in meters) averaged over IGP South Asia ( $20^\circ\text{N}$ - $32^\circ\text{N}$ ,  $70^\circ\text{E}$ - $95^\circ\text{E}$ ) (right)

Changes in the revised manuscript:-

Line no. 377-380, 382 -386, 393-401 and 513-514

Figure no. 7 added in revised manuscript

**Despite some potential calibration issue w.r.t. certain observations, there seems to be no obvious inconsistency with the NH<sub>3</sub> observations used in this study. Instead, both issues (model vs surface and total column observations) rather point to an incomplete model set-up w.r.t. the gas-aerosol partitioning assumptions. Nevertheless, I also recommend that the authors make sure that the study is based on (or includes) quality controlled surface observations.**

The quality control and assurance method followed by CPCB for these air quality monitoring stations is given at CPCB (2011 and 2020). The calibration procedures for the NH<sub>3</sub> analyzer conforms to USEPA (the United States Environmental Protection Agency) methodologies and include daily calibration checks, biweekly precision checks, and linearity checks every six weeks. All analyzers undergo full calibration every six weeks. For detail on calibration procedure, refer to CPCB (2020); Technical Specifications for Continuous Real Time Ambient Air Quality Monitoring Analysers (2016). Furthermore, we take the following steps to reassure the quality of NH<sub>3</sub> observations from the CPCB network stations. For data quality, we rejected all the observation values below 1  $\mu\text{g m}^{-3}$  and above 250  $\mu\text{g m}^{-3}$  at a given site if other sites in the network do not show values outside this range. This step aims to eliminate any short-term local influence that cannot be captured in the models and retain the regional-scale variability. Second, we removed single peaks characterized by a change of more than 100  $\mu\text{g m}^{-3}$  in just one hour for all the data in CPCB monitoring stations. This step filters random fluctuations in the observations. Third, we removed some very high NH<sub>3</sub> values that appeared in the time series right after the missing values. For any given day, we removed the sites from the consideration that either experience instrument malfunction and/or appear to be very heavily influenced by strong local sources. This information is updated in the revised manuscript.

In order to verify the data quality of the CBCB monitoring site, we have inter compared the NH<sub>3</sub> measurement at CPCB monitoring station (R.K. Puram) in Delhi with the NH<sub>3</sub> measurements at Indira Gandhi International (IGI) Airport taken during the Winter Fog Experiment (WiFEX) (Ghude et al., 2017) using MARGA (Measurement of Aerosols and Gases) instrument during the winter season of 2017-2018. More details on the NH<sub>3</sub> measurements using MARGA is available with Acharja et al. (2020). Both sites were situated in the same area of Delhi (less than 1km). Our inter-comparison shows that NH<sub>3</sub> measured at CPCB monitoring station by chemiluminescence method are slightly (on an average 9.8  $\mu\text{g m}^{-3}$ ) on the higher side than NH<sub>3</sub> measured by ion chromatography (IC) using MARGA (Fig. 2 below). The observed differences could partly be related to the different NH<sub>3</sub> measurement techniques and partly to the locations of the two monitoring sites that were not place exactly at the same location. Apparently, the difference of 9.8  $\mu\text{g m}^{-3}$  indicates that the NH<sub>3</sub> measurements from the CPCB do not suffer from the calibration issue. However, rigorous validation is required in the future with more data sets.

In the revised manuscript we have now included above discussion.

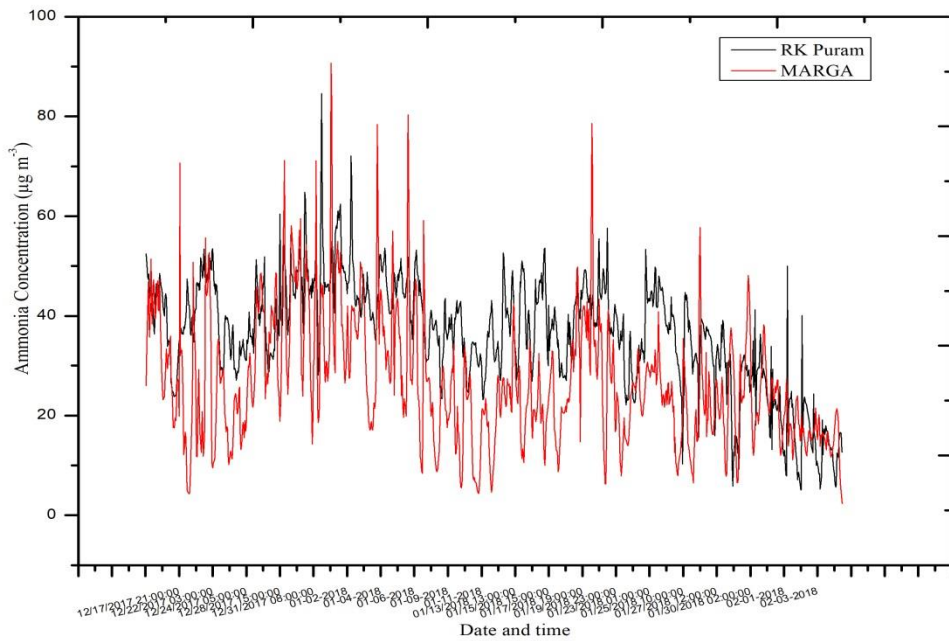


Figure 2. Comparison of  $\text{NH}_3$  ( $\mu\text{g m}^{-3}$ ) concentration from MARGA instrument with RK Puram (CPCB) station

Changes in the revised manuscript:-

Line no. 248-276

Added Figure no. S1 in the revised supplement

R1C3:

Regarding the modeling assumptions, it should be noted that the chosen set-up has its limitations w.r.t. the  $\text{NH}_3/\text{NH}_4^+$  partitioning. The main issue here is that in the current set-up, both (i) cations other than  $\text{NH}_4^+$ , e.g., sodium ( $\text{Na}^+$ ), potassium ( $\text{K}^+$ ), calcium ( $\text{Ca}^{2+}$ ), and magnesium ( $\text{Mg}^{2+}$ ), have been neglected, as well as (ii) organic acids were omitted for the gas-aerosol partitioning calculations. Both are, however, important for the  $\text{NH}_3/\text{NH}_4^+$  partitioning w.r.t. to real world observations. Nevertheless, since mineral cations and organic acids have been neglected in conjunction, the presented model results could be in terms of yearly averages more or less “right” for the wrong reason, as indicated by a study published sometimes ago in ACP 2006 (<https://acp.copernicus.org/articles/6/2549/2006/>). On shorter time scales, however, the incomplete model set-up could be a cause of the observed discrepancies.

Yes, we agree with the reviewer's comment that the current modeling setup has limitations w.r.t.  $\text{NH}_3/\text{NH}_4^+$ . In this present work, the ammonium nitrate

distribution is determined from  $\text{NH}_3$  emissions based on the parameterization of gas/aerosol partitioning by Metzger et al. (2002), which is a set of approximations to the equilibrium constant calculation (Seinfeld et al., 1998), based on the level of sulfate present. The application of any equilibrium models (EQMs) in global atmospheric studies is associated with considerable uncertainties. We followed, equilibrium simplified aerosol model (EQSAM)- gas-aerosol partitioning calculations by Metzger et al. (2002) the current setup. The assumptions used in this study are limited to the ammonium-sulfate-nitrate-water system, which is valid for only inorganic salt compounds. This latter was updated (EQSAM2) to account for ammonium-sulfate-nitrate-sodium-chloride-water system, mineral citation, and organic acids (Metzger et al., 2006). Metzger et al. (2006) found that the total ammonium partitioning calculated by updated-EQSAM2 parameterization was 15 % lower than that calculated from the parameterization similar to Metzger et al., (2002). Ammonia has a stronger affinity towards the neutralization of sulphuric acid ( $\text{H}_2\text{SO}_4$ ) than nitric acid ( $\text{HNO}_3$ ), whereas the formation of ammonium chloride ( $\text{NH}_4\text{Cl(s)}$  or  $\text{(aq)}$ ) in the atmosphere is unstable and can dissociate reversibly to  $\text{NH}_3$  and  $\text{HCl}$ . These aerosols in both dry and aqueous phase evaporate faster than the corresponding ammonium nitrate ( $\text{NH}_4\text{NO}_3$ ) aerosols (Seinfeld and Pandis, 2012).

We agree with the reviewer's comment that neglecting sodium-chloride organic acids and mineral cations in the parameterization of gas/aerosol partitioning system in the present work may cause some observed discrepancies. Overall consideration of major mineral cations could lead to more free ammonia, which will potentially increase  $\text{NH}_3$  total columns. This will further increase differences (total column) between MOZART-4 and IASI over IGP and a decrease in differences (total column) between MOZART-4 and IASI over NCP. However, the influence of mineral cations on the  $\text{NH}_3$  gas-particle partitioning might be limited (Acharja et al., 2020; Dao et al., 2014) and requires further focused studies over south Asia. Discussion is added in the revised manuscript.

**Changes in the revised manuscript:-**

**Line no. 143-162**

**Line no. 342-347**

**R1C4:**

**The reason is that in this model set-up, the  $\text{NH}_3/\text{NH}_4^+$  partitioning is mainly controlled by sulfate and subsequently by nitrate, which might be in reality not the case in Asia. Consideration of at least the major mineral cations (e.g.,  $\text{Na}^+$ ,  $\text{K}^+$ ,  $\text{Ca}^{2+}$ ,  $\text{Mg}^{2+}$ ) might be necessary, since all of them are ubiquitous and preferentially neutralize sulfate, which directly affects the  $\text{NH}_3/\text{NH}_4^+$  partitioning. In contrast to the semi-volatile compound**

ammonium nitrate ( $\text{NH}_4\text{NO}_3$ ), mineral cations form more stable compounds that exhibit a distinct different temperature dependent dissociation and water uptake, but no volatilization, as it is here the case only for  $\text{NH}_4\text{NO}_3$ . Thus, consideration of additional (mineral) cations could lead to more free ammonia (w.r.t. sulfate neutralization), which, in addition could lead to a larger fraction of ammonia being neutralized by nitric acid (e.g. resulting from lightning and thus adding up in the vertical model column as ammonium nitrate). And, since  $\text{NH}_4\text{NO}_3$  is unstable at higher temperatures and low humidities, both cases could result in higher simulated  $\text{NH}_3$  concentrations during the summer months resulting in potentially closer  $\text{NH}_3$  total column concentrations w.r.t. IASI observations.

Yes, we agree with the reviewer's comment that in our modeling system, the  $\text{NH}_3/\text{NH}_4^+$  partitioning is mainly controlled by sulfate and subsequently by nitrate since major mineral cations (e.g.,  $\text{Na}^+$ ,  $\text{K}^+$ ,  $\text{Ca}^{2+}$ ,  $\text{Mg}^{2+}$ ) are not included. We would like to draw attention to one of our recent study (Acharja et al., 2020) based on analysis of water-soluble inorganic chemical ions of  $\text{PM}_1$ ,  $\text{PM}_{2.5}$ , and atmospheric trace gases over Indo-Gangetic plain (IGP), South Asia, which were monitored by Monitoring AeRosol and Gases in Ambient Air (MARGA). The study revealed that  $\text{NH}_4^+$  was one of the dominant ions, collectively with  $\text{Cl}^-$ ,  $\text{NO}_3^-$  and  $\text{SO}_4^-$  constituted more than 95 % of the measured ionic mass in both  $\text{PM}_1$  and  $\text{PM}_{2.5}$ . The remaining ionic species (e.g.,  $\text{Na}^+$ ,  $\text{K}^+$ ,  $\text{Ca}^{2+}$ ,  $\text{Mg}^{2+}$ ) formed constituted only about 3 % of the total measured ions. Although major mineral cations (e.g.,  $\text{Na}^+$ ,  $\text{K}^+$ ,  $\text{Ca}^{2+}$ ,  $\text{Mg}^{2+}$ ) contribute actively in a neutralization reaction, but their concentration in IGP was found to be very low. Whereas over NCP,  $\text{NO}_3^-$  and  $\text{SO}_4^-$  were found to be dominant ions followed by  $\text{NH}_4^+$  and  $\text{Cl}^-$  which collectively contributed more than 86-90 % in both  $\text{PM}_1$  and  $\text{PM}_{2.5}$ . Other mineral cations contributed less than 5 % in  $\text{PM}_1$  and  $\text{PM}_{2.5}$  (Dao et al., 2014). Furthermore, in one of the studies, over East Asia, the neutralization capacities of major cations (e.g.,  $\text{K}^+$ ,  $\text{Ca}^{2+}$ ,  $\text{Mg}^{2+}$  and  $\text{NH}_4^+$ ) were individually estimated by estimating the Neutralization Factors (NFs) for interpretations. It was found that  $\text{NH}_4^+$  was the predominant neutralizing cation with the highest NF (above 1), whereas  $\text{K}^+$ ,  $\text{Ca}^{2+}$  and  $\text{Mg}^{2+}$  contributed relatively low in the neutralization of aerosol acidity with the lowest NF (below 0.2) (Xu et al., 2017). Hence, consideration of mineral cations may contribute in minor in the neutralization of acidic aerosol over Asian region; still, a rigorous study is needed in future. Therefore, consideration of mineral cations and organic acids on the  $\text{NH}_3/\text{NH}_4^+$  partitioning might be limited and will not significantly impact the results of this study.

Changes in the revised manuscript:-

Line no. 143-162

Line no. 342-347

### **R1C5:**

Also, the underestimation of the surface  $\text{NH}_3$  concentrations throughout the year over both South and East Asia could be a result of missing mineral cations in this model set-up. In reality, a larger fraction of sulphate might be neutralized by mineral cations rather than just by ammonium, which could lead to a larger fraction of free ammonia near the surface. Also, since both nitrates and sulfates preferentially react with mineral cations, nitric acid (e.g. from the traffic sector) might be neutralized by ammonia in a lower amount in reality, as it seems to be the case in this model set-up. In any case, consideration of mineral cations could also lead to a larger fraction of free ammonia near the surface, which might be even sufficient to explain discrepancies with surface observations.

Metzger et al. (2006) results have shown that only if (soluble) mineral components and (lumped) organic acids are accounted for, the observed gas-aerosol partitioning of ammonia and nitric acid can be accurately reproduced for air pollution episodes. Hence, while comparing model results with surface observations, incorporating mineral cations may lead to an increase in free ammonia near the surface, but change will not be significant (considering a 15 % increase) (Metzger et al., 2006). We have added the above description in the discussion section for explaining discrepancies with surface observations in the revised manuscript.

### **Changes in the revised manuscript:-**

Line no. 143-162

Line no. 342-347

Line no. 488-491

### **R1C6:**

Furthermore, due to the excess of ammonia in this model set-up, ammonium nitrate can be formed in both regions, although the simulated sulfate concentrations (burden) are higher in East Asia compared to South Asia. And, due to its semi-volatile character, the seasonal variability of  $\text{NH}_4\text{NO}_3$  and the associated  $\text{NH}_3$  concentrations differ in both regions as observed. Since  $\text{NH}_4\text{NO}_3$  is unstable at higher temperatures, more  $\text{NH}_3$  bound as  $\text{NH}_4\text{NO}_3$  (compared to ammonium sulfate) can lead to higher  $\text{NH}_3$  concentrations during summer, as it is observed in East Asia. In South Asia, where both ammonia and sulfate concentrations are lower, also  $\text{NH}_4\text{NO}_3$  concentrations are lower and thus the seasonality of  $\text{NH}_3$  is less pronounced, which is consistent with the surface observations.. In South Asia, where both ammonia and sulfate concentrations are lower, also  $\text{NH}_4\text{NO}_3$  concentrations are lower and thus the seasonality of  $\text{NH}_3$  is less pronounced, which is consistent with the surface observations.

Yes, we agree with reviewer.

We have added this information in the revised manuscript. We agree with the reviewer, the seasonal variability of  $\text{NH}_4\text{NO}_3$  is strong during summer over East Asia as shown in the below Fig. 3 (Fig. S6 in the revised Supplement), which can lead to higher  $\text{NH}_3$  concentrations during summer over East Asia.

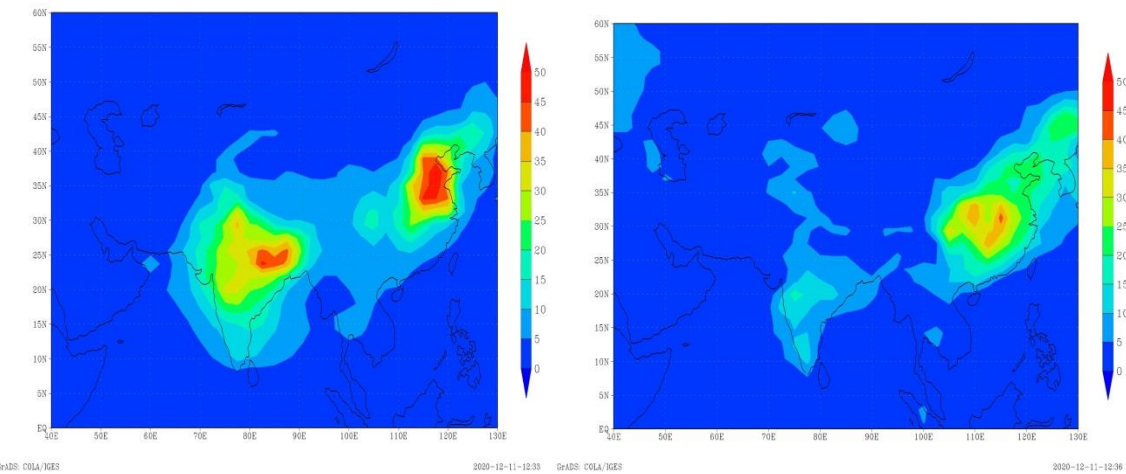


Figure 3. MOZART-4 model estimate of  $\text{NH}_3\text{NO}_3$  wet deposition flux ( $\times 10^{-9} \text{ kg m}^{-2} \text{ s}^{-1}$ ) during summer (JJA) season (left) and during winter (DJF) season (right)

Changes in the revised manuscript:-

Line no. 488-491

Figure no. S6 in the revised Supplement

R1C7:

**On the other hand, the overestimation of the IASI total column  $\text{NH}_3$  concentrations over South Asia, for most of the year except the summer months, could be also a result of missing anions, e.g., of organic acids, assuming the vertical exchange processes are more or less realistically modelled. However, considering mineral cations without additional acids, could likely cause even larger differences in this case (for details see e.g., <https://acp.copernicus.org/articles/6/2549/2006/>).**

Yes, we agree with the reviewer's comment that the current modeling setup has a limitation with respect to missing anions of organic acids and could be one of the regions between observed and model discrepancies. We want to bring to reviewers' notice that model  $\text{NH}_3$  total column concentrations are larger than IASI total column over South Asia (Fig. 4 in the revised manuscript) during most of the years, except during summer months where IASI total columns are larger than the model (Fig. 8 in the revised manuscript). It can be seen in above Fig. 1 (reply to R1C2) that during winter month's higher atmospheric stability prevents the mixing of boundary layer

$\text{NH}_3$  to the free troposphere over IGP, which is reflected in the higher wintertime values of MOZART-4  $\text{NH}_3$  columns. Similarly, higher  $\text{NH}_3/\text{NH}_4^+$  ratio and lower dry and wet deposition of  $\text{NH}_3$  over IGP in winter month enhances the accumulation of  $\text{NH}_3$  in the boundary layer compared. Limited sensitivity of IASI measurements to detect boundary layer  $\text{NH}_3$  (Van Damme et al., 2014) could be one of the reasons for large differences between MOZART-4 and IASI in winter seasons. On the other hand, heating of the landmass due to large solar incidence suppresses the wintertime subsidence over the IGP and leads to a deeper boundary layer during spring and early summer (the average PBLH is about 1100 m, 600 m deeper during spring and summer compared to winter over IGP). During this season, significant transport of the boundary pollution in the mid and upper troposphere due to enhanced convective activities and large scale vertical motion can be noticed. Vertical motion associated with the convective activities is expected to redistribute the  $\text{NH}_3$  concentration in the column, leading to more  $\text{NH}_3$  at the higher altitudes where the satellite's detection sensitivity is more than that of the surface (Clarisso et al., 2010). As a result, more  $\text{NH}_3$  gets detected by the satellite, and we see less difference between observations and model over the IGP.

Therefore, the addition of missing anions will further cause a larger difference between Model and IASI total column  $\text{NH}_3$  concentrations over South Asia during most of the months, except during summer where the difference between Model and IASI total  $\text{NH}_3$  column will decrease.

#### Changes in the revised manuscript:-

Line no. 377-380, 382 -386, 393-401 and 513-514

Figure no. 7 added in revised manuscript

#### R1C8:

**Unfortunately, these processes (briefly touched on above) are missing in most modelling studies, and I fear their consideration is also beyond the scope (or possibilities) of this study?**

We thank the reviewer for putting this additional information to improve the understanding of  $\text{NH}_3/\text{NH}_4^+$  gas-aerosol partitioning. Yes, since we followed parameterization of gas/aerosol partitioning by Metzger et al. (2002), unfortunately, additional mineral cations and organic acids are missing in our modeling study, which is important in gas-aerosol partitioning of reactive nitrogen. For accurate reproducing modeling results and real comparison to observations, EQMs play an important role in determining  $\text{NH}_3/\text{NH}_4^+$  gas-aerosol partitioning.

As mentioned previously, over Asia, chemical characterization of water-soluble inorganic chemical ions of  $\text{PM}_1$ ,  $\text{PM}_{2.5}$  and atmospheric trace gases reveals that major

mineral cations' concentration is very low in PM<sub>1</sub> and PM<sub>2.5</sub>. Lack of study on the presence of organic acids over Asia limits our understanding. Hence, due to a poor understanding of the impact of organic species on aerosol (Zaveri et al., 2008), organic species are not considered in the thermodynamic calculations. However, EQMs are associated with considerable uncertainties and assumptions. According to Metzger et al. (2006), the total NH<sub>3</sub>/NH<sub>4</sub><sup>+</sup> gas-aerosol partitioning calculated ammonium-sulfate-nitrate-sodium-chloride-water system was about 15 % lower than that calculated by EQSAM2 (Equilibrium Simplified Aerosol Model) considering organic acids, and the above study was based upon Greece, which might not be the similar case for the Asian region. Thus, to study the influence of mineral cations and organic species on the NH<sub>3</sub> gas-particle partitioning need rigorous study over the Asian region. Currently, this new setup will be out of our scope. However, in future work, we will try to use EQSAM2 to study the effect of additional mineral cations and organic acids on ammonium gas-aerosol partitioning.

#### Changes in the revised manuscript:-

Line no. 143-162

Line no. 248-276

Added Figure no. S1 in the revised supplement

Line no. 342-347

Line no. 377-380, 382 -386, 393-401, 488-491 and 513-514

Figure no. 7 added in revised manuscript

Figure no. S6 in the revised Supplement

#### References

Acharja, P., Ali, K., Trivedi, D. K., Safai, P. D., Ghude, S., Prabhakaran, T. and Rajeevan, M.: Characterization of atmospheric trace gases and water soluble inorganic chemical ions of PM1 and PM2.5 at Indira Gandhi International Airport, New Delhi during 2017–18 winter, *Sci. Total Environ.*, 729, 138800, doi:10.1016/j.scitotenv.2020.138800, 2020.

Clarissee, L., Shephard, M. W., Dentener, F., Hurtmans, D., Cady-Pereira, K., Karagulian, F., Van Damme, M., Clerbaux, C. and Coheur, P. F.: Satellite monitoring of ammonia: A case study of the San Joaquin Valley, *J. Geophys. Res. Atmos.*, 115(13), 1–15, doi:10.1029/2009JD013291, 2010.

CPCB: Guidelines for Real Time Sampling & Analyses., 2011.

CPCB: Central Pollution Control Board (2020), [online] Available from: <https://cpcb.nic.in/quality-assurance-quality-control/>.

Van Damme, Wichink Kruit, R. J., Schaap, M., Clarisse, L., Clerbaux, C., Coheur, P. F., Dammers, E., Dolman, A. J. and Erisman, J. W.: Evaluating 4 years of atmospheric ammonia (NH<sub>3</sub>) over Europe using IASI satellite observations and LOTOS-EUROS model results, *J. Geophys. Res.*, 119(15), 9549–9566, doi:10.1002/2014JD021911, 2014.

Dao, X., Wang, Z., Lv, Y., Teng, E., Zhang, L. and Wang, C.: Chemical characteristics of water-soluble ions in particulate matter in three metropolitan areas in the North China Plain, *PLoS One*, 9(12), 1–16, doi:10.1371/journal.pone.0113831, 2014.

Ghude, S. D., Bhat, G. S., Prabhakaran, T., Jenamani, R. K., Chate, D. M., Safai, P. D., Karipot, A. K., Konwar, M., Pithani, P., Sinha, V., Rao, P. S. P., Dixit, S. A., Tiwari, S., Todekar, K., Varpe, S., Srivastava, A. K., Bisht, D. S., Murugavel, P., Ali, K., Mina, U., Dharua, M., Rao, Y. J., Padmakumari, B., Hazra, A., Nigam, N., Shende, U., Lal, D. M., Chandra, B. P., Mishra, A. K., Kumar, A., Hakkim, H., Pawar, H., Acharja, P., Kulkarni, R., Subbarthi, C., Balaji, B., Varghese, M., Bera, S. and Rajeevan, M.: Winter fog experiment over the Indo-Gangetic plains of India, *Curr. Sci.*, 112(4), doi:10.18520/cs/v112/i04/767-784, 2017.

Metzger, S., Dentener, F., Pandis, S. and Lelieveld, J.: Gas/aerosol partitioning: 1. A computationally efficient model, *J. Geophys. Res. Atmos.*, 107(16), doi:10.1029/2001JD001102, 2002.

Metzger, S., Mihalopoulos, N. and Lelieveld, J.: Importance of mineral cations and organics in gas-aerosol partitioning of reactive nitrogen compounds: Case study based on MINOS results, *Atmos. Chem. Phys.*, 6(9), 2549–2567, doi:10.5194/acp-6-2549-2006, 2006.

Seinfeld, J. H. and Pandis, S. N.: *Atmospheric Chemistry and Physics: From Air Pollution to Climate Change*, Wiley., 2012.

Seinfeld, J. H., Pandis, S. N. and Noone, K.: *Atmospheric Chemistry and Physics: From Air Pollution to Climate Change*, *Phys. Today*, 51(10), 88–90, doi:10.1063/1.882420, 1998.

Technical Specifications for Continuous Real Time Ambient Air Quality Monitoring Analysers: Technical Specifications for Continuous Real Time Ambient Air Quality Monitoring Analysers / Station Volume – II., 2016.

Wang, T., Song, Y., Xu, Z., Liu, M., Xu, T., Liao, W., Yin, L., Cai, X., Kang, L., Zhang, H. and Zhu, T.: Why is the Indo-Gangetic Plain the region with the largest NH<sub>3</sub> column in the globe during pre-monsoon and monsoon seasons?, *Atmos. Chem. Phys.*, 20(14), 8727–8736, doi:10.5194/acp-20-8727-2020, 2020.

Xu, J. S., He, J., Behera, S. N., Xu, H. H., Ji, D. S., Wang, C. J., Yu, H., Xiao, H., Jiang, Y. J., Qi, B. and Du, R. G.: Temporal and spatial variation in major ion chemistry and source identification of secondary inorganic aerosols in Northern Zhejiang Province, China, *Chemosphere*, 179(December 2014), 316–330, doi:10.1016/j.chemosphere.2017.03.119, 2017.

Zaveri, R. A., Easter, R. C., Fast, J. D. and Peters, L. K.: Model for Simulating Aerosol Interactions and Chemistry (MOSAIC), *J. Geophys. Res. Atmos.*, 113(13), 1–29, doi:10.1029/2007JD008782, 2008.

## Response to Anonymous Referee #2's Comments

First of all we thank the reviewer for the positive evaluation of our study and sincerely appreciate the reviewer's insightful and helpful comments.

Below we explicitly respond to each of the items raised in the comments of anonymous referee #2. These comments are indicated in **bold**, whereas the author's response is presented in **blue** and revisions in **red** in revised manuscript.

### R2C1:

**Ammonia is an important short-lived pollutant with a huge global relevance for air quality, biodiversity and climate due to the wide spread food production. Improving the nitrogen use efficiency in agriculture is of key importance, which requires an understanding of the nitrogen budgets and the ability to monitor these. The atmospheric ammonia burden is difficult to model, and hence, improving our modelling capacity is an important activity. After reading the paper in detail I recommend a major revision is required to improve the paper to a level which is beyond a simple comparison between a coarse model field and observations, which is currently basically is.**

**A major drawback of this study is the coarse resolution the modelling is performed on. Not only in a spatial sense, also the output is available on 4 hours of the day, with IASI overpass (9:30) right in between the output times (06 and 12). The description of the comparison to the satellite data is very short. Giving the strong diurnal cycle of ammonia and the fact that the satellite data availability is affected by all kinds of factors I would like to see a much more detailed description on the method and the impacts of the choices made. - Were the monthly mean comparisons made by averaging paired observations across the month? How many valid pairs were required to allow for a valid number? If pairing was not done than a motivation/discussion why this is not important should be included. Normally the large degree of variability of ammonia column densities between days requires to pair. Satellite data availability and patterns in these within a large grid cell can also impact a non-paired comparison. How was the modelled column for 09:30 estimated? Later I read that a daily mean model value is used. . . correct? - Which quality flags of the satellite data were used? - In our experience the diurnal emission cycle largely impacts the ammonia columns at overpass. What was assumed in this study?**

**Yes, we agree that we compared the monthly mean  $\text{NH}_3$  total column from the IASI overpass in the morning (9:30) with the monthly mean model  $\text{NH}_3$  total column averaging all 4 time-steps of the day. We also agree that the diurnal emission cycle largely impacts the ammonia columns at the overpass. To check the impacts of the diurnal cycle (driven by Boundary layer dynamics), we have again compared the**

monthly mean  $\text{NH}_3$  total column from the IASI overpass in the morning (9:30) with the monthly mean model output at 11:30 LT, which near to IASI overpass (Figure 1 below). If we compare satellite and model at the nearest time-step, the Normalised Mean Bias (NMB) over IGP is reducing by 6% (with daily mean NMB=42 % and with near-time step NMB=36 %, Fig 2 (left) below), and over NCP it is increasing by 6 % (with daily mean NMB= -20 % and with near-time step NMB= -26 %) (Figure 2 (right) below). Since our model was run with the flat diurnal emissions, we have not seen any significant change compared to 4 time-step mean columns and is one of the sources of uncertainties. In the revised version, we have now compared the monthly mean  $\text{NH}_3$  total column from the IASI overpass in the morning (9:30) with the monthly mean model output at 11:30 LT near the IASI overpass.

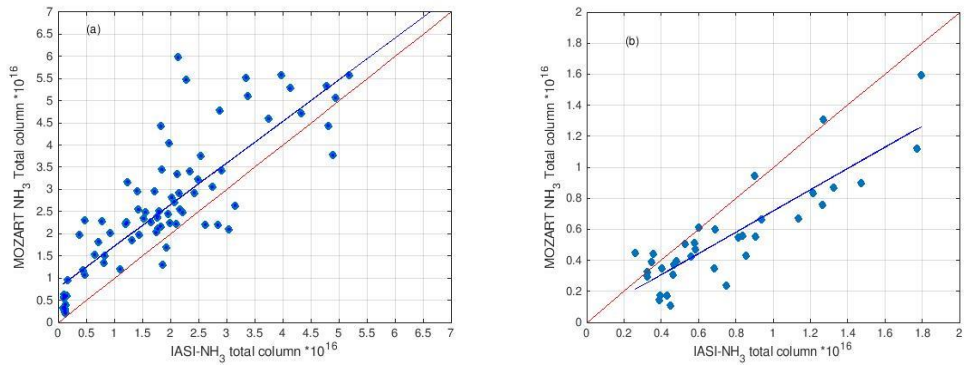
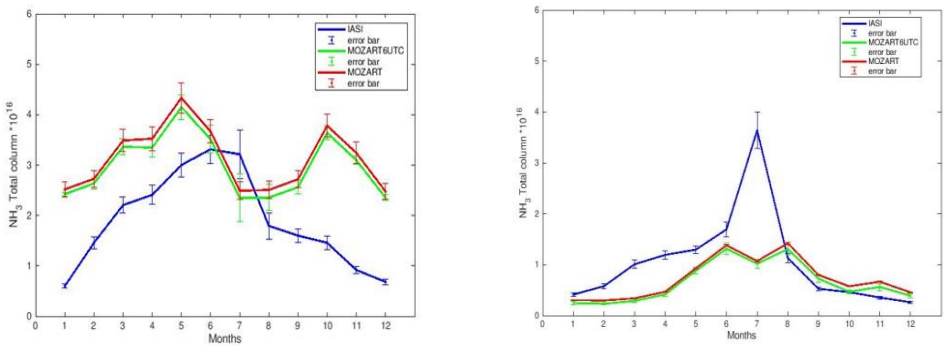


Figure 1 (a) Scatter plot between annual averaged IASI and MOZART-4 (11:30 am) simulated  $\text{NH}_3$  ( $\times 10^{16}$  molecules  $\text{cm}^{-2}$ ) total columns over IGP, South Asia (rectangle: 20°N-32°N, 70°E-95°E) and (b) Scatter plot between annual averaged IASI and MOZART-4 (11:30 am) simulated  $\text{NH}_3$  ( $\times 10^{16}$  molecules  $\text{cm}^{-2}$ ) total columns over NCP, East Asia (rectangle: 30°N-40°N, 110°E-120°E).

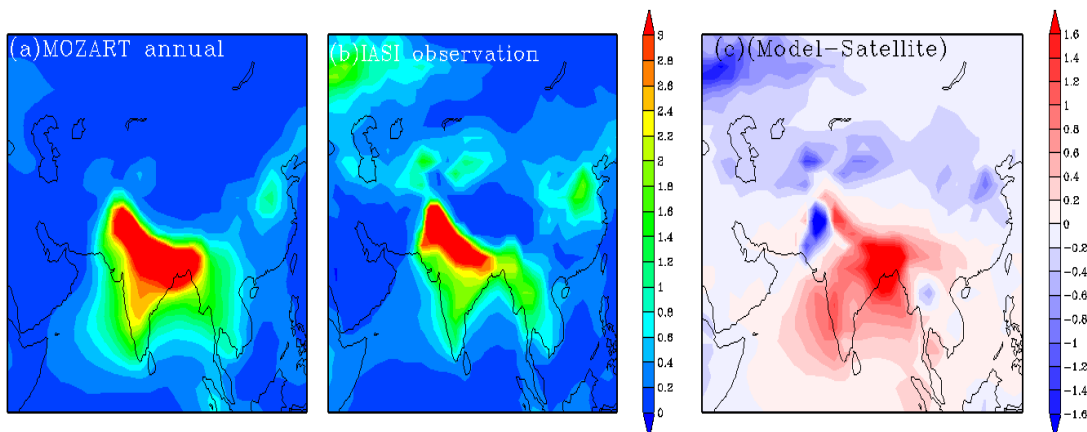


**Figure 2 (left)** Comparison between monthly averaged IASI and MOZART-4 simulated  $\text{NH}_3$  ( $\times 10^{16}$  molecules  $\text{cm}^{-2}$ ) total columns over IGP South Asia (20°N-32°N, 70°E-95°E) for daily mean (red) and near to satellite overpass (11:30, green), **(right)** Comparison between monthly averaged IASI and MOZART-4 simulated  $\text{NH}_3$

( $\times 10^{16}$  molecules  $\text{cm}^{-2}$ ) total columns over NCP East Asia (30°N-40°N, 110°E-120°E) for daily mean (red) and near to satellite overpass (11:30, green)

We agree with the reviewer's comment that a large degree of variability of ammonia column densities between days requires to pair, and Satellite data availability and patterns within a large grid cell can also impact a non-paired comparison. In the present study, we are looking at monthly, seasonal and annual data. Therefore, we considered that IASI provides representative monthly, seasonal, and annual means, despite possible biases introduced by lack of days of data due to cloud cover. We compared monthly mean column to column, as the IASI retrieval algorithm only provides total columns. We made unweighted average distributions using all the morning IASI measurements available, following the recommendation for using the dataset provided in Van Damme et al. (2017).

However, as suggested by the reviewer in the revised manuscript, we have now compared the monthly mean columns by averaging paired observations across the months. We have considered the daily  $\text{NH}_3$  cloud-free satellite total column data and compared it with the modeled daily  $\text{NH}_3$  total column averaging paired observations across the months, seasons and year. For consistency with satellite retrievals, first, the model output (11:30 LT) at each day close to satellite overpass time (09:30 LT) is interpolated in space to the location of valid satellite retrievals. Since the IASI retrieval algorithm only provides total columns, in the second step, we made the unweighted average distribution of the daily paired data to obtain a monthly mean value of satellite and model total  $\text{NH}_3$  columns at each model grid location. The following figures show the comparison between satellite and Model  $\text{NH}_3$  columns on annual (Figure 3 and 4 below) and seasonal scale (Figure 5 and 6 below) calculated by averaging paired and non-paired observations. We find that the normalized mean bias (NMB) over IGP decreased to 38 % with pair-comparison than non-paired comparison (58 %) considering the model columns close to satellite overpass time. However, normalized mean bias (NMB) increased to -41 % with pair-comparison over the NCP region than non-paired comparison (-37 %).



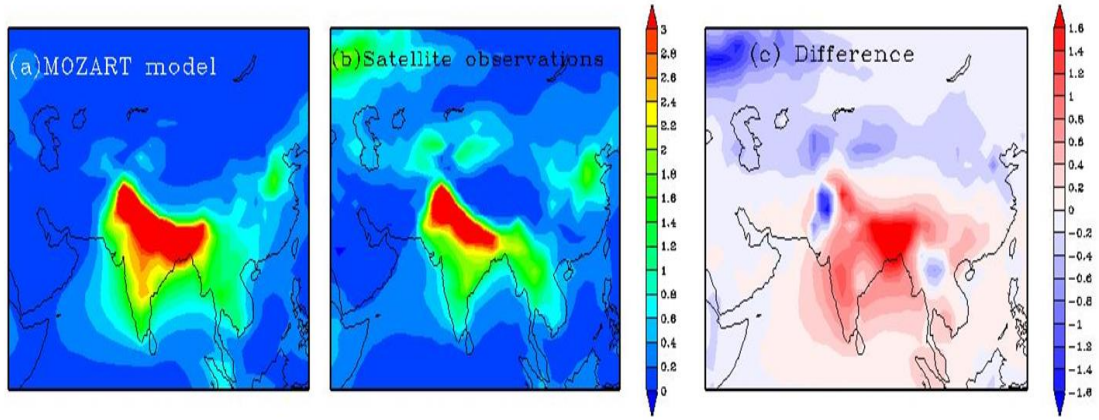


**Figure 3: (top)** Comparison between annual mean satellite and Model NH<sub>3</sub> columns calculated by averaging paired observations, **(bottom)** Comparison between annual mean satellite and Model NH<sub>3</sub> columns calculated by averaging non-paired observations.

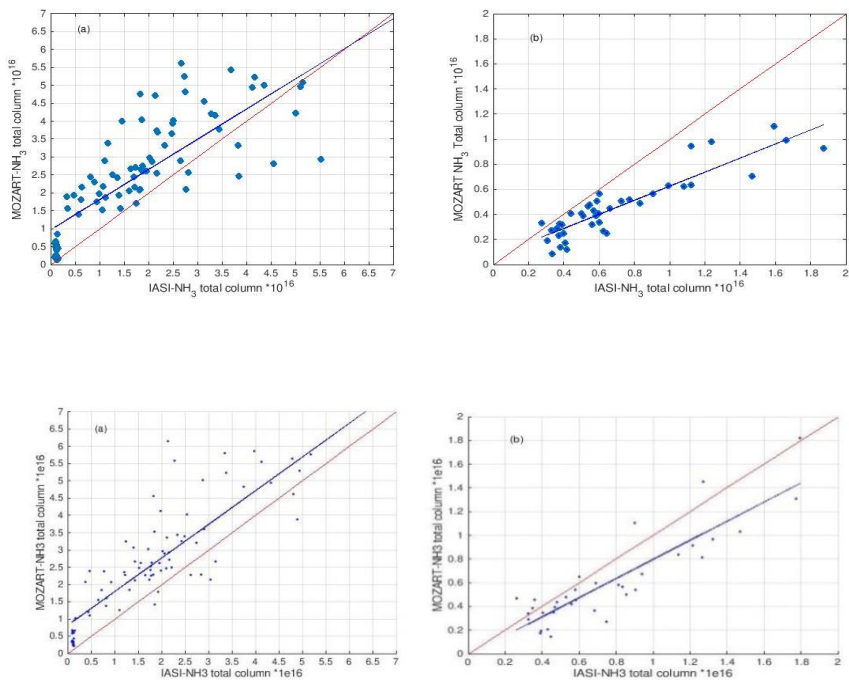


**Figure 4 (top)** Scatter plot between annual averaged IASI and MOZART-4 (11:30 am) simulated NH<sub>3</sub> total columns over IGP (left) and NCP (right) calculated by averaging **paired** observations, **(bottom)** Scatter plot between annual averaged IASI and MOZART-4 (11:30 am) simulated NH<sub>3</sub> total columns over IGP (left) and NCP (right) calculated by averaging **non-paired** observations

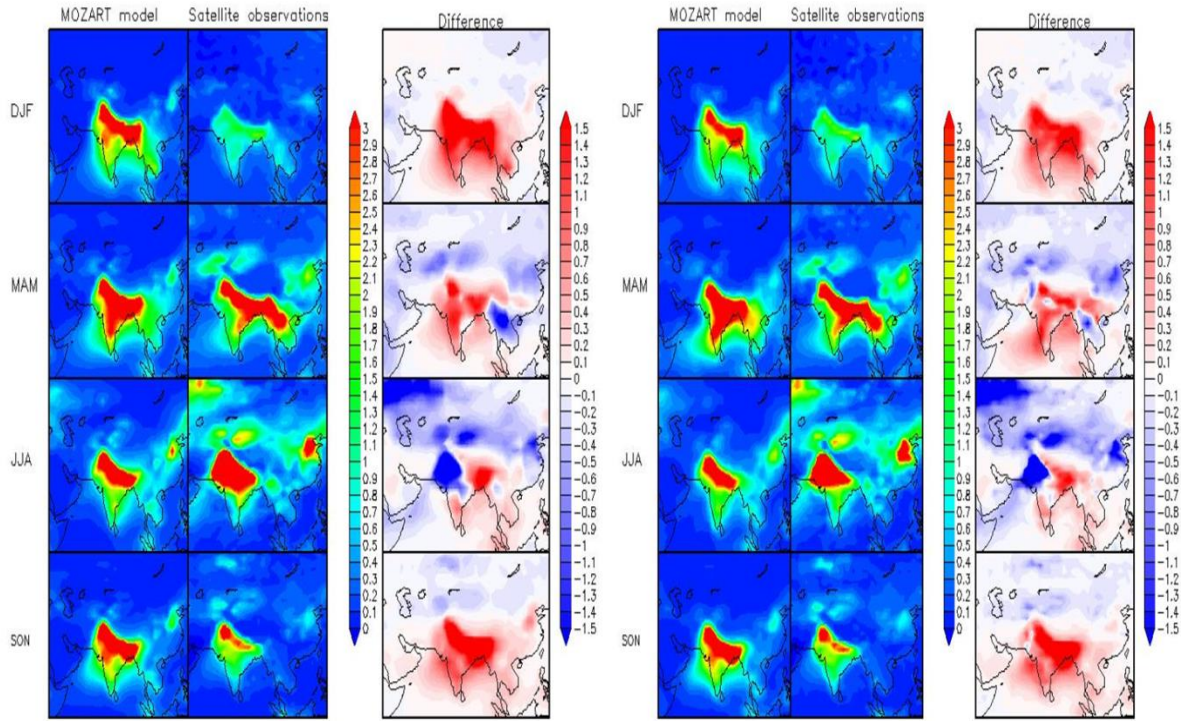


**Figure 3: (left)** Comparison between annual mean satellite and Model NH<sub>3</sub> columns calculated by averaging non-paired observations considering daily mean columns, **(right)** Comparison between annual mean satellite and Model NH<sub>3</sub> columns calculated by averaging paired observations close to satellite overpass time.

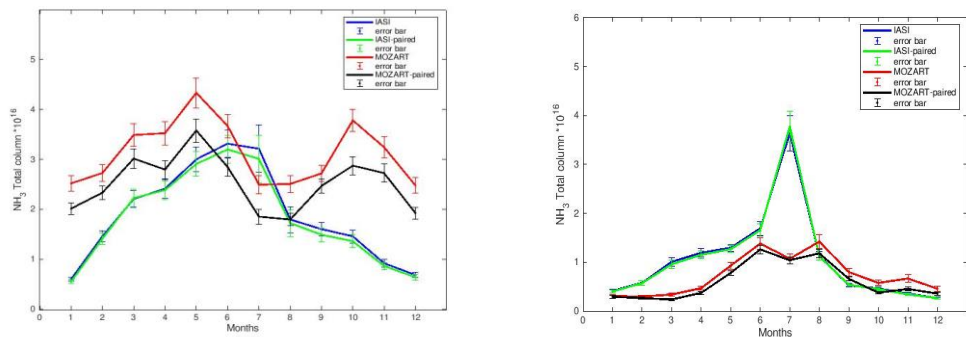


**Figure 6 (left)** Comparison between monthly averaged IASI (blue, non-paired) and MOZART-4 simulated NH<sub>3</sub> total columns for daily mean (red, non-paired) and monthly averaged IASI (paired, green) and MOZART-4 simulated NH<sub>3</sub> near to satellite overpass (black, paired) over IGP South Asia (20°N-32°N, 70°E-95°E), **(right)** Comparison between monthly averaged IASI (blue, non-paired) and MOZART-4 simulated NH<sub>3</sub> total columns for daily mean (red, non-paired) and monthly averaged IASI (green, paired) and MOZART-4 simulated NH<sub>3</sub> near to satellite overpass (black, paired) over IGP South Asia (20°N-32°N, 70°E-95°E).

monthly averaged IASI (paired, green) and MOZART-4 simulated  $\text{NH}_3$  near to satellite overpass (11:30, black, paired) over NCP East Asia ( $30^\circ\text{N}$ - $40^\circ\text{N}$ ,  $110^\circ\text{E}$ - $120^\circ\text{E}$ ).

Based on this new analysis, we have now included all the new plots (Fig. 4, Fig. 5, Fig. 6, Fig. 8) in the revised manuscript, modified Table 1, and added a detailed description of the satellite data comparison.

Further, to see the impact of finer resolution and more frequent output (1hr), we used simulated  $\text{NH}_3$  concentration for 2011 using WRF-Chem simulation for the year 2011 from Ghude et al. (2016) over south Asia at 36 km grid spacing. The model uses MOZART-4 gas-phase chemistry linked to the GOCART aerosol scheme, similar to the one used in MOZART-4 simulation in the present work. Again, we have considered the daily  $\text{NH}_3$  cloud-free satellite total column data for 2011 and compared it with the modeled daily  $\text{NH}_3$  total column averaging paired observations across the year. For consistency with satellite retrievals, first, the model output (9:30 LT) at each day is interpolated in space to the location of valid satellite retrievals at an overpass time of 09:30 LT. Since the IASI retrieval algorithm only provides total columns, in the second step, we made the unweighted average distribution of the daily paired data to obtain a yearly mean value of satellite and model total  $\text{NH}_3$  columns at each model grid location (36 km). The following figures show the comparison between satellite and Model  $\text{NH}_3$  columns on annual (Figure 7 below) scale and its scatter (Figure 8) calculated by averaging paired and non-paired observations. It can be seen that compared to coarse simulations, the bias between the model and IASI  $\text{NH}_3$  total columns are even larger with finer-scale simulations. We have included this for the reviewer's reference but not included in the revised manuscript. It gives a similar difference, but the magnitude of the difference is larger with WRF-Chem simulations.

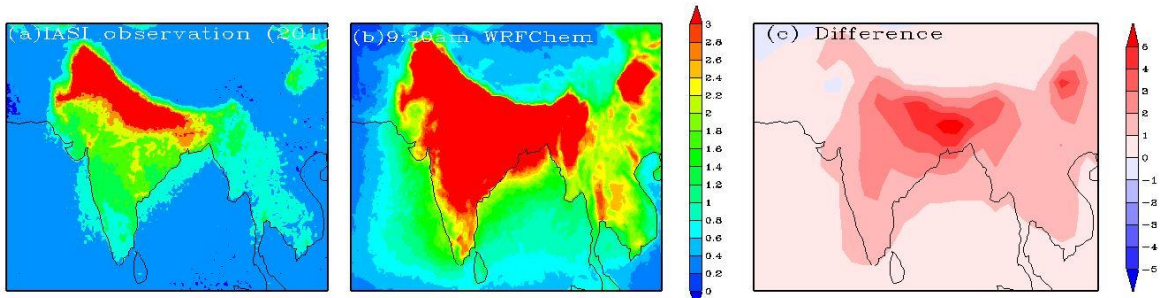


**Figure 7:** Comparison between annual mean IASI (left) and WRF-Chem (Middle)  $\text{NH}_3$  columns and their difference (Right) calculated by averaging paired observations at 09:30 am on 36 km grid resolution.

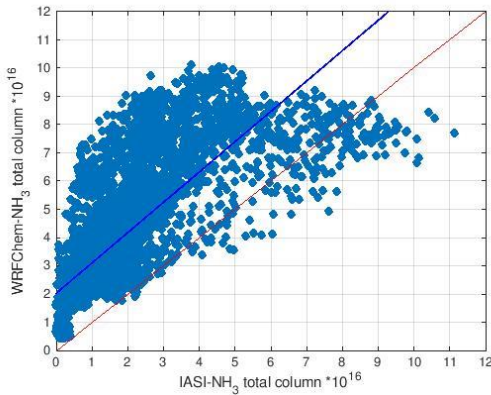


**Figure 8:** Scatter plot between annual averaged IASI and WRF-Chem (09:30 am) simulated NH<sub>3</sub> total columns over IGP.

Changes in the revised manuscript:-

Abstract

Section 2.3

Section 3.1

Section 3.2

**R2C2:**

**Given the agricultural practices in India, is it warranted to use a flat emission cycle across the year?**

We agree with the reviewer's comment. A more realistic seasonal cycle of ammonia emissions is needed for the simulations involving agriculture-based countries like India. The HTAP-V2 inventory certainly lacks this information. We aim to improve the inventory by including such a seasonal cycle for ammonia emissions in our future studies.

**R2C3:**

**The paper is severely hampered by the coarse comparison and I am afraid that the comparison methodology may impact the systematic differences seen in this paper. The differences between overpass time and a daily mean for instance relate to the daylength**

**(variability) and associated mixing, diurnal emission cycle, frequency and kind of precipitation events, etc. I would have like to see an analysis/consideration of such factors in this paper. Part of the observations might be useful for this purpose.**

We request reviewer to refer to our reply to comment R2C1.

**R2C4:**

**The discussion does not include a comparison to other modelling studies evaluating ammonia levels across Asia or studies on ammonia life time.**

Very few studies were carried out in Asia similar to Clarisse et al. (2009), which have evaluated ammonia levels and compared model simulations with satellite retrievals. In a recent study, it is shown that higher summer-time temperature along with the higher Nitrogen (N) fertilizer application rate could cause high  $\text{NH}_3$  emissions resulting in the high  $\text{NH}_3$  columns over Asia, particularly during June-July-August (JJA) (Wang et al., 2020). However, satellite and model evaluation is mostly missing in this study. Studies discussing ammonia lifetime are already mentioned in the discussion part of the manuscript.

Changes in the revised manuscript:-

Section 1 and Section 3

**R2C5:**

**I could identify many grammar mistakes in the english language use. The author list includes native speakers and I would like to urge to perform a careful language check.**

A careful check for grammar has been done.

**Minor comments:**

**R2C6:**

**Abstract: Please use past tense for the method description**

A careful check for grammar has been done.

## R2C7:

**Introduction** The introduction focusses mostly on the contribution of different agricultural activities to emission estimates in south and east Asia. The challenges with respect to the emission estimation, spatial and temporal emission variability, chemistry transport modelling and model-satellite comparison are not focused on although these are relevant to the paper and partly addressed. I would like to ask the authors to address these issues in the intro.

As suggested by the reviewer, we have now added a paragraph to address the challenges for the emission estimation, spatial and temporal emission variability, and chemistry-transport modeling and model-satellite comparison in the introduction. We hope that it addresses the reviewer's concern.

## R2C8:

**Line 43: chemical should be synthetic**

- We have replaced “chemical” with “synthetic”.

## R2C9:

**Line 50: 64 % of total means total global? if yes line 53 repeats this statement**

No, not globally, India and China together accounted for an estimated 64 % of the total amount of NH<sub>3</sub> emissions in Southern Asia during 2000-2014 (Xu et al., 2018). We have now corrected this in the revised manuscript.

## R2C10:

**Line 60-62: could you use the recent edgar numbers or this from v4.3? Should these statements be presented with the global comparison the paragraph above?**

As suggested by the reviewer, we have now provided the estimates from EDGAR v4.3.2 and included this statement where the global comparison was discussed in the

introduction section in the revised manuscript. Emission estimates provided by the latest EDGAR v4.3.2 emission inventory suggests that globally about 59 Tg of NH<sub>3</sub> was emitted in the atmosphere in 2012, out of which agricultural soils contributed about 56 %, manure management contributed about 19 %, and agricultural burning contributed about 1.5 % (Crippa et al., 2018).

**Changes in the revised manuscript:-**

Abstract has been modified.

**R2C11:**

**Line 63 and 67 are in direct contradiction to each other**

Yes, we agree with the reviewer's comment that lines 63 and 67 contradict each other. In India, around 50 % of total NH<sub>3</sub> emissions is estimated from the fertilizer application and the remaining from livestock and other NH<sub>3</sub> sources. Urea is mostly used as a fertilizer and alone contributes more than 90 % of the total fertilizer used for agricultural activities (Sharma et al., 2008). We have now corrected this in the revised manuscript.

**Changes in the revised manuscript:-**

Line no. 62-63

**R2C12:**

**Data and methodology Line 85: this sentence implies only trace gases were modelled, which is not the case I guess**

We have now revised the sentence in the revised manuscript.

**Changes in the revised manuscript:-**

Line no. 108

**R2C13:**

**Line 97: Does Mozart use a land use mosaic within a gridcell? Or dominant LUC? How do the wesely land use classes match those in the domain? Were the latter updated?**

Dry deposition of gases and aerosols were calculated online according to Wesely (1989) parameterization, and wet depositions of soluble gases were calculated as described by the method of Emmons et al. (2010). Land use cover (LUC) maps used in MOZART-4 are based on the Advanced Very High-Resolution Radiometer (AVHRR) and Moderate Resolution Imaging Spectroradiometer (MODIS) data based on NCAR Community Land Model (CLM) (Oleson et al., 2010). MOZART-4 represents the land surface as a hierarchy of sub-grid types: glacier, lake, wetland, urban and vegetated land. The vegetated land is further divided into a mosaic of Plant Function Type (PFTs). These same maps are used for the dry deposition calculations (Emmons et al., 2010; Lawrence and Chase, 2007; Oleson et al., 2010). We have now included this discussion in the revised manuscript.

**Changes in the revised manuscript:-**

Line no. 122-128

**R2C14:**

**Line 122: didn't you use emissions of all sectors?**

- We have used all the sectors for emissions as per the HTAP v2 emission inventory. The sectors are for all substances defined as follows:
- Air = international and domestic air,
- Shipping = international shipping,
- Energy = power industry,
- Industry = manufacturing, mining, metal, cement, chemical, solvent industry, transport = ground transport (incl. road, rail, pipeline, inland waterways),
- Residential = heating/cooling of buildings and equipment/lighting of buildings and waste treatment.
- For NH<sub>3</sub> there is in addition sector agriculture = agriculture (but not agricultural waste burning).
- However, for NH<sub>3</sub> HTAP-v2 emission inventory covers only 5 (agriculture, energy, transport, residential and industry) sectors and rest two sectors, aircraft and international shipping, is not considered for NH<sub>3</sub> emissions.

**Changes in the revised manuscript:-**

Line no. 180-184

**R2C15:**

**Line 133: cow dung is not fossil**

Removed word “cow dung” and replaced with “biomass combustion”.

We have now corrected it in the revised manuscript.

Changes in the revised manuscript:-

Line no. 193

**R2C16:**

**Results: Line 226: the methodology describes that nitrate is present – please explain**

We have corrected it in the revised manuscript.

Changes in the revised manuscript:-

Line no. 342

**R2C17:**

**250: the model has no maximum emissions in summer as antrop is flat and soil is a few percent of total, so this statement seems incorrect**

We agree with the reviewer's comment that over South Asia, anthropogenic emissions are flat. Although soil emissions show some increase during summer, the percentage contribution to total emissions is small and will not affect observed  $\text{NH}_3$  seasonal variability. We have now corrected it in the revised manuscript.

Changes in the revised manuscript:-

Line no. 409

**R2C18:**

**Figure 2: the scale on the upper left figure is misleading. It seems a seasonal cycle where it is basically flat.**

As per reviewer's suggestion, we have now revised the scale to make it consistent.

Changes in the revised manuscript:-

Figure 2 is modified

## References

Clarisso, L., Clerbaux, C., Dentener, F., Hurtmans, D. and Coheur, P. F.: Global ammonia distribution derived from infrared satellite observations, *Nat. Geosci.*, 2(7), 479–483, doi:10.1038/ngeo551, 2009.

Crippa, M., Guizzardi, D., Muntean, M., Schaaf, E., Dentener, F., Van Aardenne, J. A., Monni, S., Doering, U., Olivier, J. G. J., Pagliari, V. and Janssens-Maenhout, G.: Gridded emissions of air pollutants for the period 1970–2012 within EDGAR v4.3.2, *Earth Syst. Sci. Data*, 10(4), 1987–2013, doi:10.5194/essd-10-1987-2018, 2018.

Van Damme, M., Whitburn, S., Clarisse, L., Clerbaux, C., Hurtmans, D. and Coheur, P.-F.: Version 2 of the IASI NH<sub>3</sub> neural network retrieval algorithm; near-real time and reanalysed datasets, *Atmos. Meas. Tech. Discuss.*, 1–14, doi:10.5194/amt-2017-239, 2017.

Emmons, L. K., Walters, S., Hess, P. G., Lamarque, J. F., Pfister, G. G., Fillmore, D., Granier, C., Guenther, A., Kinnison, D., Laepple, T., Orlando, J., Tie, X., Tyndall, G., Wiedinmyer, C., Baughcum, S. L. and Kloster, S.: Description and evaluation of the Model for Ozone and Related chemical Tracers, version 4 (MOZART-4), *Geosci. Model Dev.*, 3(1), 43–67, doi:10.5194/gmd-3-43-2010, 2010.

Ghude, S. D.: *Geophysical Research Letters*, *Geophys. Res. Lett.*, 1–8, doi:10.1002/2013GL058740, 2016.

Lawrence, P. J. and Chase, T. N.: Representing a new MODIS consistent land surface in the Community Land Model (CLM 3.0), *J. Geophys. Res. Biogeosciences*, 112(1), doi:10.1029/2006JG000168, 2007.

Oleson, K. W., Lawrence, D. M., Bonan, G. B., Flanner, M. G., Kluzeck, E., Lawrence, P. J., Zeng, X. (2010).: Technical Description of version 4.0 of the Community Land Model (CLM), 2010.

Sharma, C., Tiwari, M. K. and Pathak, H.: Estimates of emission and deposition of reactive nitrogenous species for India, *Curr. Sci.*, 94(11), 1439–1446, 2008.

Wang, T., Song, Y., Xu, Z., Liu, M., Xu, T., Liao, W., Yin, L., Cai, X., Kang, L., Zhang, H. and Zhu, T.: Why is the Indo-Gangetic Plain the region with the largest NH<sub>3</sub> column in the globe during pre-monsoon and monsoon seasons?, *Atmos. Chem. Phys.*, 20(14), 8727–8736, doi:10.5194/acp-20-8727-2020, 2020.

Wesely, M. L.: Parameterization of surface resistances to gaseous dry deposition in regional-scale numerical models, *Atmos. Environ.*, 23(6), 1293–1304, doi:10.1016/0004-

6981(89)90153-4, 1989.

Xu, R. T., Pan, S. F., Chen, J., Chen, G. S., Yang, J., Dangal, S. R. S., Shepard, J. P. and Tian, H. Q.: Half-Century Ammonia Emissions From Agricultural Systems in Southern Asia: Magnitude, Spatiotemporal Patterns, and Implications for Human Health, *GeoHealth*, 2(1), 40–53, doi:10.1002/2017gh000098, 2018.

## Response to Editor Comments

I have taken note of the rebuttal to the reviewer's comments. Several (main) concerns have voiced with regard to the use and quality of surface observations for comparison, the use of coarse resolution model and low temporal resolution for comparison with IASI satellite data, and issues with the gas-particle partitioning. Although the responses were to some extent addressing the reviewers concerns, I encourage the authors to avoid relaying issues for 'future work', and where appropriate extend the analysis with some sensitivity studies. Further discussion is warranted wrt to quality issues of surface observations: information on calibration procedures, and in particular for what it means for this study should be described carefully.

**Reply:** We thank Editor for his comment and suggestions. We agree with both the reviewers' comments and suggestions and address their concerns that have greatly improved the manuscript's quality. We have used an additional set of simulations using the WRF-Chem model over South Asia with a consistent emission inventory and chemical scheme to see the impact of finer model resolution and high temporal resolution compared to the IASI satellite data.

We have also added the following discussion on the data quality and the quality control procedure adopted in this study.

The quality control and assurance method, followed by Central Pollution Control Board (CPCB) for these air quality monitoring stations, is given in the CPCB (2011 and 2020). Furthermore, we take the following steps to reassure the quality of  $\text{NH}_3$  observations from the CPCB network stations. For data quality, we rejected all the observations values below the lowest detection limit of the instrument ( $1 \text{ } \mu\text{g m}^{-3}$ ) (Technical specifications for CAAQM station, 2019) because most of the sites are situated in the urban environment. For cities where more than one monitoring station is available, we rejected all the observations above  $250 \text{ } \mu\text{g m}^{-3}$  at a given site if other sites in the network do not show values outside this range. This step aims to eliminate any short-term local influence that cannot be captured in the models and retain the regional-scale variability. Second, we removed single peaks characterized by a change of more than  $100 \text{ } \mu\text{g m}^{-3}$  in just one hour for all the data in CPCB monitoring stations. This step filters random fluctuations in the observations. Third, we removed some very high  $\text{NH}_3$  values that appeared in the timeseries right after the missing values. For any given day, we removed the sites from the consideration that either experience instrument malfunction, or appear to be very heavily influenced by strong local sources. In order to verify the data quality of CBCB monitoring site, we have inter compared the  $\text{NH}_3$  measurement at CPCB monitoring station (R.K. Puram) in Delhi with the  $\text{NH}_3$  measurements at Indira Gandhi International (IGI) Airport taken during Winter Fog Experiment (WiFEX) (Ghude et al., 2017) using Measurement of Aerosols and Gases (MARGA) instrument during winter season of 2017-2018. More

details on the  $\text{NH}_3$  measurements using MARGA is available with Acharja et al. (2020). Both sites were situated in the same area of Delhi (less than 1km). Our inter-comparison show that  $\text{NH}_3$  measured at CPCB monitoring station by chemiluminescence method are slightly (on an average  $9.8 \mu\text{g m}^{-3}$ ) on higher side than  $\text{NH}_3$  measured by ion chromatography (IC) using MARGA (Fig. S1 in the revised Supplement). The differences that were observed could partly be related to the different  $\text{NH}_3$  measurement techniques and partly to the locations of the two monitoring sites which were not place exactly at same location. Apparently, the difference of  $9.8 \mu\text{g m}^{-3}$  indicates that the  $\text{NH}_3$  measurements from the CPCB do not suffer from the calibration issue.

In particular, I would like to see a somewhat more in depth discussion on the potential biases derived from mismatch of temporal matching and boundary layer dynamics in the MOZART model, in particular in winter when high atmospheric stability prevents mixing, and IASI may not observe all  $\text{NH}_3$  close to the surface. A case study with higher temporal (and spatial) resolution for a limited and more frequent output and realistic assumptions on IASI effective kernels may be helpful to illustrate the sensitivity of results.

**Reply:** We have also discussed the potential biases derived from the mismatch of temporal matching and boundary dynamics in the MOZART mode. However, as suggested by the reviewer, in the revised manuscript, we have now compared the monthly mean columns by averaging paired observations across the months. We have considered the daily  $\text{NH}_3$  cloud-free satellite total column data and compared it with the modeled daily  $\text{NH}_3$  total column averaging paired observations across the months, seasons, and year. For consistency with satellite retrievals, first, the model output (11:30 LT) at each day close to satellite overpass time (09:30 LT) is interpolated in space to the location of valid satellite retrievals. Since the IASI retrieval algorithm only provides total columns, in the second step, we made the unweighted average distribution of the daily paired data to obtain a monthly mean value of satellite and model total  $\text{NH}_3$  columns at each model grid location. We find that the normalized mean bias (NMB) over IGP decreased to 38% with pair-comparison than non-paired comparison (58%) considering the model columns close to satellite overpass time. However, normalized mean bias (NMB) increased to -41% with paired-comparison over the NCP region than non-paired comparison (-37%).

IASI retrieval method used for  $\text{NH}_3$  does not produce averaging kernels as it is not based on optimal estimation. Therefore, IASI retrievals' limitation is that it does not allow the calculation of an averaging kernel to account for the vertical sensitivity of the instrument sounding to different layers in the atmosphere. We refer to Van Damme et al. (2017); Whitburn et al. (2016) for a comprehensive discussion on the advantages and disadvantage of constrained versus unconstrained retrieval approaches for  $\text{NH}_3$ . In brief, the current approach's main advantage is that a priori information does not influence the retrieval. Therefore, the  $\text{NH}_3$  column value is derived from the measurement only. We compared column to column, as the IASI retrieval algorithm

only provides total columns. We made unweighted average distributions using all the morning IASI measurements available, following the recommendation for using the dataset provided in Van Damme et al., (2017). In this paper, we have use  $\text{NH}_3$  total columns retrieved from the IASI instrument morning overpass (AM) observations (i.e., 09:30 local time).

Further, in order to see the impact of finer resolution and more frequent output (1hr), we used simulated  $\text{NH}_3$  concentration for the year 2011 using WRF-Chem simulation for the year 2011 from work reported in Ghude et al. (2016) over south Asia at 36 km grid spacing. The model uses MOZART-4 gas-phase chemistry linked to the GOCART aerosol scheme, similar to the one which is used in MOZART-4 simulation in the present work. Again, we have considered the daily  $\text{NH}_3$  cloud-free satellite total column data for 2011 and compared it with the modeled daily  $\text{NH}_3$  total column averaging paired observations across the year. For consistency with satellite retrievals, first, the model output (9:30 LT) at each day is interpolated in space to the location of valid satellite retrievals at an overpass time of 09:30 LT. Since the IASI retrieval algorithm only provides total columns, in the second step, we made the unweighted average distribution of the daily paired data to obtain a yearly mean value of satellite and model total  $\text{NH}_3$  columns at each model grid location (36 km). We found that the bias between the model and IASI  $\text{NH}_3$  total columns is even larger with finer-scale simulations compared to coarse simulations. We have included this for the reviewer's reference but not included it in the revised manuscript as it gives a similar difference, but the magnitude of the difference is larger with WRF-Chem simulations.

We requested Editor to refer to our responses and figures provided in the 'Response to Anonymous Referee #1's and Anonymous Referee #2's Comments' document enclosed with the revised manuscript.

Likewise some first order estimate of the impact of applying a temporal profile on agricultural  $\text{NH}_3$  emission would be preferable.

**Reply:** Unfortunately, the application of agriculture has significant spatial and temporal variability over South Asia, which depends on the cropping season and cropping pattern, is not well documented. However, we agree that it will contribute to the mismatch observed between observed and modeled  $\text{NH}_3$  columns to some extent. Under the on-going South Asia Nitrogen Hub (SANH) project (The Global Challenges Research Fund (GCRF) South Asia Nitrogen hub), it is planned to develop a high-resolution  $\text{NH}_3$  emission inventory over South Asia that will account for the temporal profile of agricultural  $\text{NH}_3$  emission based on agricultural statistics.

I encourage the author to resubmit, taken the review comments and my instructions as much as possible into account.

**Reply:** We requested Editor to refer to our responses in the 'Response to Anonymous Referee #1's and Anonymous Referee #2's Comments' document enclosed with the revised manuscript.

## References

Acharja, P., Ali, K., Trivedi, D. K., Safai, P. D., Ghude, S., Prabhakaran, T. and Rajeevan, M.: Characterization of atmospheric trace gases and water soluble inorganic chemical ions of PM1 and PM2.5 at Indira Gandhi International Airport, New Delhi during 2017–18 winter, *Sci. Total Environ.*, 729, 138800, doi:10.1016/j.scitotenv.2020.138800, 2020.

CPCB: Guidelines for Real Time Sampling & Analyses., 2011.

CPCB: Central Pollution Control Board (2020), [online] Available from: <https://cpcb.nic.in/quality-assurance-quality-control/>.

Van Damme, M., Whitburn, S., Clarisse, L., Clerbaux, C., Hurtmans, D. and Coheur, P.-F.: Version 2 of the IASI NH<sub>3</sub> neural network retrieval algorithm; near-real time and reanalysed datasets, *Atmos. Meas. Tech. Discuss.*, 1–14, doi:10.5194/amt-2017-239, 2017.

Ghude, S. D., Chate, D. M., Jena, C., Beig, G., Kumar, R., Barth, M. C., Pfister, G. G., Fadnavis, S. and Pithani, P.: Premature mortality in India due to PM<sub>2.5</sub> and ozone exposure, *Geophys. Res. Lett.*, 43(9), 4650–4658, doi:10.1002/2016GL068949, 2016.

Ghude, S. D., D. M. Chate, C. Jena, G. Beig, R. Kumar, M. C. Barth, G. G. Pfister, S. Fadnavis, and P. P.: Premature mortality in India due to PM<sub>2.5</sub> and ozone exposure, *Geophys. Res. Lett.*, 1–8, doi:10.1002/2013GL058740. Received, 2016.

Ghude, S. D., Bhat, G. S., Prabhakaran, T., Jenamani, R. K., Chate, D. M., Safai, P. D., Karipot, A. K., Konwar, M., Pithani, P., Sinha, V., Rao, P. S. P., Dixit, S. A., Tiwari, S., Todekar, K., Varpe, S., Srivastava, A. K., Bisht, D. S., Murugavel, P., Ali, K., Mina, U., Dharua, M., Rao, Y. J., Padmakumari, B., Hazra, A., Nigam, N., Shende, U., Lal, D. M., Chandra, B. P., Mishra, A. K., Kumar, A., Hakkim, H., Pawar, H., Acharja, P., Kulkarni, R., Subbarthi, C., Balaji, B., Varghese, M., Bera, S. and Rajeevan, M.: Winter fog experiment over the Indo-Gangetic plains of India, *Curr. Sci.*, 112(4), doi:10.18520/cs/v112/i04/767-784, 2017.

Technical specifications for CAAQM station: Technical specifications for continuous ambient air quality monitoring (CAAQM) STATION (real time) Central Pollution Control Board East Arjun Nagar , Shahdara., 2019.

The Global Challenges Research Fund (GCRF) South Asia Nitrogen hub: The Global Challenges Research Fund (GCRF) project, [online] Available from: <https://gtr.ukri.org/projects?ref=NE/S009019/>.

Whitburn, S., Damme, M. Van, Clarisse, L., Bauduin, S., Heald, C. L., Hurtmans, D., Zondlo, M. A., Clerbaux, C. and Coheur, P.: A flexible and robust neural network IASI-NH<sub>3</sub>, , 6581–6599, doi:10.1002/2016JD024828. Received, 2016.

# Analysis of atmospheric ammonia over South and East Asia based on the MOZART-4 model and its comparison with satellite and surface observations

Pooja V. Pawar<sup>1\*</sup>, Sachin D. Ghude<sup>1</sup>, Chinmay Jena<sup>1</sup>, Andrea Möring<sup>2,7</sup>, Mark A. Sutton<sup>2</sup>, Santosh Kulkarni<sup>3</sup>, Deen Mani Lal<sup>1</sup>, Divya Surendran<sup>4</sup>, Martin Van Damme<sup>5</sup>, Lieven Clarisse<sup>5</sup>, Pierre-François Coheur<sup>5</sup>, Xuejun Liu<sup>6</sup>, Gaurav Govardhan<sup>1</sup>, Wen Xu<sup>6</sup>, Jize Jiang<sup>7</sup>, and Tapan Kumar Adhya<sup>8</sup>

<sup>1</sup>Indian Institute of Tropical Meteorology (IITM), Pune, 411008, India

<sup>2</sup>Centre for Ecology & Hydrology (CEH), Edinburgh, EH26 0QB, UK

<sup>3</sup>Centre for Development of Advanced Computing, Pune, 411008, India

<sup>4</sup>Indian Meteorological Department (IMD), Pune, 411005, India

<sup>5</sup>Université libre de Bruxelles (ULB), Spectroscopy, Quantum Chemistry and Atmospheric Remote Sensing (SQUARES), Brussels, B-1050, Belgium

<sup>6</sup>College of Resources and Environmental Sciences, National Academy of Agriculture Green Development, China Agricultural University, Beijing 100193, China

<sup>7</sup>The University of Edinburgh, Scotland, EH8 9AB, UK

<sup>8</sup>Kalinga Institute of Industrial Technology, Bhubaneshwar, 751016, India

*Correspondence to:* Sachin D. Ghude (sachinghude@tropmet.res.in)

**Abstract.** Limited availability of atmospheric ammonia ( $\text{NH}_3$ ) observations, limits our understanding of controls on its spatial and temporal variability and its interactions with ecosystems. Here we used the Model for Ozone and Related chemical Tracers (MOZART-4) global chemistry transport model and the Hemispheric Transport of Air Pollution version-2 (HTAP-v2) emission inventory to simulate global  $\text{NH}_3$  distribution for the year 2010. We presented a first comparison of the model with monthly averaged satellite distributions and limited ground-based observations available across South Asia. The MOZART-4 simulations over South Asia and East Asia were evaluated with the  $\text{NH}_3$  retrievals obtained from the Infrared Atmospheric Sounding Interferometer (IASI) satellite and 69 ground based monitoring stations for air quality across South Asia, and 32 ground based monitoring stations from the Nationwide Nitrogen Deposition Monitoring Network (NNDMN) of China. We identified the northern region of India (Indo-Gangetic Plain, IGP) as a hotspot for  $\text{NH}_3$  in Asia, both using the model and satellite observations. In general, a close agreement was found between yearly-averaged  $\text{NH}_3$  total columns simulated by the model and IASI satellite measurements over the IGP, South Asia ( $r=0.81$ )

and North China Plain (NCP), of East Asia ( $r=0.90$ ). However, the MOZART-4 simulated  $\text{NH}_3$  column was substantially higher over South Asia than East Asia, as compared with the IASI retrievals, which show smaller differences. Model simulated surface  $\text{NH}_3$  concentrations indicated smaller concentrations in all seasons than surface  $\text{NH}_3$  measured by the ground based observations over South and East Asia, although uncertainties remain in the available surface  $\text{NH}_3$  measurements. Overall, the comparison of East Asia and South Asia using both MOZART-4 model and satellite observations showed smaller  $\text{NH}_3$  columns in East Asia compared with South Asia for comparable emissions, indicating rapid dissipation of  $\text{NH}_3$  due to secondary aerosol formation, which can be explained by larger emissions of acidic precursor gases in East Asia.

## 1 Introduction

Gaseous pollution due to various forms of nitrogen emissions plays an important role in environmental processes. Specifically, ammonia ( $\text{NH}_3$ ) emitted from various agricultural activities, such as use of synthetic fertilizers, animal farming, etc., together with nitrogen oxides ( $\text{NO}_x$ ) is one of the largest sources of reactive nitrogen (Nr) emission to the atmosphere. Ammonia has great environmental implications due to its substantial influence on the global nitrogen cycle and associated air pollution, ecosystem and on public health (Behera et al., 2013; Liu et al., 2017b; Zhou et al., 2016). Emission estimates provided by latest EDGAR v4.3.2. emission inventory suggests that globally about 59 Tg of  $\text{NH}_3$  was emitted in the atmosphere in 2012 out of which agricultural soils contributed about 56 %, manure management contributed about 19 %, and agricultural burning contributed about 1.5 % (Crippa et al., 2018). Ammonia is a key precursor in aerosol formation, as the reactions in the atmosphere lead to an increase in different forms of sulphates and nitrates that contribute in secondary aerosol formation (Pinder et al., 2007, 2008). India and China together accounted for an estimated 64 % of the total amount of  $\text{NH}_3$  emissions in Southern Asia during 2000-2014 (Xu et al., 2018). Emissions of  $\text{NO}_x$  and  $\text{NH}_3$  are increasing substantially over South Asia (Sutton et al., 2017), which contributes to increase in particulate mass loading, visibility degradation, acidification and eutrophication (Behera et al., 2013; Ghude et al., 2008, 2013, 2016). Asia is responsible for the largest share of global  $\text{NH}_3$  emissions (Janssens-Maenhout et al., 2012). Further increase in  $\text{NH}_3$  emission will increase its negative impacts and societal cost (Sutton et al., 2017).

In India, around 50 % of total  $\text{NH}_3$  emissions is estimated from the fertilizer application and remaining from livestock and other  $\text{NH}_3$  sources (Aneja et al., 2011; Behera et al., 2013). However, there are large uncertainties in emissions of ammonia, its deposition to surface, chemistry and transport (Sutton et al., 2013; Zhu et al., 2015). Urea is mostly used as a fertilizer (Fertilizer Association of India annual report 2018-19) and alone contributes more than 90 % of total fertilizer used for the agricultural activities (Sharma et al., 2008). India is currently the second largest consumer

of fertilizers after China, and fertilizer usage is bound to increase with further intensification of agriculture and the fertilizer input of India is expected to be doubled by 2050 (Alexandratos and Bruinsma, 2012).

Recent study based on Infrared Atmospheric Sounding Interferometer (IASI) satellite measurements show very high concentration of  $\text{NH}_3$  over Indo-Gangetic Plain (IGP) and North China Plain (NCP) which were mainly related to agricultural (Van Damme et al., 2014a, 2014b, 2015b) and industrial activity (Clarisso et al., 2019; Van Damme et al., 2018). The seasonality was shown to be more pronounced in the northern hemisphere, with peak columns in spring and summer season (Van Damme et al., 2014a). Van Damme et al., (2015a) attempted first to validate IASI- $\text{NH}_3$  measurements using existing independent ground-based and airborne data sets. This study doesn't include comparison of ground-based  $\text{NH}_3$  data sets with IASI measurements particularly over South Asia (India) due to limited availability of  $\text{NH}_3$  measurements. Liu et al. (2017a) estimated the ground-based  $\text{NH}_3$  concentrations over East Asia, combining IASI- $\text{NH}_3$  columns and  $\text{NH}_3$  profiles from MOZART-4 and validated it with forty four sites of Chinese Nationwide Nitrogen Deposition Monitoring Network (NNDMN). In one of the recent study over South Asia, interannual variability of atmospheric  $\text{NH}_3$  using IASI observations revealed large seasonal variability in atmospheric  $\text{NH}_3$  concentrations which were equivalent with highest number of urea fertilizer plants. This study highlights the importance of role of agriculture statistics and fertilizer consumption/application in determining ammonia concentration in South Asia (Kuttippurath et al., 2020). Available global ammonia emission inventory does not include a comprehensive bottom up  $\text{NH}_3$  emissions for South Asia compared to East Asia to be suitable for input to atmospheric models by taking into consideration actual statistical data of various  $\text{NH}_3$  sources such as livestock excreta, fertilizer application, agricultural soil, nitrogen-fixing plants, crop residue compost, biomass burning, urine from rural populations, chemical industry, waste disposal, traffic, etc which is currently missing (Behera et al., 2013; Huang et al., 2012; Janssens-Maenhout et al., 2015; Li et al., 2017; Zhang et al., 2010). Han et al. (2020) suggested that updated emission inventory as per the source activity is essential for south Asia to reduce the uncertainties simulated  $\text{NH}_3$  over this region. A recent study by Wang et al. (2020) examined the  $\text{NH}_3$  column observed over the IGP during summer using regional model driven with MIX emission inventory. The study suggested that large agriculture activity and high summer temperature contributes to high  $\text{NH}_3$  emission fluxes over IGP which leads to large total columns. Summer time increase in  $\text{NH}_3$  concentration at surface over certain sites in the IGP regions are also observed from the ground based monitoring network (Datta et al., 2012; Mandal et al., 2013; Saraswati et al., 2019; Sharma et al., 2012, 2014b).

In this study, we examined the spatio-temporal variability of atmospheric  $\text{NH}_3$  over Asia (South and East Asia) and focus on two hotspots regions of ammonia, the Indo-Gangetic Plain (IGP) and the North China Plain (NCP). The approach for this study is a combination of simulations using

chemical transport modelling, satellite observations and *in-situ* ammonia measurements over South Asia (69 stations) and East Asia (32 stations). The analysis applies the Model for Ozone and Related chemical tracers (MOZART-4) driven by priori ammonia emissions based on Hemispheric Transport of Air Pollution version-2 (HTAP-v2) emission inventory. It applies HTAP-v2 data for emissions to produce estimated total columns of NH<sub>3</sub> and aerosol species for the year 2010 over Asia. Model simulations were evaluated and compared with NH<sub>3</sub> data from IASI (over South and East Asia) and selected ground-based observations (noted above). In addition to the regional comparison, we examine why certain emission hotspot regions in East Asia show lower NH<sub>3</sub> total columns compared with similar hotspot regions in South Asia, when analyzed with both model and satellite observations.

## 2. Data and methodology

### 2.1 MOZART-4 model

The global chemical transport model MOZART-4 has been employed in this study to conduct a year-long (2010) simulation of **atmospheric trace gases and aerosols** over Asia using the updated HTAP-v2 emission inventory (Janssens-Maenhout et al., 2015). These simulations were earlier performed to meet the objectives of Task Force on Hemispheric Transport of Air Pollution, phase 2, multi-model experiments (Surendran et al., 2015; Surendran et al., 2016). The model domain covers entire globe at a horizontal grid resolution of 1.9° × 2.5° and 56 vertical levels from the surface upto 1hectopascal (hPa). The model has approximately 10 levels in the boundary layer (below 850 hPa). MOZART-4 takes into account surface emissions, convection, advection, boundary layer transport, photochemistry, and wet and dry deposition. The model simulations were driven by the input meteorological data set of 1.9° × 2.5° resolution from Modern Era Retrospective-analysis for Research (MERRA) and Applications of the Goddard Earth Observing System Data Assimilation System (GEOS-DAS). Model simulations were performed for the complete year of 2010 (1 January 2010 to 31 December 2010) and its outputs were saved every 6h (4 time steps each day) with a spin up time of six months (1 July 2009 to 31 December 2009). MOZART-4 includes 157 gas-phase reactions, 85 gas-phase species, 39 photolysis and 12 bulk aerosol compounds (Emmons et al., 2010). Dry deposition of gases and aerosols were calculated online according to the parameterization of Wesely (1989) and wet deposition of soluble gases were calculated as described by the method of Emmons et al. (2010). **Land use cover (LUC) maps used in MOZART-4 are based on the Advanced Very High Resolution Radiometer (AVHRR) and Moderate Resolution Imaging Spectroradiometer (MODIS) data based on NCAR Community Land Model (CLM)** (Oleson et al., 2010). MOZART-4 represents the land surface as a hierarchy of sub-grid types: glacier, lake, wetland, urban and vegetated land. The vegetated land is further divided into a mosaic of Plant Function Type (PFTs). These same maps are used for the dry deposition calculations (Emmons et al., 2010; Oleson et al.,

2010; Lawrence and Chase, 2007). In MOZART-4 the tropospheric aerosol component is built on the extended work of Tie et al. (2001 and 2005). Online fast Tropospheric Ultraviolet Visible (FTUV) scheme, based on the TUV model (Tie et al., 2003) is used for the calculation of photolysis rates in MOZART-4. For long-lived species like  $\text{CH}_4$  and  $\text{H}_2$ , surface boundary conditions are constrained by observations from NOAA/ESRL/GMD (Dlugokencky et al., 2005, 2008; Novelli et al., 1999) and as per Intergovernmental Panel  $\text{N}_2\text{O}$  concentrations are set to the value as described in Intergovernmental Panel on Climate Change 2000 report (IPCC, 2000). Biogenic emissions of isoprene and monoterpenes are calculated online using the Model of Emissions of Gases and Aerosols from Nature (MEGAN) (Guenther et al., 2006), using the implementation described by Pfister et al. (2008). Surface moisture flux and all relevant physical parameters are used to calculate water vapor ( $\text{H}_2\text{O}$ ) online. Biomass burning emissions of a wide range of gaseous components, including  $\text{NH}_3$ ,  $\text{SO}_2$  and individual volatile organic compounds were provided from the Global Fire Emission Database (GFED-v3), determined by scaling the GFED  $\text{CO}_2$  emissions by the emission factors provided on  $1.9^\circ \times 2.5^\circ$  grid resolution (Emmons et al., 2010).

In MOZART-4 the ammonium nitrate distribution is determined from  $\text{NH}_3$  emissions and the parameterization of gas/aerosol partitioning using equilibrium simplified aerosol model (EQSAM) by Metzger et al. (2002), which is a set of approximations to the equilibrium constant calculation (Seinfeld et al., 1998), based on the level of sulphate present. In Metzger et al. (2002) cations other than  $\text{NH}_4^+$ , e.g., sodium ( $\text{Na}^+$ ), potassium ( $\text{K}^+$ ), calcium ( $\text{Ca}^{2+}$ ), and magnesium ( $\text{Mg}^{2+}$ ) as well as organic acids have been neglected for the gas-aerosol partitioning calculations. Metzger et al. (2006) found that the  $\text{NH}_3/\text{NH}_4^+$  (calculated by account for ammonium-sulfate-nitrate-sodium-chloride-water system (updated-EQSAM2 parameterization considering organic acids) was 15 % lower than that calculated from the parameterization similar to EQSAM. Ammonia has stronger affinity towards neutralization of sulphuric acid ( $\text{H}_2\text{SO}_4$ ) than nitric acid ( $\text{HNO}_3$ ) whereas formation of ammonium chloride ( $\text{NH}_4\text{Cl(s)}$  or  $\text{(aq)}$ ) in atmosphere is unstable and can dissociate reversibly to  $\text{NH}_3$  and  $\text{HCl}$ . These aerosols in both dry and aqueous phase evaporate faster than the corresponding ammonium nitrate ( $\text{NH}_4\text{NO}_3$ ) aerosols (Seinfeld and Pandis, 2012). In current modelling setup  $\text{NH}_3/\text{NH}_4^+$  partitioning is mainly controlled by sulfate and subsequently by nitrate. Recent study (Acharja et al., 2020) based on analysis of water soluble inorganic chemical ions of  $\text{PM}_1$ ,  $\text{PM}_{2.5}$  and atmospheric trace gases over IGP revealed that  $\text{NH}_4^+$  was one of the dominant ions, collectively with  $\text{Cl}^-$ ,  $\text{NO}_3^-$  and  $\text{SO}_4^{2-}$  constituted more than 95 % of the measured ionic mass in both  $\text{PM}_1$  and  $\text{PM}_{2.5}$ . Remaining ionic species (i.e.,  $\text{Na}^+$ ,  $\text{K}^+$ ,  $\text{Ca}^{2+}$  and  $\text{Mg}^{2+}$ ) formed constituted only about 3 % of the total measured ions. Although major mineral cations (i.e.,  $\text{Na}^+$ ,  $\text{K}^+$ ,  $\text{Ca}^{2+}$  and  $\text{Mg}^{2+}$ ) contribute actively in neutralization reaction, but their concentration in IGP was found to be very low. Also over NCP, mineral cations contributed less than 5 % in both  $\text{PM}_1$  and  $\text{PM}_{2.5}$  (Dao et al., 2014). Furthermore, recent study by Xu et al. (2017) over East Asia revealed that  $\text{NH}_4^+$  was the predominant neutralizing cation with the

highest neutralization factor (NF) (above 1), whereas  $\text{Na}^+$ ,  $\text{K}^+$ ,  $\text{Ca}^{2+}$  and  $\text{Mg}^{2+}$  contributed relatively low (below 0.2). Therefore, consideration of mineral cations and organic acids on the  $\text{NH}_3/\text{NH}_4^+$  partitioning might be limited and will not have significant impact on the results of this study.

## 2.2 Emission inventory (HTAP-v2)

The HTAP-v2 bottom-up database is used in this study as an input for anthropogenic emissions of  $\text{NH}_3$  for the year 2010 (Janssens-Maenhout et al., 2015). HTAP-v2 dataset is embedded with the activity data as per harmonized emission factors, international standards, and gridded emissions with global proxy data. It includes important point sources providing high spatial resolution and emission grid maps with global coverage. This dataset consists of monthly mean  $\text{NH}_3$  emission maps with  $0.1^\circ \times 0.1^\circ$  grid resolution for the year 2010. The HTAP-v2 dataset is compiled using various regional gridded emission inventories by Environmental Protection Agency (EPA) for USA and Environment Canada for Canada, European Monitoring Evaluation Programme (EMEP) and Netherlands Organisation for Applied Scientific Research for Europe, and Model Inter comparison Study in Asia (MICS Asia) for China, India and other Asian countries. The emissions Database for Global Atmospheric Research (EDGAR v4.3) is used for the rest of the world (mainly South-America, Africa, Russia and Oceania). The ‘MICS Asia’ dataset incorporated into the HTAP-v2 dataset includes an anthropogenic emission inventory developed in 2010 (Li et al., 2015), which incorporates several local emission inventories, including the Multi-resolution Emission Inventory for China (MEIC),  $\text{NH}_3$  emission inventory from Peking University (Huang et al., 2012) and Regional Emission inventory in Asia version 2.1 (REAS2.1) (Kurokawa et al., 2013) for areas where local emission data are not available. A detailed description on HTAP-v2 datasets can be found in Janssens-Maenhout et al. (2015).

For this study, we used emissions from five important sectors, such as, agricultural, residential (heating/cooling of buildings and equipment/lighting of buildings and waste treatment), energy (power industry), transport (ground transport) and industries (manufacturing, mining, metal, cement, chemical, solvent industry) for the year 2010. The aircraft and international shipping is not considered for  $\text{NH}_3$  emissions in the HTAP-v2 bottom-up database. These emissions also includes natural emissions such as soil from the Community Earth System Model (CESM), and biomass burning from the Global Fire Emission Database (GFED-v3) (Randerson et al., 2013). All these emissions are regridded to  $1.9^\circ \times 2.5^\circ$  to match the model resolution.

The spatial distribution of the total  $\text{NH}_3$  emissions over Asian region is shown in Fig. 1. It shows the highest emissions over both South and East Asia, especially over the IGP and NCP region (shown with black box in Fig. 1). Agricultural sector is the main contributor to  $\text{NH}_3$  emission, including management of manure and agricultural soils (application of nitrogen fertilizers, including animal

waste). It also includes emissions from livestock, crop cultivation excluding emissions from agricultural waste burning and savannah burning (Janssens-Maenhout et al., 2015). Minor contributions from the residential sector are also observed for the Asian countries due to use of **biomass combustion** and coal burning which is also included in the emissions. Spatial proxies such as population density, road networks, and land use information have been used to allocate area of emission sources. For the REAS2 emission inventory over India, the agricultural sector follows spatial proxy of total population (Li et al., 2017). The use of this approach is expected to be the main source of spatial uncertainty in the estimated  $\text{NH}_3$  emissions to the extent that total human population is only approximately correlated with spatial distribution of fertilizer use and livestock numbers. Seasonal variation of average  $\text{NH}_3$  emission over the IGP and NCP region for Anthropogenic (HTAP-v2), biomass burning (GFED-v3) and Soil emission (CESM) is shown in Fig. 2. Anthropogenic  $\text{NH}_3$  emissions do not show any strong seasonal variability over the IGP region however over the NCP region,  $\text{NH}_3$  emissions show strong seasonality with peak emissions between May-September months. It can be seen that the magnitude of peak emissions is two times more over the NCP region than IGP region. On the other hand, seasonality in biomass burning  $\text{NH}_3$  emissions is strong over the IGP region, which shows highest emissions in the spring season (MAM). Also, contribution of  $\text{NH}_3$  emissions from the IGP region is significantly higher compared to NCP region during peak burning season, but the magnitude of biomass burning emission is six times lower compared to the magnitude of anthropogenic emissions.

### 2.3 Satellite $\text{NH}_3$ observations

The  $\text{NH}_3$  total columns data used in study are derived from the IASI space-borne remote sensing instrument on board Metop-A, which was launched in 2006 in a polar sun-synchronous orbit. The IASI operates in the thermal infrared spectral range ( $645\text{--}2760\text{ cm}^{-1}$ ) with mean local solar overpass time of 9:30 am and 9:30 pm (Clerbaux et al., 2009). It covers the globe twice a day with and each observation is composed of 4 pixels with a circular footprint of 12 Kilometer (km) diameter at nadir and elliptical at the end of the swath ( $20 \times 39\text{ km}$ ). IASI is a suitable tool for evaluation of regional and global models due to its relatively high spatial and temporal sampling and retrieval algorithms have been continuously improved (Whitburn et al., 2016). The  $\text{NH}_3$  total column retrievals show reasonable agreement with monthly averaged integrated ground-based measurements with FTIR column data (Van Damme et al., 2015a). IASI measurements are also found to be consistent with other  $\text{NH}_3$  satellite products (Clarisso et al., 2010; Someya et al., 2020; Viatte et al., 2020). In present study, we have used ANNI- $\text{NH}_3$ -v2.2R-I dataset for the year 2010 which relies on ERA-Interim ECMWF meteorological input data, along with surface temperature retrieved from a dedicated network (Van Damme et al., 2017). An improved retrieval scheme for IASI spectra relies on the calculation of a dimensionless “Hyperspectral Range Index,” which is successively converted to the

total column and allow a better identification of weak point sources of atmospheric NH<sub>3</sub> (Van Damme et al., 2017; Whitburn et al., 2016). More details about IASI satellite and NH<sub>3</sub> data product is given in Clerbaux et al. (2009), Van Damme et al. (2017) and Whitburn et al. (2016). We have considered the daily NH<sub>3</sub> cloud-free satellite total column data and compared with the modelled daily NH<sub>3</sub> total column averaging paired observations across the months, seasons and year. We have used only morning overpasses at 9:30 am measurements, as the relative errors due to the lower thermal contrast are larger for the night-time measurements (9:30 pm overpass). For consistency with satellite retrievals, first the model output (11:30 LT) at each day close to satellite overpass time (9:30 LT) is interpolated in space to the location of valid satellite retrievals. Since IASI retrieval algorithm only provides total columns, in second step, we made unweighted average distribution of the daily paired data to obtain a monthly, seasonal and annual mean value of satellite and model total NH<sub>3</sub> columns at each horizontal resolution of the model (1.9° × 2.5°).

#### 2.4 Ground based observations

To evaluate model performance in South Asia, we used hourly NH<sub>3</sub> measurements from the air quality monitoring station (AQMS) network operated by Central Pollution Control Board (CPCB) across India. CPCB follows a national program for sampling of ambient air quality as well as weather parameters measurements. An automatic analyzer (continuous) method is adopted at each monitoring location. NH<sub>3</sub> is measured by the chemiluminescence method as NO<sub>x</sub> following oxidation of NH<sub>3</sub> to NO<sub>x</sub>. In this approach, NH<sub>3</sub> is determined from the difference between NO<sub>x</sub> concentration with and without inclusion of NH<sub>3</sub> oxidation (CPCB, 2011). The quality assurance and control process followed for these air quality monitoring instruments is given in CPCB (2014, 2020). Surface observations of NH<sub>3</sub> are taken from 69 different stations in South Asia. Most of the NH<sub>3</sub> monitoring stations from India used in the current study are situated in the cities representing the urban environment. Sampling of ambient NH<sub>3</sub> is done through a sampling inlet of 1 meter (m) above the roof top of container AQMS having height of 2.5 m (Technical specifications, 2019). The details of these monitoring locations are given in Table S1 (in the Supplement) and the geographical locations are shown in Fig. 3. Out of these stations thirty five locations in Delhi, six in Bangalore city, four in Hyderabad, and two in Jaipur city are averaged to get single value for the same geographical location and the remaining 22 locations are considered independently representing 26 respective cities. Hourly NH<sub>3</sub> concentrations (in  $\mu\text{g m}^{-3}$ ) used in the study are for the duration of 2016 to 2019. The quality control and assurance method, followed by Central Pollution Control Board (CPCB) for these air quality monitoring stations, is given in the CPCB (2011 and 2020). The calibration procedures for NH<sub>3</sub> analyzer conforms to United States Environmental Protection Agency (USEPA) methodologies and include daily calibration checks, biweekly precision checks and linearity checks every six weeks. All analyzers undergo full calibration every six weeks. For detail on calibration procedure refer to

Technical Specifications for Continuous Real Time Ambient Air Quality Monitoring Analysers (2016) and CPCB (2020). Furthermore, we take the following steps to reassure the quality of  $\text{NH}_3$  observations from the CPCB network stations. For data quality, we rejected all the observations values below the lowest detection limit of the instrument ( $1 \mu\text{g m}^{-3}$ ) (Technical specifications for CAAQM station, 2019) because most of the sites are situated in the urban environment. For cities where more than one monitoring station is available, we rejected all the observations above  $250 \mu\text{g m}^{-3}$  at a given site if other sites in the network do not show values outside this range. This step aims to eliminate any short-term local influence that cannot be captured in the models and retain the regional-scale variability. Second, we removed single peaks characterized by a change of more than  $100 \mu\text{g m}^{-3}$  in just one hour for all the data in CPCB monitoring stations. This step filters random fluctuations in the observations. Third, we removed some very high  $\text{NH}_3$  values that appeared in the timeseries right after the missing values. For any given day, we removed the sites from the consideration that either experience instrument malfunction, or appear to be very heavily influenced by strong local sources. In order to verify the data quality of CBCB monitoring site, we have inter compared the  $\text{NH}_3$  measurement at CPCB monitoring station (R.K. Puram) in Delhi with the  $\text{NH}_3$  measurements at Indira Gandhi International (IGI) Airport taken during Winter Fog Experiment (WiFEX) (Ghude et al., 2017) using Measurement of Aerosols and Gases (MARGA) instrument during winter season of 2017-2018. More details on the  $\text{NH}_3$  measurements using MARGA is available with Acharja et al. (2020). Both sites were situated in the same area of Delhi (less than 1km). Our inter-comparison show that  $\text{NH}_3$  measured at CPCB monitoring station by chemiluminescence method are slightly (on an average  $9.8 \mu\text{g m}^{-3}$ ) on higher side than  $\text{NH}_3$  measured by ion chromatography (IC) using MARGA (Fig. S1 in the Supplement). The differences that were observed could partly be related to the different  $\text{NH}_3$  measurement techniques and partly to the locations of the two monitoring sites which were not place exactly at same location. Apparently, the difference of  $9.8 \mu\text{g m}^{-3}$  indicates that the  $\text{NH}_3$  measurements from the CPCB do not suffer from the calibration issue. However, rigorous validation is required in the future with more data sets. Given the presence of relatively high  $\text{NO}_x$  concentrations, especially at urban locations, it is recognized that the measurement of  $\text{NH}_3$  by difference (i.e., between  $\text{NO}_x$  and  $\text{NO}_x$  plus oxidized  $\text{NH}_3$ ), is a potentially significant source of uncertainty. Future measurement inter-comparisons are planned (rescheduled from 2020 to 2021 because of COVID-19) to allow the chemiluminescence method as used in the Indian network to be compared with a range of other  $\text{NH}_3$  measurement methods (A. Moring et. al, 2020; The Global Challenges Research Fund (GCRF) South Asia Nitrogen hub).

To further evaluate model performance over East Asia, we used monthly mean  $\text{NH}_3$  measurements from the 32 stations of the Nationwide Nitrogen Deposition Monitoring Network (NNDMN) of China, operated by China Agricultural University. The details of these monitoring locations are given in Table S2 (in the Supplement) and the geographical locations are shown in Fig. 3. Monthly mean

$\text{NH}_3$  concentrations (in  $\mu\text{g m}^{-3}$ ) used in the study are for the duration of 2010 to 2015. Ambient concentrations of gaseous  $\text{NH}_3$  were measured using an active Denuder for Long-Term Atmospheric sampling (DELTa) system. More detail about the data product is given by Xu et al. (2019). To compare the model with observation, simulated  $\text{NH}_3$  from the model are compared with the surface-based observations by using bi-linear interpolation of model output to the geographical location and elevation of the observational sites.

### 3. Results and Discussion

#### 3.1 Annual mean $\text{NH}_3$ total columns over South Asia

Yearly-averaged 2010 distribution of  $\text{NH}_3$  total columns over Asia simulated by MOZART-4 model and also retrieved with IASI instrument are shown in Fig. 4a and 4b. The total  $\text{NH}_3$  columns simulated by the model show high Tropospheric Vertical Column Densities (TVCDs) of about  $0.5\text{--}7 \times 10^{16}$  molecules  $\text{cm}^{-2}$  over IGP region of India compared to any other regions of Asia. This may reflect the larger range of  $\text{NH}_3$  column values for the South Asian model domain, with both more polluted and cleaner conditions. These high TVCDs values coincide with the high fertilizer-N and livestock numbers, as scaled according to human population density in Fig. 1.

Spatial differences between model simulated data and satellite data for  $\text{NH}_3$  total column distribution are shown in Fig. 4c. On a quantitative level, the MOZART-4 model is found to overestimates the  $\text{NH}_3$  total column compared with IASI by  $1\text{--}4 \times 10^{16}$  molecules  $\text{cm}^{-2}$  over South Asia, especially over northeast India and Bangladesh. Conversely, the MOZART-4 model underestimates  $\text{NH}_3$  in comparison with IASI over the arid region of north western India (state of Rajasthan adjacent to Pakistan) and centering on Pakistan. There are several possible reasons for the spatial differences shown in Fig. 4c, including: a) uncertainties in the mapped  $\text{NH}_3$  emissions data (e.g., between Afghanistan, Bangladesh, India and Pakistan, due to different relationships between human population and livestock/fertilizer activities); b) uncertainties related to turbulent mixing and dispersion (this may affect both the simulations in MOZART-4 and the assumed vertical profiles for the IASI retrievals); and c) uncertainties related to precipitation scavenging of ammonia and ammonium, noting that the eastern part of the IGP is substantially wetter than the western part.

According to Fig. 1, the magnitude of  $\text{NH}_3$  emissions over NCP is similar to IGP. By contrast, much smaller TVCDs of the  $\text{NH}_3$  columns are estimated by MOZART-4 and IASI over NCP compared with IGP. The MOZART-4 and IASI estimates are found to be in close agreement, with slightly smaller values estimated by MOZART-4. The possible reasons for the difference in  $\text{NH}_3$  concentrations in IGP and NCP are discussed in Sect. 3.4. The relationship between modelled and IASI retrieved  $\text{NH}_3$  total columns are further analysed in terms of scatter plots in Fig. 5a and 5b, over IGP region of South

Asia (20°N-32°N, 70°E-95°E) and NCP region of East Asia (30°N-40°N, 110°E-120°E) (rectangular areas shown in Fig. 1). Correlation coefficients (r) between model and satellite observed annual mean total columns over IGP and NCP are found to be 0.81 and 0.90 respectively for 2010. This indicates that spatial variability in simulated NH<sub>3</sub> by the model and satellite observation is in closer agreement, both over IGP and NCP region. The Model simulated **annual mean total NH<sub>3</sub> columns** gives larger values over IGP region (Normalised Mean Bias (NMB) = 38 %) as well as over entire South Asia (NMB = 44 %). Whereas over the NCP region (NMB = -35 %) and entire East Asia (NMB = -32 %), the model gives values which are smaller than IASI. Other statistical indicators are summarised in Table 1. Larger estimates of NH<sub>3</sub> columns from an atmospheric Chemistry Transport Model (CTM) compared with IASI was also found in an earlier study for South Asia (Clarisse et al., 2009).

The overall higher value of the model simulated NH<sub>3</sub> over South Asia compared with IASI could be due to the combination of the uncertainties in both approaches. This includes uncertainties in emissions from the HTAP-v2 datasets used for the model simulations, inaccurate modelling of the chemistry in MOZART-4, errors in dry and wet deposition schemes used in the model, and biases inherent to infrared satellite remote sensing. For IASI, firstly, only cloud-free satellite scenes are processed, which could result in missing partly some of the NH<sub>3</sub> values during cloudy periods and biomass burning events. Secondly, NH<sub>3</sub> vertical columns retrieved from the IASI observations are actually sampled around 9:30 local time **while the MOZART-4 simulated model output close to overpass time (11:30 LTC) was used**. Finally, the retrieval of NH<sub>3</sub> from infrared satellites is sensitive to inaccuracies in the temperature profile, and biases in the IASI L2 temperature profiles can result in biases in the retrieved NH<sub>3</sub> (Whitburn et al., 2016). The HTAP-v2 dataset use proxy values for agricultural activities (i.e., distributed by human population) instead of actual values for field fertilizer application and livestock excretion over the South Asia. This could also result in additional uncertainty of NH<sub>3</sub> emissions from the agricultural activities. Further work is on-going to integrate NH<sub>3</sub> emissions inventories for different countries in South Asia based on national datasets, which should allow the emissions related uncertainties to be reduced in future. Similarly, slight underestimation over East Asia might originates from the country specific emission inventory used for China (Huang et al., 2012) in MOSAIC HTAP-v2 emission inventory and the limitations discussed above. **The application of any equilibrium models (EQMs) in global atmospheric studies is associated with considerable uncertainties. In MOZART-4 chemistry, the ammonium nitrate distribution is determined from NH<sub>3</sub> emissions and the parameterization of gas/aerosol partitioning by Metzger et al. (2002), based on the level of sulphate present. The emission fluxes of SO<sub>2</sub> and NO<sub>x</sub> in HTAP-v2 data set also has large uncertainties over the IGP (Jena et al., 2015b; Wang et al., 2020), which can introduce additional uncertainty in NH<sub>3</sub>/NH<sub>4</sub><sup>+</sup> gas/aerosol partitioning.** In MOZART-4 chemistry, uncertainty can be also associated in dry and wet deposition scheme which can result in overestimation (Emmons et al., 2010).

### 3.2 Seasonal variability of $\text{NH}_3$ total columns

Figure 6 shows the model (left) and IASI satellite (middle) seasonal distributions of  $\text{NH}_3$  total columns over Asia. These seasons are represented as 3-month periods: Winter, December-January-February (DJF, first row), Spring, March-April-May (MAM, second row), Summer, June-July-August (JJA, third row), and Autumn, September-October-November (SON, fourth row). It can be seen in Fig. 6, that there is larger seasonal variation in IASI  $\text{NH}_3$  total columns while MOZART-4 presents limited seasonality as in South Asia compare to better seasonal variation estimated in East Asia, as shown by both IASI and the MOZART-4 model. In general, during autumn, spring, summer and winter seasons MOZART-4 shows higher  $\text{NH}_3$  total column compared with IASI estimates over most of South Asia. However, this difference is more pronounced during autumn (SON) and winter (DJF) seasons (Fig. 6; Right). We have seen that (Fig. 2) anthropogenic emission of  $\text{NH}_3$  is nearly same in all months and biomass burning has peak during MAM over South Asia in the MOZART-4 model. Whereas, seasonality is better represented in  $\text{NH}_3$  emission for East Asia.

Major drivers in anthropogenic  $\text{NH}_3$  seasonal variation include differences in management and timing of fertilizer, which is not well represented in the emission over South Asia (Janssens-Maenhout et al., 2012). This can be expected to have the direct effect on  $\text{NH}_3$  total column over South Asia. It is recognized that  $\text{NH}_3$  emission can be strongly affected by both short term meteorological variation and longer term climatic differences (Sutton et al., 2013). This means that  $\text{NH}_3$  emissions may be expected to increase in warm summer conditions than in winter (Battye and Barrows, 2004). However, magnitude of these emissions is expected to be smaller in comparison with anthropogenic emissions and may not contribute significantly to larger summer time  $\text{NH}_3$  columns observed from IASI retrievals over South Asia and East Asia than MOZART-4. Additional driver in  $\text{NH}_3$  seasonal variation include meteorological variation. For example, strong subsidence, lower temperature and lighter winds over South Asia in the autumn and winter months prevent venting of low altitude pollution to the higher altitudes. This means that emitted air pollutants tend to accumulate close to the source region in winter time conditions (Ghude et al., 2010, 2011). Considering the comparison of IGP with NCP, accumulation of pollutants in the boundary layer is more pronounced over IGP region due to flat land topography, and it is more during winter than the autumn months (Surendran et al., 2016). We saw that simulated mean Planetary boundary layer height (PBLH) is lower (approximately 400 m, Fig. S2 in the Supplement), and winds are lighter in winter months, compared to summer months, over South Asia, and particularly over IGP region (Surendran et al., 2016). Figure 7 (left) and 7 (right) shows the time-height distribution of  $\text{NH}_3$  and mean PBLH averaged over the IGP region, respectively. It can be seen that during winter months higher atmospheric stability prevents mixing of boundary layer  $\text{NH}_3$  to the free troposphere over IGP (Fig. 7 (left)), which is reflected in the higher wintertime values of MOZART-4  $\text{NH}_3$  columns. Similarly, higher  $\text{NH}_3/\text{NH}_4$  ratio (Fig. S3 in the Supplement) and lower dry and wet deposition (Fig. S4 and S5 in the Supplement) of  $\text{NH}_3$  over IGP

in winter month enhances the accumulation of  $\text{NH}_3$  in the boundary layer compared to summer months. On the other hand, very less  $\text{NH}_3$  gets detected by the satellite at the higher altitudes where detection sensitivity of the satellite is more than that at the surface (Clarisson et al., 2010). Limited sensitivity of IASI measurements to detect boundary layer  $\text{NH}_3$  (Van Damme et al., 2014a) could be one of the reasons for large differences ( $1-4 \times 10^{16}$  molecules  $\text{cm}^{-2}$ ) between MOZART-4 and IASI in winter seasons. Also, sowing of wheat crop over IGP involves higher rate of fertilizer application during peak winter month (Sharma et al., 2014) that release significant quantity of  $\text{NH}_3$  into the atmosphere. However, this seasonality is largely missing in the emissions (Fig. 2 (top, left)) indicating that higher MOZART-4  $\text{NH}_3$  is largely driven by the winter-time meteorology over this region.

It is interesting to note from Fig. 6 (right) that during spring the difference between modelled and observed column  $\text{NH}_3$  is smaller over the IGP region compared with the winter season. Heating of the landmass due to large solar incidence suppresses the wintertime subsidence over the IGP and leads to deeper boundary layer during spring and early summer. It can be seen that (Fig. 7 (right) and Fig. S2 in the Supplement) the average PBLH is about 1100 m and 600 m deeper during spring and summer compared to winter over IGP. During this season, significant transport of the boundary pollution in the mid and upper troposphere due to enhanced convective activities and large scale vertical motion can be noticed in Fig. 7 (left) and is consistent with the earlier studies over this region (Lal et al., 2014; Surendran et al., 2016). Vertical motion associated with the convective activities is expected to redistribute the  $\text{NH}_3$  concentration in the column, which leads to more  $\text{NH}_3$  at the higher altitudes where detection sensitivity of the satellite is more than that at the surface (Clarisson et al., 2010). As a result, more  $\text{NH}_3$  gets detected by the satellite and we see less difference between observations and model over the IGP. This may also partly explain the higher IASI estimates of  $\text{NH}_3$  column for summertime prior to the monsoon season. However, this hypothesis needs to be tested with higher sensitivity experiments as a part of future work. During spring season, MOZART-4 reflects widespread  $\text{NH}_3$  total column from the entire Indian land mass and IASI observations does capture increase in  $\text{NH}_3$  total column at least for seasonal mean cycle (Fig. 8a). This seasonal maximum in  $\text{NH}_3$  total column identified both in IASI and MOZART-4 over South Asia can be explained by the two factors: Meteorology factor and biomass burning emissions. Volatilization of  $\text{NH}_3$  enhances with increase in temperature (Sutton et al., 2013), hence higher temperature during this drier periods over IGP partly enhances  $\text{NH}_3$  emission to the environment which is also evident from the soil  $\text{NH}_3$  emissions in Fig. 2 (bottom). However, magnitude of these emissions is expected to be smaller in comparison with anthropogenic emissions. In the Indian region, emissions from the biomass burning (crop-residue burning) peaks in March to May (Jena et al., 2015a) and emission of  $\text{NH}_3$  from biomass burning is maximum during this period (Fig. 2 (middle)). However, MOZART-4 estimates smaller  $\text{NH}_3$  total columns compared with IASI over Myanmar, Laos and Thailand during the period March-May (Fig. 6 (right)). This period is estimated to be associated with large scale forest fires (and open

crop burning) (Chan, 2017; Wu et al., 2018; Zheng et al., 2017), the effect of which appears to be underestimated in the MOZART-4 simulations. It suggests that the Global Fire Emissions Database (GFED-v3) used in this study is low over this region agreeing with Zhang et al. (2020) and Huang et al. (2013). During the monsoon season (JJA) (Fig. 6 (right)) and summer, IASI- $\text{NH}_3$  total columns are larger than the MOZART-4 estimates over north-western arid region of South Asia, where monsoon rainfall is lowest (less than 30 cm). On the other hand,  $\text{NH}_3$  columns estimated by IASI are lower in the North-western IGP than the MOZART-4 simulations.

Figure 8 shows the comparison between IASI and modelled monthly time series of  $\text{NH}_3$  total columns over IGP ( $20^{\circ}\text{N}$ - $32^{\circ}\text{N}$ ,  $70^{\circ}\text{E}$ - $95^{\circ}\text{E}$ ) and NCP ( $30^{\circ}\text{N}$ - $40^{\circ}\text{N}$ ,  $110^{\circ}\text{E}$ - $120^{\circ}\text{E}$ ), respectively (rectangular areas shown on Fig. 1). We found a better consistency between modelled and measured seasonal  $\text{NH}_3$  total column over NCP than IGP. Monthly  $\text{NH}_3$  columns over the IGP show bimodal distribution in the model. However, IASI does not show such bimodal variation. Seasonal statistics show large normalised mean bias (38 %) and poor correlation ( $r=0.41$ ) between model and IASI. The bimodal distribution in  $\text{NH}_3$  total columns is partly driven by the biomass burning emissions, which show major peak in spring and another small peak in autumn (Fig. 2 (middle)), and partly by the meteorology as discussed in the previous section. During monsoon months (JJA), when South Asia receives significant rainfall all over, model simulations present lower  $\text{NH}_3$  total column, which is not seen in the IASI observations and also in the surface observations (Fig. 8a and 9b) over IGP. The reason for this discrepancy may be related with the flat  $\text{NH}_3$  emission over South Asia (Fig. 2). Usually large amount of fertilization application is expected during the warm month of June and July in the IGP which is not represented in the HTAP-v2 emissions and therefore lower values in the model during monsoon month is mostly driven by the model meteorology. Lower values observed during monsoon season in general are attributed to increase wet scavenging of  $\text{NH}_3$  due to monsoon rain (Fig. S5 (left) in the Supplement) and influx of cleaner marine air from the Bay of Bengal and Arabian Sea through south-easterly and south-westerly wind (Ghude et al., 2008). On the other hand, monthly variation in IASI  $\text{NH}_3$  total columns over East Asia is found to be captured well by the model (Fig. 8b) and seems to follow the variation observed in the anthropogenic  $\text{NH}_3$  emission (Fig. 2), except for the month of July where IASI estimates substantially higher  $\text{NH}_3$  total columns than the model. The reason for this peak in the IASI data for July may be related to urea fertilizer application in warm July conditions (see temporal course of Enhanced Vegetation Index (Li et al., 2014)), which seems to be not represented well in the HTAP-v2 emissions. The overall statistics show slight good correlation ( $r=0.61$ ) between observed and simulated  $\text{NH}_3$  columns and negative normalised mean bias (NMB = -41 %).

### 3.3 Comparison between surface NH<sub>3</sub> measurements and simulated NH<sub>3</sub> concentrations in South and East Asia

To evaluate modelled surface NH<sub>3</sub> concentrations in South Asia, we have used NH<sub>3</sub> surface measurements from 69 monitoring locations over India for the years from 2016 to 2019. As 2010 data was not available, we make the hypothesis that measurement from 2016-2019 can be considered as representative from what have been measured in 2010. Out of these stations thirty five locations in Delhi, six in Bangalore city, four in Hyderabad, and two in Jaipur city are averaged to get single value for the same geographical location and the remaining 22 locations are considered independently representing 26 respective cities. Due to the lack of ground-based measurements performed in 2010, the following comparison will mainly be qualitative, although it is estimated that the main spatial features of Indian agriculture and NH<sub>3</sub> emissions will be consistent between 2010 and 2016-2019. As per the RCP 8.5 (Kumar et al., 2018) NH<sub>3</sub> emission from South Asia is expected to increase by less than 20 % from 2010 to 2020. Assuming a linear relationship between emission and surface concentration, it is expected that NH<sub>3</sub> concentrations could be higher by about 10-15 % in 2016 to 2019.

It is interesting to note that the correlation between annual and monthly mean MOZART-4 simulated and measured NH<sub>3</sub> concentration ( $r=0.82$  and  $r=0.62$ ) is better than the comparison between MOZART-4 and IASI for South Asia (Fig. 9). However, the MOZART-4 has systematically smaller estimated NH<sub>3</sub> concentrations compared with the ground based measurement network (NMB = -47 %). It should be noted that most of the monitoring stations are situated in urban regions(cities) of India and therefore represents the urban environment, which may have locally higher NH<sub>3</sub> concentrations due to traffic and human activities (Sharma et al., 2014). Since the MOZART-4 model is run relatively at coarse ( $1.9^\circ \times 2.5^\circ$ ) grid resolution the emissions may not capture the true variability in emissions at city scale. These surface NH<sub>3</sub> sites are influenced by local emissions that are therefore not resolved by the MOZART-4 model. Therefore, when comparing coarse-scale models to observations, the model may have difficulties in resolving local scales effects (Surendran et al., 2015). Until the planned further evaluation of the chemiluminescence monitoring method for ammonia (measured by difference with NO<sub>x</sub>) is evaluated (as noted in Sect. 2.4), it is not possible to be certain the extent to which possible uncertainties in the measurement method contribute to the differences shown in Fig. 9b. While noting these uncertainties, it is worth noting that the ground based NH<sub>3</sub> observation network confirms the occurrence of higher ground-level NH<sub>3</sub> concentrations in autumn and winter, as simulated using MOZART-4 using the HTAP-v2 emissions inventory (Fig. 9b).

Comparison of Fig. 8a and 9b shows that the time course of ground level NH<sub>3</sub> concentrations (as estimated by MOZART-4) is significantly different to the time course of total NH<sub>3</sub> column (as also

estimated by MOZART-4). Whereas the total column is largest in the summer (reflective of deeper atmospheric mixing and recirculation), and the ground level concentrations are largest during winter. Although it is not easy to use the IASI data to infer ground level  $\text{NH}_3$  concentrations, the stronger summer maximum of IASI (Fig. 8a) compared with MOZART-4, suggests that IASI would be in less close agreement with the ground based measurement network than MOZART-4 (Fig. 9b). While recognizing uncertainties in this interpretation, the key point is that large  $\text{NH}_3$  columns estimated by IASI for May-July are not reflected in the ground-based  $\text{NH}_3$  measurements from the Indian monitoring network.

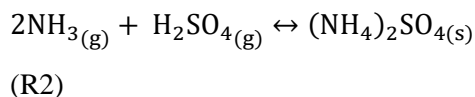
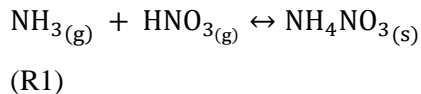
Figure 10 shows the comparison between monthly mean (from 2010 to 2015 observations)  $\text{NH}_3$  surface measurements from 32 monitoring locations over China and modelled surface  $\text{NH}_3$  concentrations from the same location over East. Similar to South Asia the MOZART-4 has systematically smaller estimated  $\text{NH}_3$  concentrations compared with the ground based measurement network (NMB = -44 %) over East Asia. Figure 10b shows maximum  $\text{NH}_3$  concentration occurred in summer (JJA) denotes agreement with IASI measurements. Other statistical indicators are summarised in Table 2. Furthermore, high  $\text{NH}_3$  concentration from ground based measurements during JJA is consistent with the higher HTAP-v2 emissions (Fig. 2) (Huang et al., 2012) and higher  $\text{NH}_4\text{NO}_3$  concentration (Fig. S6 in the Supplement). Higher concentration of  $\text{NH}_4\text{NO}_3$  and can also lead to higher  $\text{NH}_3$  concentrations especially during summer due to its semi-volatile and unstable character at higher temperatures, as it is observed in East Asia. This implies that the  $\text{NH}_3$  emissions may play a vital role in determining the seasonal pattern of the ground  $\text{NH}_3$  concentrations. Summer peak may originate from fertilizer application, livestock emissions and volatilization of  $\text{NH}_3$  which is enhanced in higher temperature (Liu et al., 2017a).

### 3.4 Why were $\text{NH}_3$ total columns low over high $\text{NH}_3$ emission over East Asia compared to high $\text{NH}_3$ emission region of South Asia?

Fine-scale details of the  $\text{NH}_3$  emissions over Asia in Fig. 1 and 2 clearly revealed larger emission values in areas where there is intensive agricultural management. This is the case especially in the NCP and IGP (Fig. 1, shown with box). Earlier emission estimates suggest that fertilizer application and livestock contribute 2.6 Tg per year ( $\text{yr}^{-1}$ ) and 1.7 Tg  $\text{yr}^{-1}$   $\text{NH}_3$  emissions respectively from South Asia (Aneja et al., 2011). Over South Asia, urea accounts for emissions of 2.5 Tg  $\text{yr}^{-1}$  which contributes to 95 % of the fertilizer emission, and 58 % of total estimated agricultural emissions (Fertilizer Association of India annual report 2018-19). For East Asia, livestock manure management accounts for approximately 54 % (5.3 Tg  $\text{yr}^{-1}$ ) of the total emissions and fertilizer application accounts for 33 % (3.2 Tg  $\text{yr}^{-1}$ ) emissions, with 13 % of emissions from other sources. Combined the model areas for NCP and IGP (as shown in Fig. 1) accounts for ~45 % of the  $\text{NH}_3$  emitted from fertilization in East Asia and South Asia (Huang et al., 2012).

We find that satellite observations show larger  $\text{NH}_3$  columns over IGP than over similar higher emission regions of NCP. However, in addition, we also find that the MOZART-4 model is able to capture this contrasting columnar  $\text{NH}_3$  levels between IGP and NCP. This indicates that the difference between IGP and NCP is unrelated to differences between the mosaic of emissions over South Asia and East Asia in HTAP-v2 and similarly not related to uncertainties in satellite retrievals. Instead, the analysis from MOZART-4 demonstrates that the difference can be explained by differences in atmospheric chemistry between the two regions, linked to higher  $\text{SO}_2$  and  $\text{NO}_x$  emissions in the NCP than in the IGP. **Recent study by Wang et al. (2020), shows that emission fluxes of  $\text{SO}_2$  and  $\text{NO}_x$  over IGP are only one-fourth of that over NCP.**

As ammonia is a highly alkaline gas with an atmospheric lifetime usually of few hours (and rarely a few days) (Dammers et al., 2019), it readily reacts with acid present in the atmosphere to form aerosols, which are eventually deposited to the earth's surface by either dry or wet deposition processes (Fig. S4 and S5 in the Supplement). In the atmosphere, ammonia therefore reacts rapidly with atmospheric sulphuric acid ( $\text{H}_2\text{SO}_4$ ), nitric acids ( $\text{HNO}_3$ ) and hydrochloric acid ( $\text{HCl}$ ) to contribute to ambient levels of fine particles, forming ammonium sulphate, ammonium nitrate and ammonium chloride. Following reaction (R1) and (R2)



In the atmosphere, ammonium ion ( $\text{NH}_4^+$ ) as an aerosol is estimated to have a lifetime of about 1–15 days (Aneja et al., 1998), though this is obviously dependent on the amount of atmospheric acids (Seinfeld and Pandis, 2012). In addition to the large fertilizer application and livestock management activities which are characteristic of both IGP and NCP, industrial and transportation activities are higher over the NCP (China) which also results in higher emission of  $\text{NO}_x$  and  $\text{SO}_2$  over NCP compared with IGP (Zhao et al., 2013). Ammonia has greater affinity towards oxides of sulphur, hence it first reacts to form ammonium sulphate, and then the remaining ammonia further reacts to form ammonium nitrate (Seinfeld et al., 1998). The differences in the secondary aerosol formation over NCP and IGP are compared by considering the MOZART-4 model estimates of volume mixing ratio (VMR) in parts per billion ( $\times 10^9$  ppb) of total sulphate, ammonium, ammonium nitrate at surface and total column of  $\text{NO}_x$  (Fig. 11). Although vertical profiles of the aerosol components are small, there are strong vertical gradients in  $\text{NO}_x$  concentrations, and for this reason we consider the

comparison with the total  $\text{NO}_x$  column more reflective of overall  $\text{NO}_x$  chemistry than the ground level  $\text{NO}_x$  VMR.

Figure 11 shows that total sulphate VMR (Fig. 11a) and  $\text{NO}_x$  total column (Fig. 11c) are significantly higher over NCP region than IGP. Similarly, total ammonium VMR (Fig. 11b) is significantly larger over NCP than IGP indicating how a higher fraction of the gaseous ammonia is transformed to form ammonium over NCP region. In addition, Fig. 11d shows higher estimated levels of ammonium nitrate in MOZART-4 over NCP, reflective of the higher  $\text{NO}_x$  emissions in this region. As a consequence of the different  $\text{SO}_2$  and  $\text{NO}_x$  sources, gaseous  $\text{NH}_3$  is more quickly removed from atmosphere over East Asia with residence time of approximately 6 hours (Fig. S7 in the Supplement) (higher values indicates lower mean residence time), which is reflected in the higher VMR of ammonium, sulphate and ammonium nitrate (Fig. 11a, b and d). It can be seen that  $\text{NH}_3/\text{NH}_4^+$  ratio denotes lower values 0-1 (Fig. S3 in the Supplement) over East Asia than South Asia suggesting  $\text{NH}_4^+$  partitioning is more over East Asia. As a result the  $\text{NH}_3$  total columns over NCP are much smaller than over IGP, even though magnitude of  $\text{NH}_3$  emission fluxes is greater over NCP than IGP.

#### 4. Conclusion

In this work, we have compared  $\text{NH}_3$  total columns simulated by the MOZART-4 model with IASI  $\text{NH}_3$  satellite observations over South and East Asia. The annual mean distribution reveals a consistent spatial pattern between MOZART-4 and IASI, but MOZART-4 tends to show larger  $\text{NH}_3$  columns over South Asia than IASI, particularly over the Indo-Gangetic Plain (IGP), whereas it is in close agreement over East Asia (including the North China Plain, NCP), with the exception of a July peak seen in the IASI dataset, which may be related to specific timing of fertilizer-related  $\text{NH}_3$  emissions. Comparison for seasonally and monthly resolved IASI total column with the MOZART-4 simulations shows inconsistencies in spatial and temporal pattern over South Asia. This inconsistency is due to the uncertainties in emission estimate which doesn't include seasonality pattern in HTAP-v2 over South Asia, as well as uncertainties in the processing of the IASI data. Both the MOZART-4 results and IASI estimates involve assumptions that could considerably affect the comparison between total columns of  $\text{NH}_3$ .

Comparison with estimates from a ground based  $\text{NH}_3$  monitoring network for both South and East Asia, our results showed that MOZART-4 systematically gives smaller  $\text{NH}_3$  concentration estimates than the monitoring network. The  $\text{NH}_3$  measurement sites used in present study mostly represent urban locations and model may not be able to capture actual concentration at point location due to coarser grid resolution over India. In addition, further assessment is needed to demonstrate the reliability of the  $\text{NH}_3$  measurement technique used in the monitoring network, where  $\text{NH}_3$  is measured

by difference with  $\text{NO}_x$  concentrations, which may be uncertain in urban areas with high  $\text{NO}_x$  concentrations.

Despite the high  $\text{NH}_3$  emission over both South and East Asia, a larger  $\text{NH}_3$  total column is observed over South Asia in both the IASI and MOZART-4 estimates. This difference is explained by the MOZART-4 simulation, which treat the full atmospheric chemistry interaction with  $\text{SO}_2$  and  $\text{NO}_x$  emissions, leading to aerosol formation. The MOZART-4 model showed higher sulphate volume mixing ratio and  $\text{NO}_x$  total column over East Asia, especially in the NCP, which is reflected in ammonium aerosol volume mixing ratio (VMR) over East Asia. This suggests that the formation of ammonium aerosols (dominated by ammonium, sulphate and ammonium nitrate) is quicker over East Asia than in South Asia, leading to lower  $\text{NH}_3$  total columns in East Asia.

To examine the present findings future studies should investigate the effect of changing emissions of  $\text{NO}_x$  and  $\text{SO}_2$  on  $\text{NH}_3$  columns, for example by using perturbation of these emissions through counterfactual modeling scenarios. The comparison between model simulations using MOZART-4, satellite derived estimates from IASI and ground-based monitoring of  $\text{NH}_3$  concentrations has highlighted the known uncertainties in emissions, satellite retrievals and measurements at point locations. In order to reduce the uncertainties in ammonia emission, it would be a key to create an  $\text{NH}_3$  emission inventory specifically over South Asia, which is now currently under development as part of the GCRF South Asian Nitrogen Hub. This includes work to improve the bottom-up  $\text{NH}_3$  emission inventory, taking into account primary agricultural statistics on fertilizer use and animal number distributions. There is also potential for top-down (inverse modelling) for  $\text{NH}_3$  and  $\text{NO}_x$  by taking inference from the model, satellite and ground-based evidence. Here it is essential to recognize the need for more ground-based observational sites to measure  $\text{NH}_3$  air concentrations in rural areas where agriculture activity is predominant. Such measurements at present are currently very few for South Asia. Coarser global models fail to resolve the local-scale emissions, hence higher resolution regional models with advance chemistry are also needed to resolve the sources and chemical processes on urban and rural scales.

## **Data availability**

The  $0.1^\circ \times 0.1^\circ$  emission grid maps can be downloaded from the EDGAR website on [https://edgar.jrc.ec.europa.eu/htap\\_v2/index.php?SECURE=\\_123](https://edgar.jrc.ec.europa.eu/htap_v2/index.php?SECURE=_123) per year per sector. The model data can be downloaded upon request from the AeroCom database (<http://www.htap.org/>, last accessed June 22, 2020) (TF HTAP, 2018). The model data is available at Prithvi (IITM) super-computer and can be provided upon request to corresponding author. The morning overpass  $\text{NH}_3$  total columns measured through IASI can be accessed from data center at <http://cds-espri.ipsl.upmc.fr/etherTypo/index.php?id=1700&L=1>. For India, ground based hourly  $\text{NH}_3$  measurements can be obtained from CPCB website on <https://app.cpcbccr.com/CCR>. For China,

ground based monthly mean NH3 datasets can be downloaded from [https://figshare.com/articles/Data\\_Descriptor\\_Xu\\_et\\_al\\_20181211\\_Scientific\\_data\\_docx/7451357](https://figshare.com/articles/Data_Descriptor_Xu_et_al_20181211_Scientific_data_docx/7451357). Author contributions

### **Author contributions**

All authors contributed to the research; SDG designed the research; PVP conducted the research; PVP and SDG wrote the paper; CJ and DS performed the MOZART model simulations; AM and MAS formulated the research; MVD, LC and PFC performed the IASI experiments; SK, DML, XL, WU, JJ, and TKA contributed to writing.

### **Competing interests**

The authors declare that they have no conflict of interest.

### **Acknowledgments**

We wish to thank the National Centre for Atmospheric Research (NCAR), funded by the U.S. National Science Foundation and operated by the University Corporation for Atmospheric Research, for access to the MOZART-4. All model runs were carried out on a Prithvi IBM High Performance Computing system at the Indian Institute of Tropical Meteorology (IITM), Pune India. We thank the Director, IITM for providing all the essential facilities required to complete the work. We wish to acknowledge the availability of CPCB data from CPCB webportal (<https://app.cpcbCCR.com/CCR>). Research at ULB has been supported by the Belgian State Federal Office for Scientific, Technical and Cultural Affairs (Prodex arrangement IASI.FLOW). L.C. and M.V.D are respectively research associate and postdoctoral researcher with the Belgian F.R.S-FNRS. Cooperation between IITM and CEH has been facilitated through the NEWS India-UK Virtual Joint Centre, supported at CEH by the Biotechnological and Biological Sciences Research Council, and the Natural Environment Research Council of UK Research and Innovation (UKRI), and through the UKRI Global Challenges Research Fund (GCRF) South Asian Nitrogen Hub. The Nationwide Nitrogen Deposition Monitoring Network (NNDMN) of China was supported by the Chinese National Natural Science Foundation (41425007) and the Chinese National Research Program for Key Issues in Air Pollution Control (DQGG0208).

### **Financial support**

This research has been supported by “Urban modeling C-DAC” sponsored project.

## References

A. Moring et. al: Nitrogen challenges and opportunities for agricultural and environmental science in India, *Frontiers* (Boulder)., doi:10.3389/fsufs.2021.505347, 2020.

Acharja, P., Ali, K., Trivedi, D. K., Safai, P. D., Ghude, S., Prabhakaran, T. and Rajeevan, M.: Characterization of atmospheric trace gases and water soluble inorganic chemical ions of  $PM_1$  and  $PM_{2.5}$  at Indira Gandhi International Airport, New Delhi during 2017–18 winter, *Sci. Total Environ.*, 729, 138800, doi:10.1016/j.scitotenv.2020.138800, 2020.

Alexandratos, N. and Bruinsma, J.: World Agriculture Towards 2030 / 2050 The 2012 Revision. Global Perspective Studies Team, FAO Agricultural Development Economics Division. ESA Working Paper No. 12-03, (12), 2012.

Aneja, V. P., Murray, G. C. and Southerland, J.: Atmospheric nitrogen compounds: Emissions, transport, transformation, deposition, and assessment, *EM Air Waste Manag. Assoc. Mag. Environ. Manag.*, 22–25, 1998.

Aneja, V. P., Battye, W., Behera, S. N., Erisman, J. W., Schlesinger, W. H. and Sharma, M.: Reactive nitrogen emissions from crop and livestock farming in India, *Atmos. Environ.*, 47, 92–103, doi:10.1016/j.atmosenv.2011.11.026, 2011.

Battye, W. and B. R.: Review of Ammonia Emission Modeling Techniques for Natural Landscapes and Fertilized Soils, *Work Assign. No. 2-09*, 27517(68), 2004.

Behera, S. N., Sharma, M., Aneja, V. P. and Balasubramanian, R.: Ammonia in the atmosphere: a review on emission sources, atmospheric chemistry and deposition on terrestrial bodies, *Environ. Sci. Pollut. Res.*, 20(11), 8092–8131, doi:10.1007/s11356-013-2051-9, 2013.

Chan, K. L.: Biomass burning sources and their contributions to the local air quality in Hong Kong, *Sci. Total Environ.*, 596–597, 212–221, doi:10.1016/j.scitotenv.2017.04.091, 2017.

Clarisso, L., Clerbaux, C., Dentener, F., Hurtmans, D. and Coheur, P. F.: Global ammonia distribution derived from infrared satellite observations, *Nat. Geosci.*, 2(7), 479–483, doi:10.1038/ngeo551, 2009.

Clarisso, L., Shephard, M. W., Dentener, F., Hurtmans, D., Cady-Pereira, K., Karagulian, F., Van Damme, M., Clerbaux, C. and Coheur, P. F.: Satellite monitoring of ammonia: A case study of the San Joaquin Valley, *J. Geophys. Res. Atmos.*, 115(13), 1–15, doi:10.1029/2009JD013291, 2010.

Clarisso, L., Van Damme, M., Clerbaux, C. and Coheur, P. F.: Tracking down global  $NH_3$  point sources with wind-adjusted superresolution, *Atmos. Meas. Tech.*, 12(10), 5457–5473,

doi:10.5194/amt-12-5457-2019, 2019.

Clerbaux, C., Boynard, A., Clarisse, L., George, M., Hadji-Lazaro, J., Herbin, H., Hurtmans, D., Pommier, M., Razavi, A., Turquety, S., Wespes, C. and Coheur, P. F.: Monitoring of atmospheric composition using the thermal infrared IASI/MetOp sounder, *Atmos. Chem. Phys.*, 9(16), 6041–6054, doi:10.5194/acp-9-6041-2009, 2009.

CPCB: Guidelines for Real Time Sampling and Analyses., 2011.

CPCB: Annual Report 2014-15., 2014.

CPCB: Central Pollution Control Board (2020), [online] Available from: <https://cpcb.nic.in/quality-assurance-quality-control/>.

Crippa, M., Guizzardi, D., Muntean, M., Schaaf, E., Dentener, F., Van Aardenne, J. A., Monni, S., Doering, U., Olivier, J. G. J., Pagliari, V. and Janssens-Maenhout, G.: Gridded emissions of air pollutants for the period 1970–2012 within EDGAR v4.3.2, *Earth Syst. Sci. Data*, 10(4), 1987–2013, doi:10.5194/essd-10-1987-2018, 2018.

Van Damme, M., Whitburn, S., Clarisse, L., Clerbaux, C., Hurtmans, D. and Coheur, P.-F.: Version 2 of the IASI NH<sub>3</sub> neural network retrieval algorithm; near-real time and reanalysed datasets, *Atmos. Meas. Tech. Discuss.*, 1–14, doi:10.5194/amt-2017-239, 2017.

Van Damme, M., Clarisse, L., Whitburn, S., Hadji-Lazaro, J., Hurtmans, D., Clerbaux, C. and Coheur, P. F.: Industrial and agricultural ammonia point sources exposed, *Nature*, 564(7734), 99–103, doi:10.1038/s41586-018-0747-1, 2018.

Van Damme, Wichink Kruit, R. J., Schaap, M., Clarisse, L., Clerbaux, C., Coheur, P. F., Dammers, E., Dolman, A. J. and Erisman, J. W.: Evaluating 4 years of atmospheric ammonia (NH<sub>3</sub>) over Europe using IASI satellite observations and LOTOS-EUROS model results, *J. Geophys. Res.*, 119(15), 9549–9566, doi:10.1002/2014JD021911, 2014a.

Van Damme, M., Hurtmans, D., Coheur, P. F., Clerbaux, C., Dolman, A. J., Erisman, J. W., Clarisse, L., Ngadi, Y. and Heald, C. L.: Global distributions, time series and error characterization of atmospheric ammonia (NH<sub>3</sub>) from IASI satellite observations, *Atmos. Chem. Phys.*, 14(6), 2905–2922, doi:10.5194/acp-14-2905-2014, 2014b.

Van Damme, Dammers, E., Flechard, C. R., Coheur, P. F., Xu, W., Erisman, J. W., Galy-Lacaux, C., Neuman, J. A., Clerbaux, C., Van Damme, M., Tang, Y. S., Liu, X., Sutton, M. A., Nowak, J. B. and Clarisse, L.: Towards validation of ammonia (NH<sub>3</sub>) measurements from the IASI satellite, *Atmos.*

Meas. Tech., 8(3), 1575–1591, doi:10.5194/amt-8-1575-2015, 2015a.

Van Damme, Erisman, J. W., Clarisse, L., Dammers, E., Whitburn, S., Clerbaux, C., Dolman, A. J. and Coheur, P.: Worldwide spatiotemporal atmospheric ammonia (NH<sub>3</sub>), Geophys. Res. Lett., 1–9, doi:10.1002/2015GL065496, 2015b.

Dammers, E., McLinden, C. A., Griffin, D., Shephard, M. W., Van Der Graaf, S., Lutsch, E., Schaap, M., Gainairu-Matz, Y., Fioletov, V., Van Damme, M., Whitburn, S., Clarisse, L., Cady-Pereira, K., Clerbaux, C., Francois Coheur, P. and Erisman, J. W.: NH<sub>3</sub> emissions from large point sources derived from CrIS and IASI satellite observations, Atmos. Chem. Phys., 19(19), 12261–12293, doi:10.5194/acp-19-12261-2019, 2019.

Dao, X., Wang, Z., Lv, Y., Teng, E., Zhang, L. and Wang, C.: Chemical characteristics of water-soluble ions in particulate matter in three metropolitan areas in the North China Plain, PLoS One, 9(12), 1–16, doi:10.1371/journal.pone.0113831, 2014.

Datta, A., Sharma, S. K., Harit, R. C., Kumar, V., Mandal, T. K. and Pathak, H.: Ammonia emission from subtropical crop land area in india, Asia-Pacific J. Atmos. Sci., 48(3), 275–281, doi:10.1007/s13143-012-0027-1, 2012.

Slugokenky, E. J., Myers, R. C., Lang, P. M., Masarie, K. A., Crotwell, A. M., Thoning, K. W., Hall, B. D., Elkins, J. W. and Steele, L. P.: Conversion of NOAA atmospheric dry air CH<sub>4</sub> mole fractions to a gravimetrically prepared standard scale, J. Geophys. Res. D Atmos., 110(18), 1–8, doi:10.1029/2005JD006035, 2005.

Emmons, L. K., Walters, S., Hess, P. G., Lamarque, J. F., Pfister, G. G., Fillmore, D., Granier, C., Guenther, A., Kinnison, D., Laepple, T., Orlando, J., Tie, X., Tyndall, G., Wiedinmyer, C., Baughcum, S. L. and Kloster, S.: Description and evaluation of the Model for Ozone and Related chemical Tracers, version 4 (MOZART-4), Geosci. Model Dev., 3(1), 43–67, doi:10.5194/gmd-3-43-2010, 2010.

Fertilizer Association of India annual report 2018-19: Fertilizer Association of India annual report 2018-19., 2018.

Ghude, S. D., Fadnavis, S., Beig, G., Polade, S. D. and van der A, R. J.: Detection of surface emission hot spots, trends, and seasonal cycle from satellite-retrieved NO<sub>2</sub> over India, J. Geophys. Res., 113(D20), D20305, doi:10.1029/2007JD009615, 2008.

Ghude, S. D., Lal, D. M., Beig, G., van der A, R. and Sable, D.: Rain-Induced Soil NO<sub>x</sub> Emission From India During the Onset of the Summer Monsoon: A Satellite Perspective, J. Geophys. Res.,

115(D16), D16304, doi:10.1029/2009JD013367, 2010.

Ghude, S. D., Beig, G., Kulkarni, P. S., Kanawade, V. P., Fadnavis, S., Remedios, J. J. and Kulkarni, S. H.: Regional co pollution over the Indian-subcontinent and various transport pathways as observed by mopitt, *Int. J. Remote Sens.*, 32(21), 6133–6148, doi:10.1080/01431161.2010.507796, 2011.

Ghude, S. D., Kulkarni, S. H., Jena, C., Pfister, G. G., Beig, G., Fadnavis, S. and Van Der, R. J.: Application of satellite observations for identifying regions of dominant sources of nitrogen oxides over the indian subcontinent, *J. Geophys. Res. Atmos.*, 118(2), 1075–1089, doi:10.1029/2012JD017811, 2013.

Ghude, S. D., Chate, D. M., Jena, C., Beig, G., Kumar, R., Barth, M. C., Pfister, G. G., Fadnavis, S. and Pithani, P.: Premature mortality in India due to PM<sub>2.5</sub> and ozone exposure, *Geophys. Res. Lett.*, 43(9), 4650–4658, doi:10.1002/2016GL068949, 2016.

Ghude, S. D., Bhat, G. S., Prabhakaran, T., Jenamani, R. K., Chate, D. M., Safai, P. D., Karipot, A. K., Konwar, M., Pithani, P., Sinha, V., Rao, P. S. P., Dixit, S. A., Tiwari, S., Todekar, K., Varpe, S., Srivastava, A. K., Bisht, D. S., Murugavel, P., Ali, K., Mina, U., Dharua, M., Rao, Y. J., Padmakumari, B., Hazra, A., Nigam, N., Shende, U., Lal, D. M., Chandra, B. P., Mishra, A. K., Kumar, A., Hakkim, H., Pawar, H., Acharja, P., Kulkarni, R., Subbarthi, C., Balaji, B., Varghese, M., Bera, S. and Rajeevan, M.: Winter fog experiment over the Indo-Gangetic plains of India, *Curr. Sci.*, 112(4), doi:10.18520/cs/v112/i04/767-784, 2017.

Guenther, A., Karl, T., Harley, P., Wiedinmyer, C., Palmer, P. I. and Geron, C.: Estimates of global terrestrial isoprene emissions using MEGAN (Model of Emissions of Gases and Aerosols from Nature), *Atmos. Chem. Phys.*, 6(11), 3181–3210, doi:10.5194/acp-6-3181-2006, 2006.

Han, X., Zhu, L., Liu, M., Song, Y. and Zhang, M.: Numerical analysis of the impact of agricultural emissions on PM<sub>2.5</sub> in China using a high-resolution ammonia emissions inventory, *Atmos. Chem. Phys.*, (March), 1–31, doi:10.5194/acp-2019-1128, 2020.

Huang, K., Fu, J. S., Hsu, N. C., Gao, Y., Dong, X., Tsay, S. C. and Lam, Y. F.: Impact assessment of biomass burning on air quality in Southeast and East Asia during BASE-ASIA, *Atmos. Environ.*, 78(2012), 291–302, doi:10.1016/j.atmosenv.2012.03.048, 2013.

Huang, X., Song, Y., Li, M., Li, J., Huo, Q., Cai, X., Zhu, T., Hu, M. and Zhang, H.: A high-resolution ammonia emission inventory in China, *Global Biogeochem. Cycles*, 26(1), 1–14, doi:10.1029/2011GB004161, 2012.

Janssens-Maenhout G., Dentener F., Van Aardenne J., Monni S., Pagliari V., Orlandini L., Klimont

Z., Kurokawa J., Akimoto H., Ohara T., Wankmueller R., Battye B., Grano D., Zuber A., K. T. .: EDGAR-HTAP: a Harmonized Gridded Air Pollution Emission Dataset Based on National Inventories, Ispra (Italy): European Commission Publications Office, , (February), 1–18, doi:ISBN 978-92-79-23122-0, ISSN 1831-9424, 2012.

Janssens-Maenhout, G., Dentener, F. J., Aardenne, J. Van, Monni, S., Pagliari, V., Orlandini, L., Klimont, Z., Kurokawa, J., Akimoto, H., Ohara, T., Wankmüller, R., Battye, B., Grano, D., Zuber, A. and Keating, T.: EDGAR-HTAP: a harmonized gridded air pollution emission dataset based on national inventories., 2012.

Janssens-Maenhout, G., Koffi, B., Crippa, M., Pouliot, G., Zhang, Q., Wankmüller, R., Frost, G., Dentener, F., Li, M., Guizzardi, D., Denier van der Gon, H., Darras, S., Kuenen, J. J. P., Keating, T., Klimont, Z., Kurokawa, J. and Muntean, M.: HTAP\_v2.2: a mosaic of regional and global emission grid maps for 2008 and 2010 to study hemispheric transport of air pollution, *Atmos. Chem. Phys.*, 15(19), 11411–11432, doi:10.5194/acp-15-11411-2015, 2015.

Jena, C., Ghude, S. D., Pfister, G. G., Chate, D. M., Kumar, R., Beig, G., Surendran, D. E., Fadnavis, S. and Lal, D. M.: Influence of springtime biomass burning in South Asia on regional ozone ( $O_3$ ): A model based case study, *Atmos. Environ.*, 100, 37–47, doi:10.1016/j.atmosenv.2014.10.027, 2015a.

Jena, C., Ghude, S. D., Beig, G., Chate, D. M., Kumar, R., Pfister, G. G., Lal, D. M., Surendran, D. E., Fadnavis, S. and van der A, R. J.: Inter-comparison of different NOx emission inventories and associated variation in simulated surface ozone in Indian region, *Atmos. Environ.*, 117, 61–73, doi:10.1016/j.atmosenv.2015.06.057, 2015b.

Kumar, R., Barth, M. C., Pfister, G. G., Delle Monache, L., Lamarque, J. F., Archer-Nicholls, S., Tilmes, S., Ghude, S. D., Wiedinmyer, C., Naja, M. and Walters, S.: How Will Air Quality Change in South Asia by 2050?, *J. Geophys. Res. Atmos.*, 123(3), 1840–1864, doi:10.1002/2017JD027357, 2018.

Kurokawa, J., Ohara, T., Morikawa, T., Hanayama, S., Janssens-Maenhout, G., Fukui, T., Kawashima, K. and Akimoto, H.: Emissions of air pollutants and greenhouse gases over Asian regions during 2000-2008: Regional Emission inventory in ASia (REAS) version 2, *Atmos. Chem. Phys.*, 13(21), 11019–11058, doi:10.5194/acp-13-11019-2013, 2013.

Kuttippurath, J., Singh, A., Dash, S. P., Mallick, N., Clerbaux, C., Van Damme, M., Clarisse, L., Coheur, P. F., Raj, S., Abhishek, K. and Varikoden, H.: Record high levels of atmospheric ammonia over India: Spatial and temporal analyses, *Sci. Total Environ.*, 740, 139986, doi:10.1016/j.scitotenv.2020.139986, 2020.

Lal, D. M., Ghude, S. D., Singh, J. and Tiwari, S.: Relationship between Size of Cloud Ice and Lightning in the Tropics, , doi:10.1155/2014/471864, 2014.

Lawrence, P. J. and Chase, T. N.: Representing a new MODIS consistent land surface in the Community Land Model (CLM 3.0), J. Geophys. Res. Biogeosciences, 112(1), doi:10.1029/2006JG000168, 2007.

Li, L., Friedl, M. A., Xin, Q., Gray, J., Pan, Y. and Frolking, S.: Mapping Crop Cycles in China Using MODIS-EVI Time Series, , (September), doi:10.3390/rs6032473, 2014.

Li, M., Zhang, Q., Kurokawa, J., Woo, J., He, K. B., Lu, Z. and Ohara, T.: MIX : a mosaic Asian anthropogenic emission inventory for the MICS-Asia and the HTAP projects, , 34813–34869, doi:10.5194/acpd-15-34813-2015, 2015.

Li, M., Zhang, Q., Kurokawa, J. I., Woo, J. H., He, K., Lu, Z., Ohara, T., Song, Y., Streets, D. G., Carmichael, G. R., Cheng, Y., Hong, C., Huo, H., Jiang, X., Kang, S., Liu, F., Su, H. and Zheng, B.: MIX: A mosaic Asian anthropogenic emission inventory under the international collaboration framework of the MICS-Asia and HTAP, Atmos. Chem. Phys., 17(2), 935–963, doi:10.5194/acp-17-935-2017, 2017.

Liu, L., Zhang, X., Xu, W., Liu, X., Li, Y., Lu, X., Zhang, Y. and Zhang, W.: Temporal characteristics of atmospheric ammonia and nitrogen dioxide over China based on emission data, satellite observations and atmospheric transport modeling since 1980, Atmos. Chem. Phys., 17(15), 9365–9378, doi:10.5194/acp-17-9365-2017, 2017a.

Liu, X., Xu, W., Duan, L., Du, E., Pan, Y., Lu, X., Zhang, L., Wu, Z., Wang, X., Zhang, Y., Shen, J., Song, L., Feng, Z., Liu, X., Song, W., Tang, A., Zhang, Y., Zhang, X. and Collett, J. L.: Atmospheric Nitrogen Emission, Deposition, and Air Quality Impacts in China: an Overview, Curr. Pollut. Reports, 3(2), 65–77, doi:10.1007/s40726-017-0053-9, 2017b.

Mandal, T. K., Saxena, M., Rohtash, Sharma, S. K., Gupta, N. C., Kumar, M. and Saraswati: Characteristics of ambient ammonia over Delhi, India, Meteorol. Atmos. Phys., 124(1–2), 67–82, doi:10.1007/s00703-013-0299-8, 2013.

Metzger, S., Dentener, F., Pandis, S. and Lelieveld, J.: Gas/aerosol partitioning: 1. A computationally efficient model, J. Geophys. Res. Atmos., 107(16), doi:10.1029/2001JD001102, 2002.

Metzger, S., Mihalopoulos, N. and Lelieveld, J.: Importance of mineral cations and organics in gas-aerosol partitioning of reactive nitrogen compounds: Case study based on MINOS results, Atmos. Chem. Phys., 6(9), 2549–2567, doi:10.5194/acp-6-2549-2006, 2006.

Oleson, K. W., Lawrence, D. M., Bonan, G. B., Flanner, M. G., Kluzek, E., Lawrence, P. J., Zeng, X. (2010).: Technical Description of version 4.0 of the Community Land Model (CLM)., 2010.

Pfister, G. G., Emmons, L. K., Hess, P. G., Lamarque, J. F., Orlando, J. J., Walters, S., Guenther, A., Palmer, P. I. and Lawrence, P. J.: Contribution of isoprene to chemical budgets: A model tracer study with the NCAR CTM MOZART-4, *J. Geophys. Res. Atmos.*, 113(5), doi:10.1029/2007JD008948, 2008.

Pinder, R. W., Adams, P. J. and Pandis, S. N.: Ammonia Emission Controls as a Cost-Effective Strategy for Reducing Atmospheric Particulate Matter in the Eastern United States, *Environ. Sci. Technol.*, 41(2), 380–386, doi:10.1021/es060379a, 2007.

Pinder, R. W., Gilliland, A. B. and Dennis, R. L.: Environmental impact of atmospheric NH<sub>3</sub> emissions under present and future conditions in the eastern United States, *Geophys. Res. Lett.*, 35(12), doi:10.1029/2008GL033732, 2008.

Pollution, C. and Board, C.: Guidelines for Manual Sampling and Analyses., 2011.

Randerson, J., Werf, G. Van Der, Giglio, L., DAAC, G. C.-O. and 2015, Global Fire Emissions Database, Version 4.1 (GFEDv4), daac.ornl.gov.

Saraswati, George, M. P., Sharma, S. K., Mandal, T. K. and Kotnala, R. K.: Simultaneous Measurements of Ambient NH<sub>3</sub> and Its Relationship with Other Trace Gases, PM<sub>2.5</sub> and Meteorological Parameters over Delhi, India, *Mapan - J. Metrol. Soc. India*, 34(1), 55–69, doi:10.1007/s12647-018-0286-0, 2019.

Seinfeld, J. H. and Pandis, S. N.: Atmospheric Chemistry and Physics: From Air Pollution to Climate Change, Wiley., 2012.

Seinfeld, J. H., Pandis, S. N. and Noone, K.: Atmospheric Chemistry and Physics: From Air Pollution to Climate Change, *Phys. Today*, 51(10), 88–90, doi:10.1063/1.882420, 1998.

Sharma, S. K., Saxena, M., Saud, T., Korpole, S. and Mandal, T. K.: Measurement of NH<sub>3</sub>, NO, NO<sub>2</sub> and related particulates at urban sites of indo gangetic plain (IGP) of India, *J. Sci. Ind. Res. (India)*, 71(5), 360–362, 2012.

Sharma, S. K., Harit, R. C., Kumar, V., Mandal, T. K. and Pathak, H.: Ammonia Emission from Rice-Wheat Cropping System in Subtropical Soil of India, *Agric. Res.*, 3(2), 175–180, doi:10.1007/s40003-014-0107-9, 2014a.

Sharma, S. K., Kumar, M., Rohtash, Gupta, N. C., Saraswati, Saxena, M. and Mandal, T. K.:

Characteristics of ambient ammonia over Delhi, India., 2014b.

Someya, Y., Imasu, R., Shiomi, K. and Saitoh, N.: Atmospheric ammonia retrieval from the TANSO-FTS/GOSAT thermal infrared sounder, *Atmos. Meas. Tech.*, 13(1), 309–321, doi:10.5194/amt-13-309-2020, 2020.

Surendran, D., Jena, C., Beig, G., Chate, D. M. and Ghude, S. D.: Quantifying the sectoral contribution of pollution transport from South Asia during summer and winter monsoon seasons in support of HTAP-2 experiment, *Atmos. Environ.*, 145, 60–71, doi:10.1016/j.atmosenv.2016.09.011, 2016.

Surendran, D. E., Ghude, S. D., Beig, G., Emmons, L. K., Jena, C., Kumar, R., Pfister, G. G. and Chate, D. M.: Air quality simulation over South Asia using Hemispheric Transport of Air Pollution version-2 (HTAP-v2) emission inventory and Model for Ozone and Related chemical Tracers (MOZART-4), *Atmos. Environ.*, 122, 357–372, doi:10.1016/j.atmosenv.2015.08.023, 2015.

Sutton, M. A., Reis, S., Riddick, S. N., Dragosits, U., Nemitz, E., Theobald, M. R., Tang, Y. S., Braban, C. F., Vieno, M., Dore, A. J., Mitchell, R. F., Wanless, S., Daunt, F., Fowler, D., Blackall, T. D., Milford, C., Flechard, C. R., Loubet, B., Massad, R., Cellier, P., Personne, E., Coheur, P. F., Clarisse, L., Van Damme, M., Ngadi, Y., Clerbaux, C., Skjøth, C. A., Geels, C., Hertel, O., Kruit, R. J. W., Pinder, R. W., Bash, J. O., Walker, J. T., Simpson, D., Horváth, L., Misselbrook, T. H., Bleeker, A., Dentener, F. and de Vries, W.: Towards a climate-dependent paradigm of ammonia emission and deposition, *Philos. Trans. R. Soc. B Biol. Sci.*, 368(1621), 20130166–20130166, doi:10.1098/rstb.2013.0166, 2013.

Sutton, M. A., J. Drewer, A. Moring, T.K Adhya, A. Ahmed and A. Bhatia: The Indian nitrogen assessment : sources of reactive nitrogen, environmental and climate effects, management options, and policies, in The Indian Nitrogen Assessment, edited by Y. P. Abrol, T. K. Adhya, V. P. Aneja, N. Raghuram, H. Pathak, U. Kulshrestha, C. Sharma, and B. Singh, pp. 9–25, Elsevier., 2017.

Technical specifications for CAAQM station: Technical specifications for continuous ambient air quality monitoring (CAAQM) STATION (real time) Central Pollution Control Board East Arjun Nagar, Shahdara., 2019.

Technical Specifications for Continuous Real Time Ambient Air Quality Monitoring Analysers: Technical Specifications for Continuous Real Time Ambient Air Quality Monitoring Analysers / Station Volume – II., 2016.

The Global Challenges Research Fund (GCRF) South Asia Nitrogen hub: The Global Challenges Research Fund (GCRF) project, [online] Available from:

<https://grtr.ukri.org/projects?ref=NE/S009019/1>.

Tie, X., Brasseur, G., Emmons, L., Horowitz, L. and Kinnison, D.: Effects of aerosols on tropospheric oxidants: A global model study, *J. Geophys. Res. Atmos.*, 106(D19), 22931–22964, doi:10.1029/2001JD900206, 2001.

Tie, X., Madronich, S., Walters, S., Zhang, R., Rasch, P. and Collins, W.: Effect of clouds on photolysis and oxidants in the troposphere, , 108, doi:10.1029/2003JD003659, 2003.

Tie, X., Madronich, S., Walters, S., Edwards, D. P., Ginoux, P., Mahowald, N., Zhang, R. Y., Lou, C. and Brasseur, G.: Assessment of the global impact of aerosols on tropospheric oxidants, *J. Geophys. Res. D Atmos.*, 110(3), 1–32, doi:10.1029/2004JD005359, 2005.

Viatte, C., Wang, T., Van Damme, M., Dammers, E., Meleux, F., Clarisse, L., Shephard, M. W., Whitburn, S., Coheur, P. F., Cady-Pereira, K. E. and Clerbaux, C.: Atmospheric ammonia variability and link with particulate matter formation: a case study over the Paris area, *Atmos. Chem. Phys.*, 20(1), 577–596, doi:10.5194/acp-20-577-2020, 2020.

Wang, T., Song, Y., Xu, Z., Liu, M., Xu, T., Liao, W., Yin, L., Cai, X., Kang, L., Zhang, H. and Zhu, T.: Why is the Indo-Gangetic Plain the region with the largest  $\text{NH}_3$  column in the globe during pre-monsoon and monsoon seasons?, *Atmos. Chem. Phys.*, 20(14), 8727–8736, doi:10.5194/acp-20-8727-2020, 2020.

Wesely, M. L.: Parameterization of surface resistances to gaseous dry deposition in regional-scale numerical models, *Atmos. Environ.*, 23(6), 1293–1304, doi:10.1016/0004-6981(89)90153-4, 1989.

Whitburn, S., Damme, M. Van, Clarisse, L., Bauduin, S., Heald, C. L., Hurtmans, D., Zondlo, M. A., Clerbaux, C. and Coheur, P.: A flexible and robust neural network IASI- $\text{NH}_3$ , , 6581–6599, doi:10.1002/2016JD024828. Received, 2016.

Wu, J., Kong, S., Wu, F., Cheng, Y., Zheng, S., Yan, Q., Zheng, H., Yang, G., Zheng, M., Liu, D., Zhao, D. and Qi, S.: Estimating the open biomass burning emissions in central and eastern China from 2003 to 2015 based on satellite observation, *Atmos. Chem. Phys.*, 18(16), 11623–11646, doi:10.5194/acp-18-11623-2018, 2018.

Xu, J. S., He, J., Behera, S. N., Xu, H. H., Ji, D. S., Wang, C. J., Yu, H., Xiao, H., Jiang, Y. J., Qi, B. and Du, R. G.: Temporal and spatial variation in major ion chemistry and source identification of secondary inorganic aerosols in Northern Zhejiang Province, China, *Chemosphere*, 179(December 2014), 316–330, doi:10.1016/j.chemosphere.2017.03.119, 2017.

Xu, R. T., Pan, S. F., Chen, J., Chen, G. S., Yang, J., Dangal, S. R. S., Shepard, J. P. and Tian, H. Q.: Half-Century Ammonia Emissions From Agricultural Systems in Southern Asia: Magnitude, Spatiotemporal Patterns, and Implications for Human Health, *GeoHealth*, 2(1), 40–53, doi:10.1002/2017gh000098, 2018.

Xu, W., Zhang, L. and Liu, X.: A database of atmospheric nitrogen concentration and deposition from the nationwide monitoring network in China, , (December 2018), 2–7, 2019.

Zhang, X., Liu, J., Han, H., Zhang, Y., Jiang, Z., Wang, H., Meng, L., Li, Y. C. and Liu, Y.: Satellite-Observed Variations and Trends in Carbon Monoxide over Asia and Their Sensitivities to Biomass Burning, *Remote Sens.*, 12(5), 830, doi:10.3390/rs12050830, 2020.

Zhang, Y., Dore, A. J., Ma, L., Liu, X. J., Ma, W. Q., Cape, J. N. and Zhang, F. S.: Agricultural ammonia emissions inventory and spatial distribution in the North China Plain, *Environ. Pollut.*, 158(2), 490–501, doi:10.1016/j.envpol.2009.08.033, 2010.

Zhao, B., Wang, S. X., Liu, H., Xu, J. Y., Fu, K., Klimont, Z., Hao, J. M., He, K. B., Cofala, J. and Amann, M.: NO<sub>x</sub> emissions in China: Historical trends and future perspectives, *Atmos. Chem. Phys.*, 13(19), 9869–9897, doi:10.5194/acp-13-9869-2013, 2013.

Zheng, J., Hu, M., Du, Z., Shang, D., Gong, Z., Qin, Y., Fang, J., Gu, F., Li, M., Peng, J., Li, J., Zhang, Y., Huang, X., He, L., Wu, Y. and Guo, S.: Influence of biomass burning from South Asia at a high-altitude mountain receptor site in China, *Atmos. Chem. Phys.*, 17(11), 6853–6864, doi:10.5194/acp-17-6853-2017, 2017.

Zhou, Y., Zhang, Y., Tian, D. and Mu, Y.: Impact of dicyandiamide on emissions of nitrous oxide, nitric oxide and ammonia from agricultural field in the North China Plain, *J. Environ. Sci. (China)*, 40, 20–27, doi:10.1016/j.jes.2015.08.016, 2016.

Zhu, L., Henze, D. K., Bash, J. O., Cady-Pereira, K. E., Shephard, M. W., Luo, M. and Capps, S. L.: Sources and Impacts of Atmospheric NH<sub>3</sub>: Current Understanding and Frontiers for Modeling, Measurements, and Remote Sensing in North America, *Curr. Pollut. Reports*, 1(2), 95–116, doi:10.1007/s40726-015-0010-4, 2015.

## FIGURE CAPTIONS

**Figure 1.** Spatial distribution of total  $\text{NH}_3$  emissions ( $\times 10^{10} \text{ kg m}^{-2} \text{s}^{-1}$ ) over Asia. Data are shown at  $0.1^\circ \times 0.1^\circ$  grid resolution from Hemispheric Transport of Air Pollution version-2 (HTAP-v2) emission inventory. The solid rectangles indicate the Indo-Gangetic plain, IGP ( $20^\circ\text{N}-32^\circ\text{N}$ ,  $70^\circ\text{E}-95^\circ\text{E}$ ) and the North China Plain, NCP ( $30^\circ\text{N}-40^\circ\text{N}$ ,  $110^\circ\text{E}-120^\circ\text{E}$ ).

**Figure 2.** Monthly variation of anthropogenic (HTAP-v2) (molecules  $\text{cm}^{-2} \text{s}^{-1}$ ) (top), Biomass Burning (GEFED-v3) (molecules  $\text{cm}^{-2} \text{s}^{-1}$ ) (middle) and Soil (CESM) (molecules  $\text{cm}^{-2} \text{s}^{-1}$ ) (bottom)  $\text{NH}_3$  emission averaged from Indo-Gangetic plain ( $20^\circ\text{N}-32^\circ\text{N}$ ,  $70^\circ\text{E}-95^\circ\text{E}$ ) and the North China Plain ( $30^\circ\text{N}-40^\circ\text{N}$ ,  $110^\circ\text{E}-120^\circ\text{E}$ ).

**Figure 3.** Geographical locations of surface  $\text{NH}_3$  observational sites (69 locations) from the air quality automatic monitoring network operated by the Central Pollution Control Board (CPCB, 2020), India and observational sites (32 locations) from Nationwide Nitrogen Deposition Monitoring Network (NNDMN) operated by China Agricultural University, China.

**Figure 4.** Spatial distributions annual mean  $\text{NH}_3$  ( $\times 10^{16} \text{ molecules cm}^{-2}$ ) total columns over Asia for the year 2010. (a) Simulated by MOZART-4, (b) from the IASI satellite observations and (c) spatial

difference between MOZART-4 and IASI.

**Figure 5.** (a) Scatter plot between annual averaged IASI and MOZART-4 simulated  $\text{NH}_3$  ( $\times 10^{16} \text{ molecules cm}^{-2}$ ) total columns over IGP, South Asia (rectangle:  $20^\circ\text{N}-32^\circ\text{N}$ ,  $70^\circ\text{E}-95^\circ\text{E}$ ) and (b) Scatter plot between annual averaged IASI and MOZART-4 simulated  $\text{NH}_3$  ( $\times 10^{16} \text{ molecules cm}^{-2}$ ) total columns over NCP, East Asia (rectangle:  $30^\circ\text{N}-40^\circ\text{N}$ ,  $110^\circ\text{E}-120^\circ\text{E}$ ).

**Figure 6.** Seasonal  $\text{NH}_3$  total columns distribution ( $\times 10^{16} \text{ molecules cm}^{-2}$ ) in 2010 (left) simulated by MOZART-4, (middle) measured by IASI satellite and (right) spatial differences between MOZART-4 and IASI during (top to bottom) winter (DJF) spring (MAM) summer (JJA) and autumn (SON) seasons.

**Figure 7.** Daily vertical distribution of distribution of  $\text{NH}_3$  (ppb) averaged over IGP South Asia ( $20^{\circ}\text{N}$ - $32^{\circ}\text{N}$ ,  $70^{\circ}\text{E}$ - $95^{\circ}\text{E}$ ) (left) and daily mean Planetary Boundary Layer height (PBLH in meters) averaged over IGP South Asia ( $20^{\circ}\text{N}$ - $32^{\circ}\text{N}$ ,  $70^{\circ}\text{E}$ - $95^{\circ}\text{E}$ ) (right).

**Figure 8.** (a) Comparison between monthly averaged IASI and MOZART-4 simulated  $\text{NH}_3$  ( $\times 10^{16}$  molecules  $\text{cm}^{-2}$ ) total columns over IGP South Asia ( $20^{\circ}\text{N}$ - $32^{\circ}\text{N}$ ,  $70^{\circ}\text{E}$ - $95^{\circ}\text{E}$ ), (b) Comparison of monthly averaged IASI and MOZART-4 simulated  $\text{NH}_3$  ( $\times 10^{16}$  molecules  $\text{cm}^{-2}$ ) total columns over NCP East Asia ( $30^{\circ}\text{N}$ - $40^{\circ}\text{N}$ ,  $110^{\circ}\text{E}$ - $120^{\circ}\text{E}$ ) (bar indicates standard error of 88 and 35 pixels in IGP and NCP respectively).

**Figure 9.** (a) Scatter plot between annual averaged surface observations from 69 monitoring sites (Fig. 2) over South Asia and MOZART-4 simulated surface  $\text{NH}_3$  ( $\mu\text{g m}^{-3}$ ) (992 hPa) interpolated at the locations of 69 sites (b) Comparison between monthly mean surface observations from 69 monitoring sites and MOZART-4 simulated monthly mean  $\text{NH}_3$  ( $\mu\text{g m}^{-3}$ ) concentration interpolated at the locations of 69 sites over South Asia.

**Figure 10.** (a) Scatter plot between annual averaged surface observations from 32 monitoring sites (Fig. 2) over East Asia and MOZART-4 simulated surface  $\text{NH}_3$  ( $\mu\text{g m}^{-3}$ ) (992 hPa) interpolated at the locations of 32 sites (b) Comparison between monthly mean surface observations from 32 monitoring sites and MOZART-4 simulated monthly mean  $\text{NH}_3$  ( $\mu\text{g m}^{-3}$ ) concentration interpolated at the locations of 32 sites over East Asia.

**Figure 11.** MOZART-4 simulated spatial distribution of annual averaged (a) total sulphate aerosol ( $\times 10^9$  ppb), (b) total Ammonium aerosol ( $\times 10^9$  ppb), (c)  $\text{NO}_x$  total columns ( $\times 10^{16}$  molecules  $\text{cm}^{-2}$ ) and (d) total ammonium nitrate aerosol ( $\times 10^9$  ppb) over Asia.

**TABLES**

**Table 1** Model performance statistics for NH<sub>3</sub> total columns over Asia from IASI and MOZART-4 simulations for the year 2010

Statistics indicator	IGP, South Asia	NCP, East Asia
Mean (Model-IASI )	0.68	-0.24
( $\times 10^{16}$ molecules cm $^{-2}$ )		
Normalized Mean Bias (NMB)	0.38	-0.35
Variance ( $\times 10^{16}$ molecules cm $^{-2}$ )	1.39	-0.83
Root Mean Square Error (RMSE) ( $\times 10^{16}$ molecules cm $^{-2}$ )	0.125	0.05
Correlation Coefficient (r)	0.81	0.90

**Table 2 Model performance statistics for NH<sub>3</sub> concentration over East and South Asia from MOZART-4 simulations and observational network for the year 2010**

<b>Statistics indicator</b>	<b>IGP, South Asia</b>	<b>NCP, East Asia</b>
Mean (Model-Observations) ( $\mu\text{g m}^{-3}$ )	-13.47	3.1
Normalized Mean Bias (NMB)	0.44	-0.46
Variance ( $\mu\text{g m}^{-3}$ )	-0.629	-0.88
Root Mean Square Error (RMSE) ( $\mu\text{g m}^{-3}$ )	1.91	0.728
Correlation Coefficient (r)	0.82	0.65

**Figure 1**

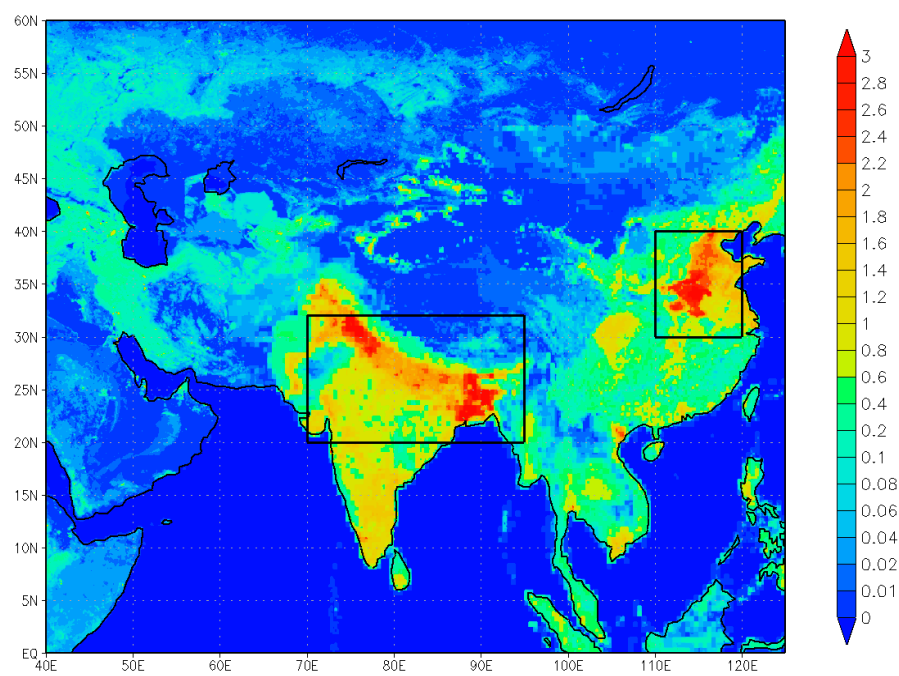


**Figure 2**

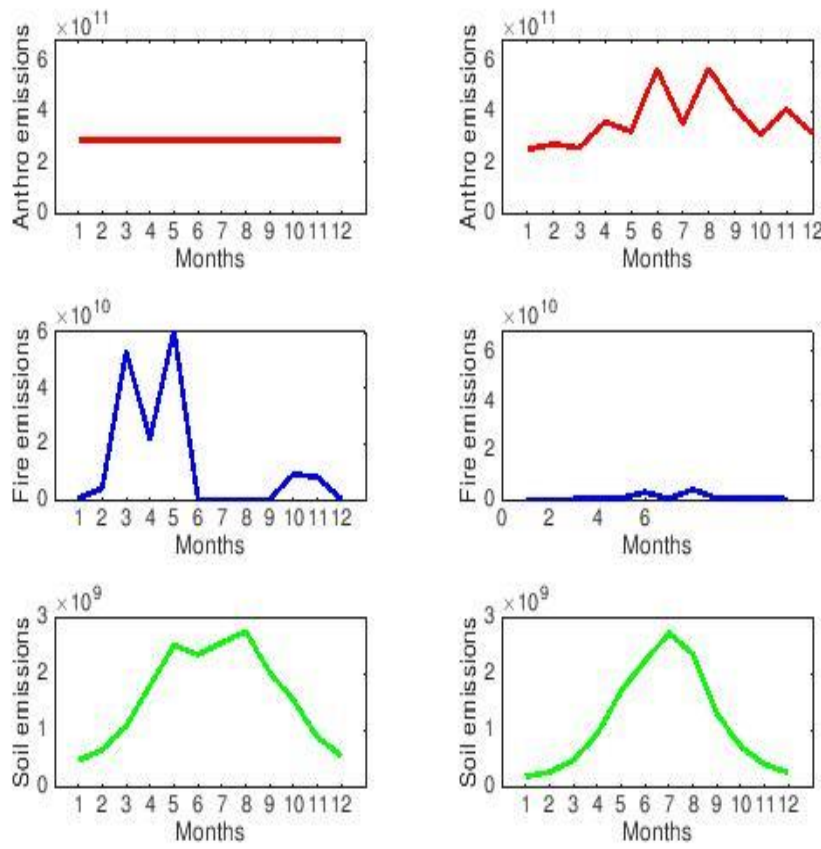


**Figure 3**

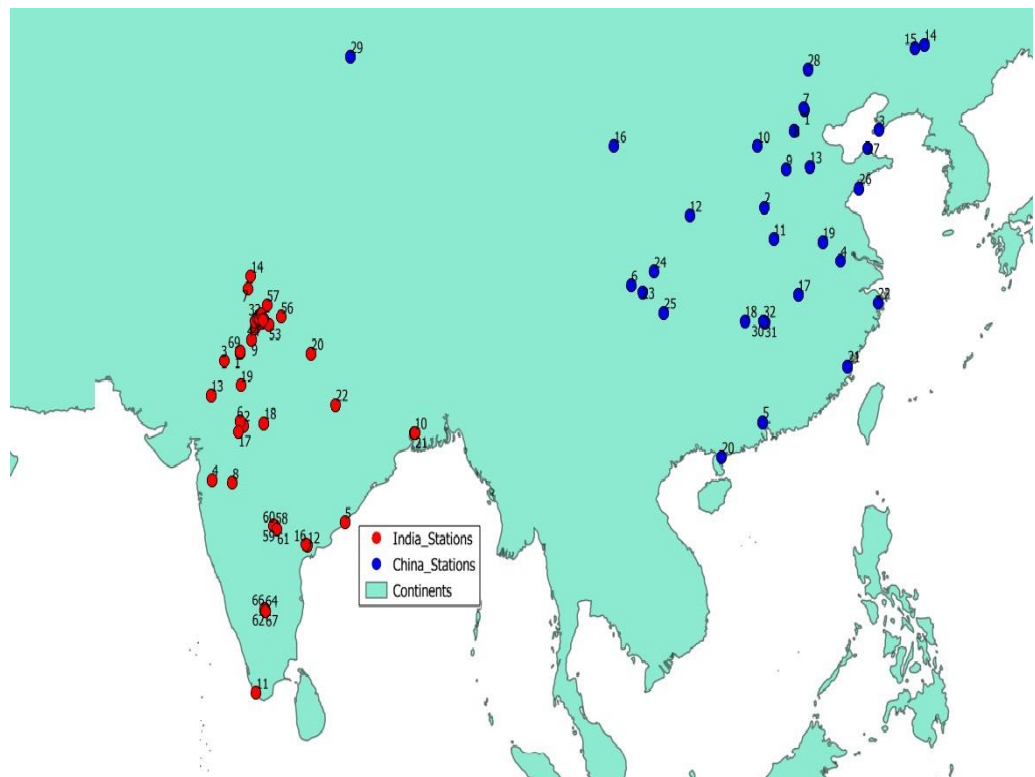


**Figure 4**

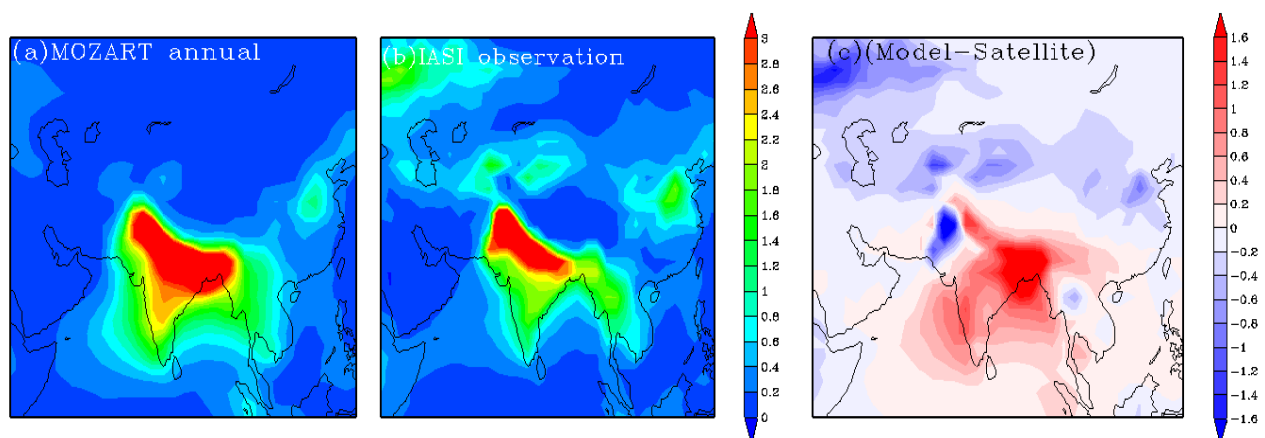


**Figure 5**

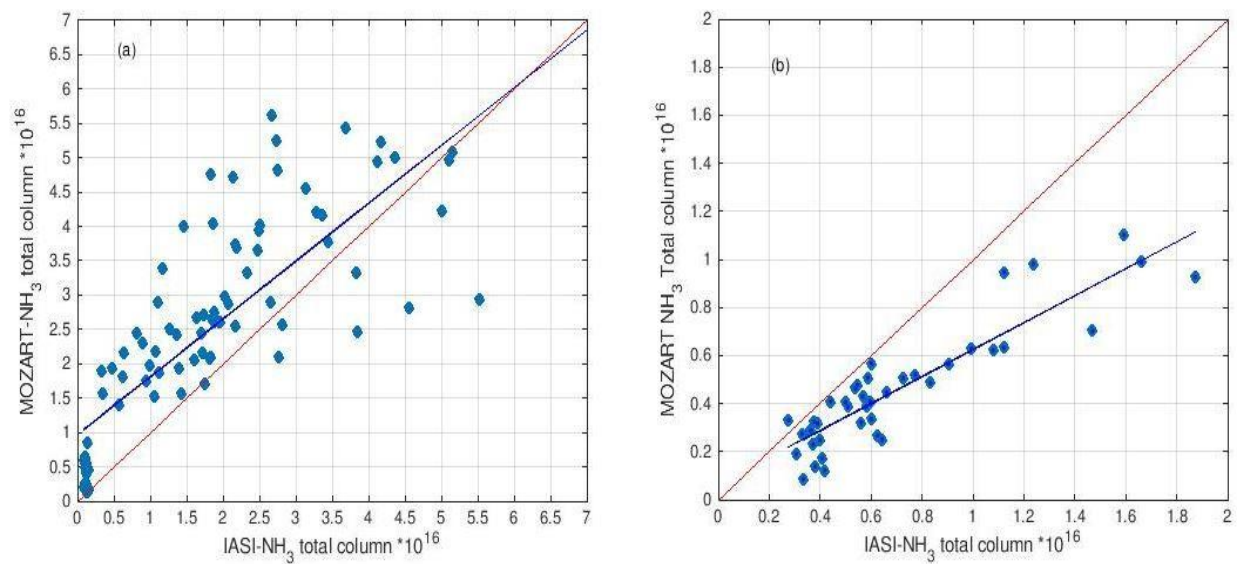


**Figure 6**

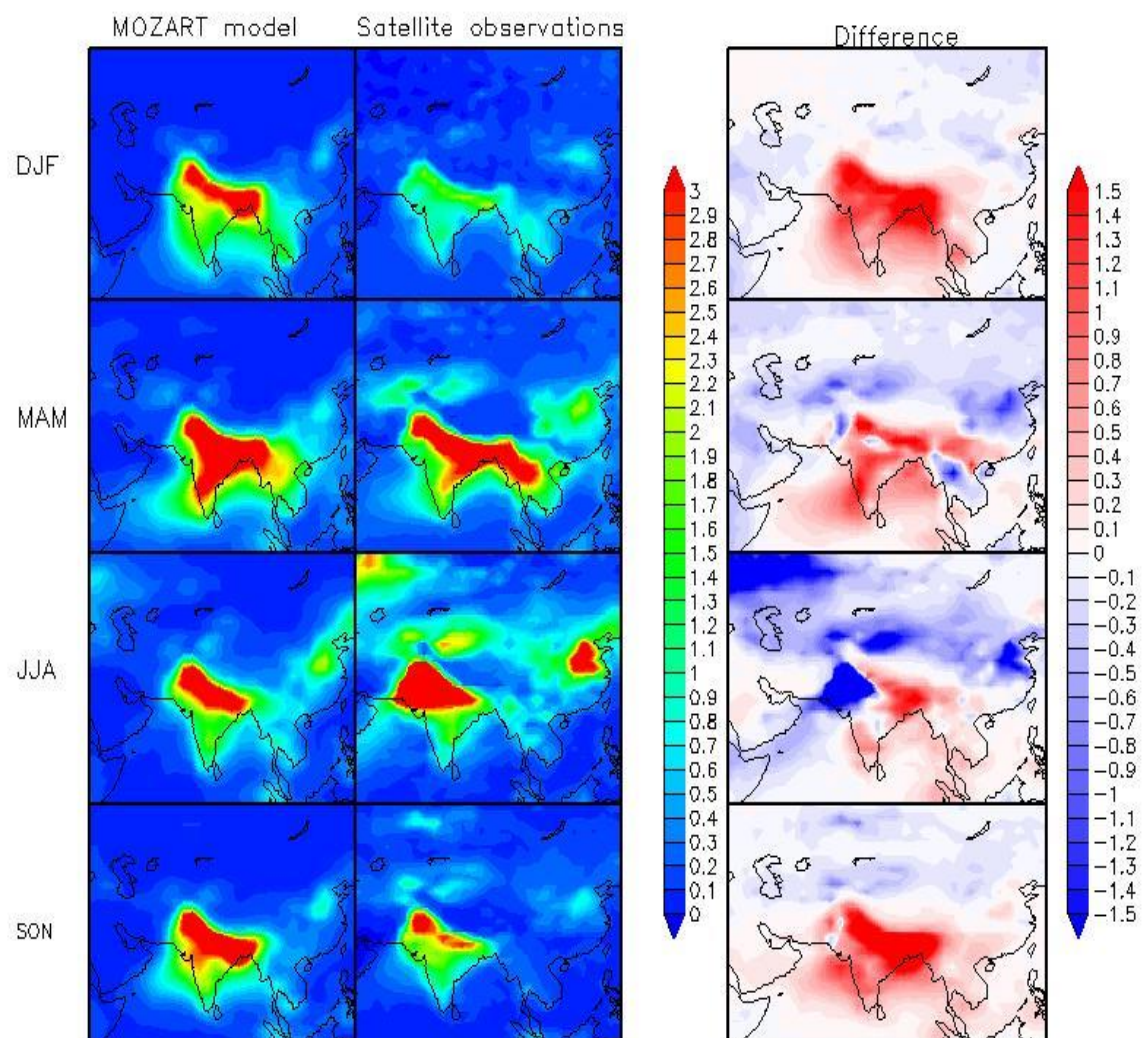


**Figure 7**

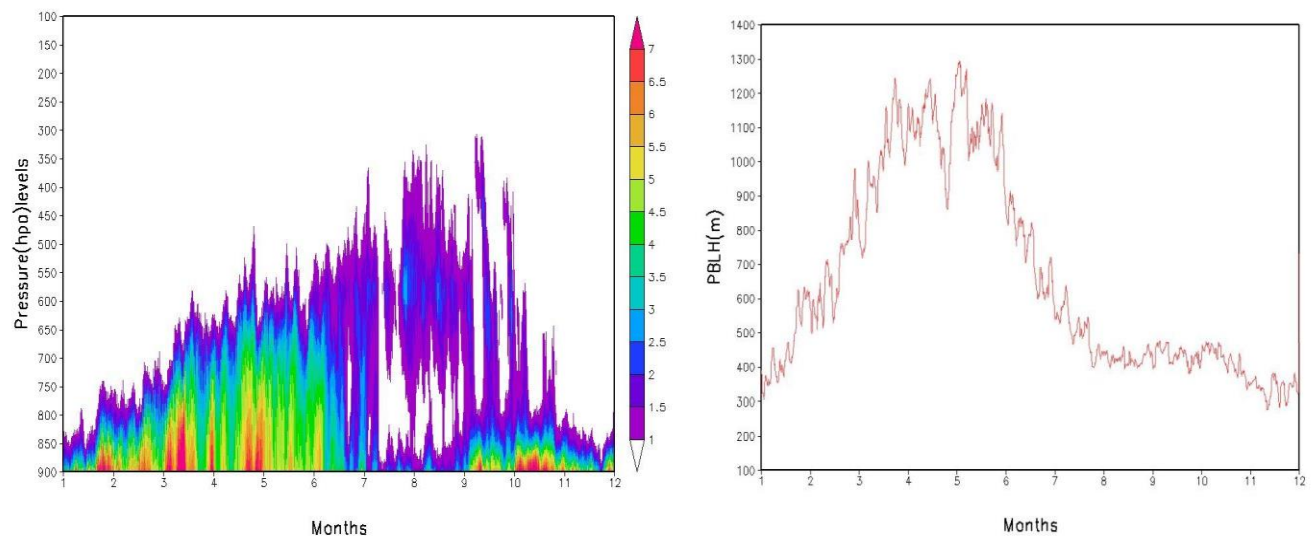


**Figure 8**

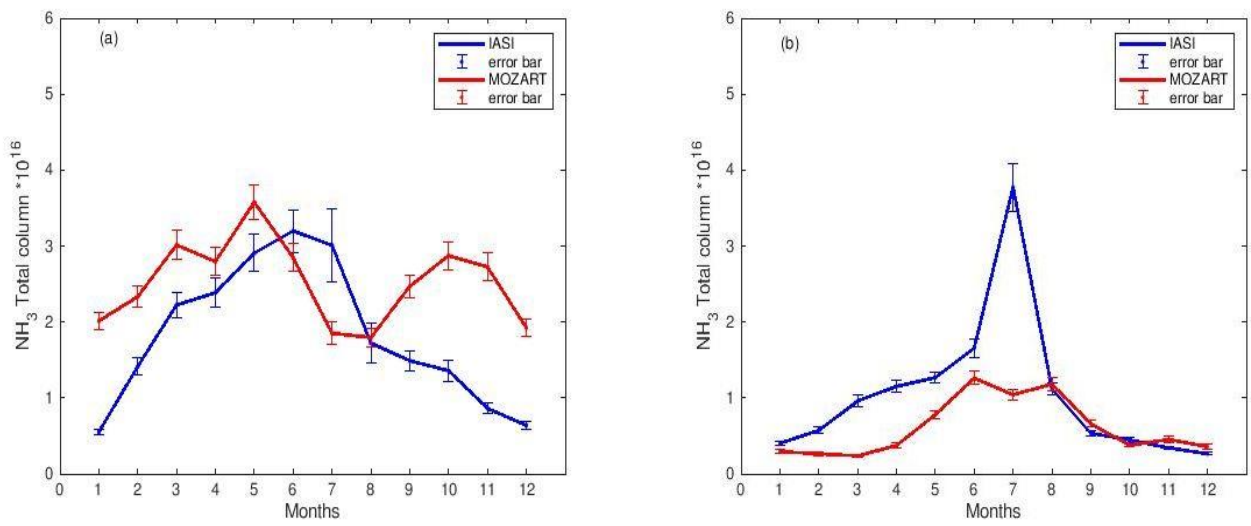


**Figure 9**

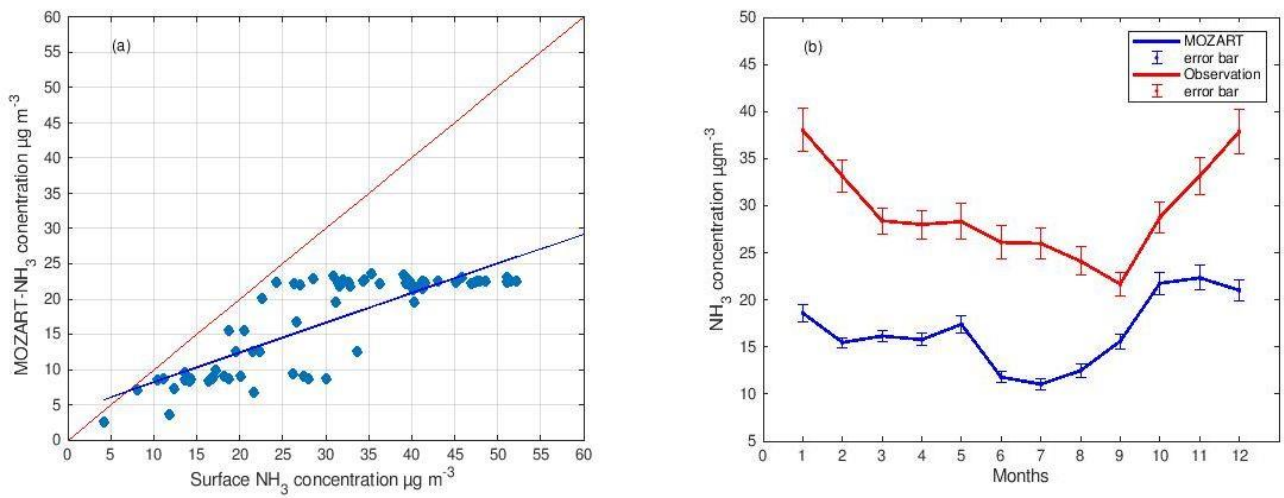


**Figure 10**

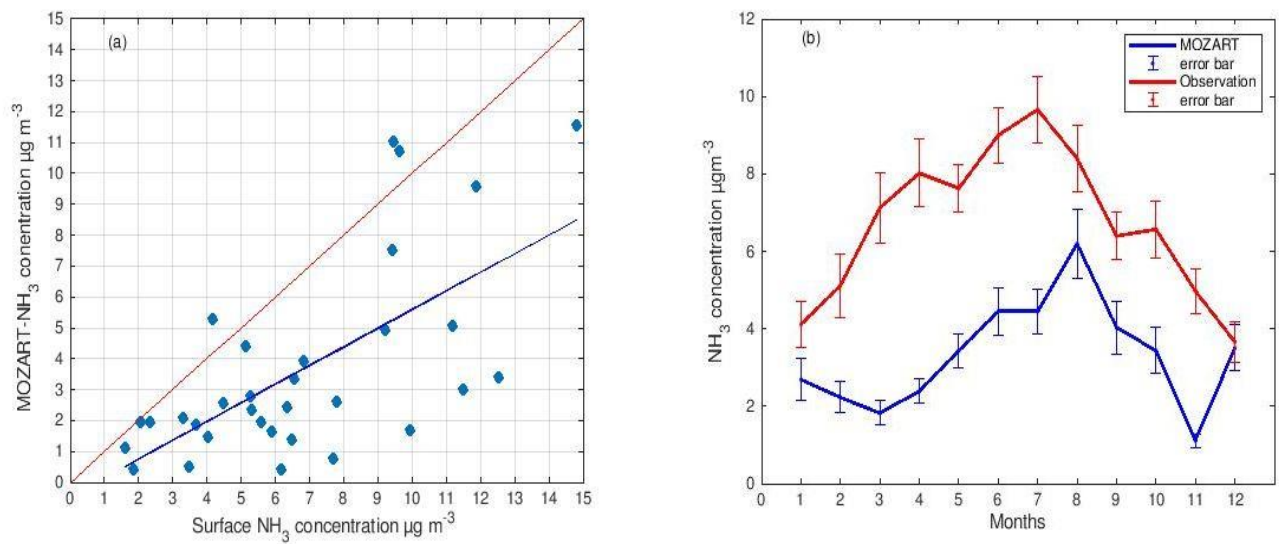
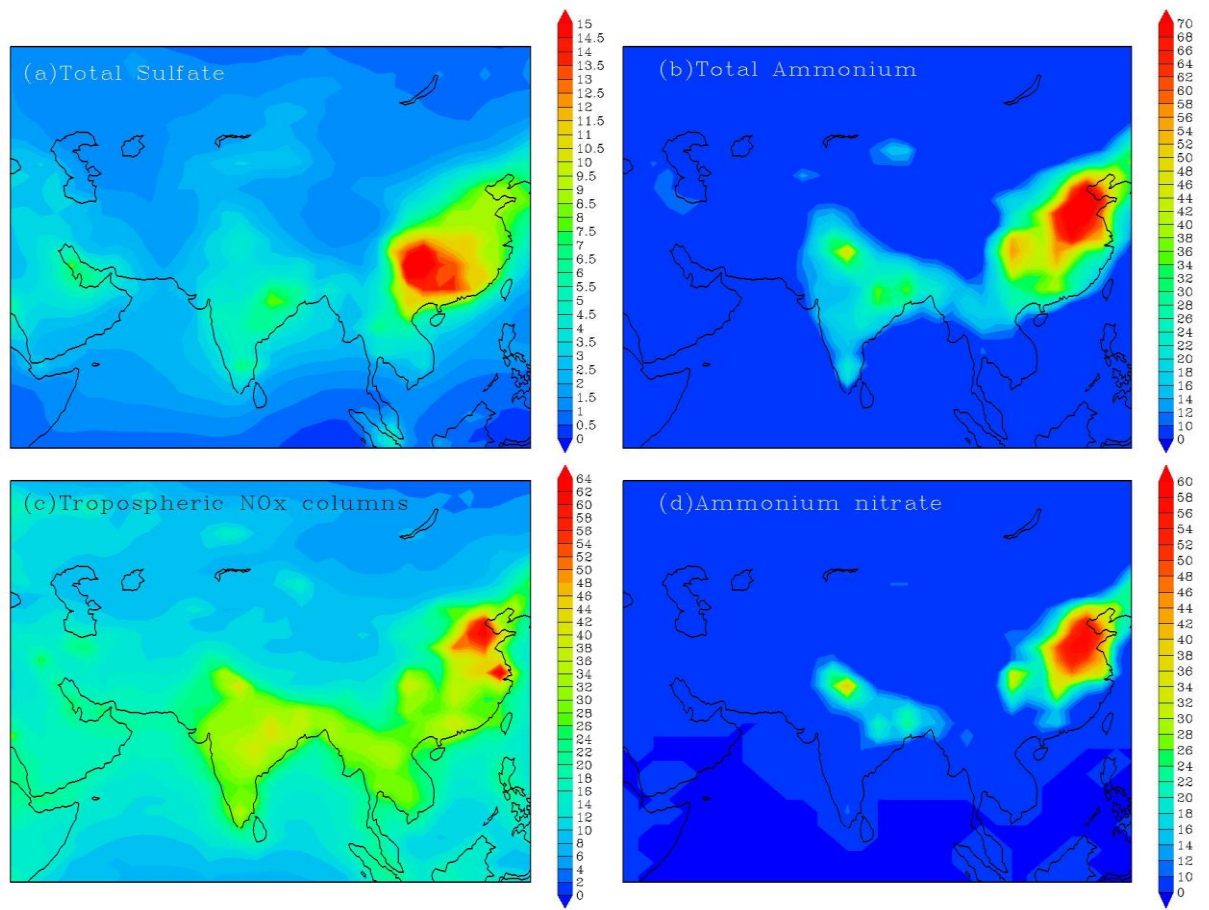


**Figure 11**



*Supplement of*

**Analysis of atmospheric ammonia over South and East Asia  
based on the MOZART-4 model and its comparison with  
satellite and surface observations**

**Pooja Pawar et al.**

*Correspondence to:* Sachin D. Ghude (sachinghude@tropmet.res.in)

## **Supplementary material**

# **Analysis of atmospheric ammonia over South and East Asia based on the MOZART-4 model and its comparison with satellite and surface observations**

Pooja V. Pawar<sup>1\*</sup>, Sachin D. Ghude<sup>1</sup>, Chinmay Jena<sup>1</sup>, Andrea Móring<sup>2,7</sup>, Mark A. Sutton<sup>2</sup>, Santosh Kulkarni<sup>3</sup>, Deen Mani Lal<sup>1</sup>, Divya Surendran<sup>4</sup>, Martin Van Damme<sup>5</sup>, Lieven Clarisse<sup>5</sup>, Pierre-François Coheur<sup>5</sup>, Xuejun Liu<sup>6</sup>, **Gaurav Govardhan<sup>1</sup>**, Wen Xu<sup>6</sup>, Jize Jiang<sup>7</sup>, and Tapan Kumar Adhya<sup>8</sup>

<sup>1</sup>Indian Institute of Tropical Meteorology (IITM), Pune, 411008, India

<sup>2</sup>Centre for Ecology & Hydrology (CEH), Edinburgh, EH26 0QB, UK

<sup>3</sup>Centre for Development of Advanced Computing, Pune, 411008, India

<sup>4</sup>Indian Meteorological Department (IMD), Pune, 411005, India

<sup>5</sup>Université libre de Bruxelles (ULB), Spectroscopy, Quantum Chemistry and Atmospheric Remote Sensing (SQUARES), Brussels, B-1050, Belgium

<sup>6</sup>College of Resources and Environmental Sciences, National Academy of Agriculture Green Development, China Agricultural University, Beijing 100193, China

<sup>7</sup>The University of Edinburgh, Scotland, EH8 9AB, UK

<sup>8</sup>Kalinga Institute of Industrial Technology, Bhubaneshwar, 751016, India

*Correspondence to:* Sachin D. Ghude (sachinghude@tropmet.res.in)

**Table S1. Location of NH<sub>3</sub> measurement sites from the air quality monitoring network operated by the Central Pollution Control Board, India (see also Figure 3)**

Site No.	Location name	Latitude	Longitude	Elevation (m)	Area
1	Adarsh Nagar	26.8754	75.8167	433	Rural
2	Devas	22.9688	76.0636	563	Rural
3	Ajmer	26.4727	74.6415	494	Urban
4	Nashik	20.0073	73.7762	580	Urban
5	Visakhapatnam	17.72	83.3	26	Urban
6	Ujjain	23.1793	75.7849	497	Urban
7	Patiala	30.3448	76.3708	256	Urban
8	Aurangabad	19.8406	75.2466	521	Urban
9	Alwar	27.5591	76.6021	276	Urban
10	Howrah	22.5707	88.3008	8	Coastal
11	Kerela	8.5141	76.9477	23	Urban
12	Vijaywada	16.5064	80.632	25	Urban
13	Udaipur	24.589	73.7022	575	Urban
14	Ratnapura	31.029	76.5734	274	Rural
15	Bhiwadi	28.207	76.8577	268	Industrial
16	Amravati	16.5151	80.5182	14	Rural
17	Pithampur	22.6248	75.6752	616	Rural
18	Mandideep	23.099	77.505	445	Industrial
19	Kota	25.136	75.8247	297	Urban
20	Lucknow	26.834	80.8917	126	Urban

21	Kolkata	22.5449	88.3425	18	Urban
22	Singrauli	24.0886	82.6478	287	Rural
23	Delhi1	28.8229	77.102	212	Urban
24	Delhi2	28.6508	77.3152	224	Urban
25	Delhi3	28.6687	77.23	218	Urban
26	Delhi4	28.7762	77.0511	218	Industrial
27	Delhi5	28.4997	77.2671	257	Rural
28	Delhi6	28.7501	77.1177	214	Urban
29	Delhi7	28.5713	77.0644	220	Urban
30	Delhi8	28.6803	77.2012	226	Urban
31	Delhi9	28.6317	77.2494	230	Urban
32	Delhi10	28.7255	77.1587	225	Urban
33	Delhi11	28.6687	77.1599	217	Urban
34	Delhi12	28.6124	77.2351	204	Urban
35	Delhi13	28.6338	77.198	219	Urban
36	Delhi14	28.6823	77.0349	217	Urban
37	Delhi15	28.6072	76.9459	218	Urban
38	Delhi16	28.6072	76.8408	212	Urban
39	Delhi17	28.6644	77.1704	238	Urban
40	Delhi18	28.5393	77.2687	233	Urban
41	Delhi19	28.6287	77.2946	220	Urban
42	Delhi20	28.6637	77.1196	22	Urban
43	Delhi21	28.632	77.1555	219	Urban
44	Delhi22	28.5646	77.167	225	Urban

45	Delhi23	28.7406	77.0577	212	Urban
46	Delhi24	28.5438	77.331	201	Urban
47	Delhi25	28.5504	77.2116	222	Urban
48	Delhi26	28.7373	77.2274	203	Urban
49	Delhi27	28.5062	77.2492	243	Urban
50	Delhi28	28.6688	77.3131	207	Urban
51	Delhi29	28.6981	77.1517	215	Urban
52	Delhi30	28.9575	77.2723	211	Urban
53	Delhi31	28.407	77.8498	197	Urban
54	Delhi32	28.694	77.455	226	Urban
55	Delhi33	28.6679	77.4498	208	Urban
56	Delhi34	28.8253	78.7213	193	Urban
57	Delhi35	29.4677	77.7116	245	Urban
58	Hyderabad1	17.4567	78.3264	580	Rural
59	Hyderabad2	17.5111	78.2752	544	Rural
60	Hyderabad3	17.5325	78.1849	545	Industrial
61	Hyderabad4	17.3507	78.4513	505	Urban
62	Bengaluru1	12.9568	77.5397	851	Urban
63	Bengaluru2	12.9135	77.5951	917	Urban
64	Bengaluru3	12.9756	77.6035	923	Urban
65	Bengaluru4	12.9172	77.5834	921	Urban
66	Bengaluru5	13.029	77.5197	909	Urban
67	Bengaluru6	12.9177	77.6238	882	Urban
68	Jaipur1	26.916	75.8017	435	Urban

69 Jaipur2 26.9503 75.801 470 Urban

---

**Table S2. Location of NH<sub>3</sub> measurement sites from the Nationwide Nitrogen Deposition Monitoring Network (NNDMN) operated by China Agricultural University, China (see also Figure 3)**

Site No.	Location name	Latitude	Longitude	Elevation (m)	Area
1	China Agricultural University	40.02	116.28	50	Urban
2	Zhengzhou	34.75	113.37	167	Urban
3	Dalian	38.92	121.58	18	Urban
4	Nanjing	31.84	118.85	9	Urban
5	Baiyun	23.16	113.27	16	Urban
6	Wenjiang	30.55	103.84	477	Urban
7	Shangzhuang	40.11	116.20	44	Rural
8	Baoding	38.85	115.48	15	Rural
9	Quzhou	36.78	114.94	44	Rural
10	Yangqu	38.05	112.89	1276	Rural
11	Zhumadian	33.02	114.05	69	Rural
12	Yangling	34.31	108.01	554	Rural
13	Yucheng	36.94	116.63	24	Rural
14	Gongzhuling	43.53	124.83	201	Rural
15	Lishu	43.36	124.17	129	Rural
16	Wuwei	38.07	102.60	1493	Rural
17	Wuxue	30.01	115.79	16	Rural
18	Taojiang	28.61	111.97	130	Rural
19	Fengyang	32.88	117.56	66	Rural
20	Zhanjiang	21.26	110.33	24	Rural
21	Fuzhou	26.17	119.36	432	Rural

22	Fenghua	29.61	121.53	34	Rural
23	Ziyang	30.13	104.63	360	Rural
24	Yanting	31.28	105.47	506	Rural
25	Jiangjin	29.06	106.18	292	Rural
26	Lingshadao	35.77	120.18	0	Coastal
27	Changdao	37.93	120.75	59	Coastal
28	Duolun	42.20	116.49	1239	Grassland
29	Bayingbuluke	42.88	83.71	2468	Grassland
30	Feiyue	28.56	113.34	77	Forest
31	Huinong	28.52	113.41	96	Forest
32	Xishan	28.61	113.31	230	Forest

---

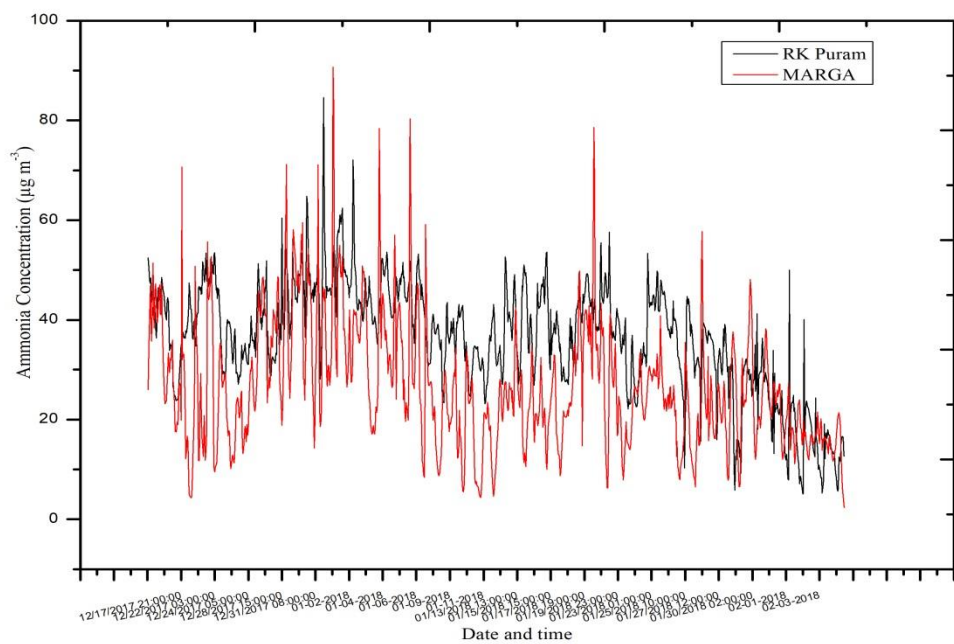


**Figure S1. Comparison of  $\text{NH}_3$  ( $\mu\text{g m}^{-3}$ ) concentration from MARGA instrument with RK Puram (CPCB) station**

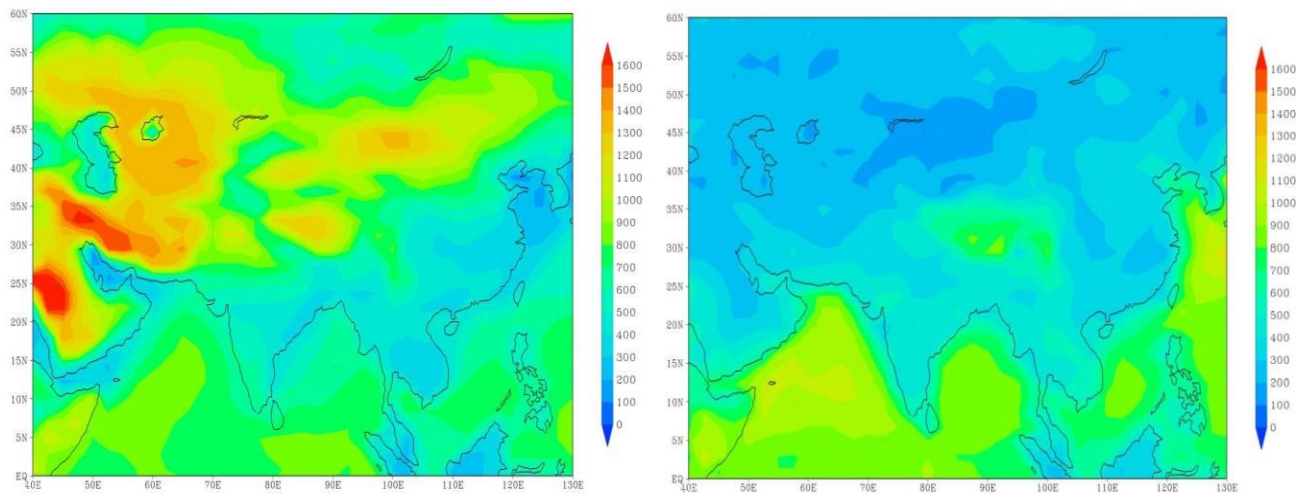


**Figure S2. MOZART-4 model estimate of Planetary boundary layer height (PBLH) (m) during summer (JJA) season (left) and during winter (DJF) season (right).**

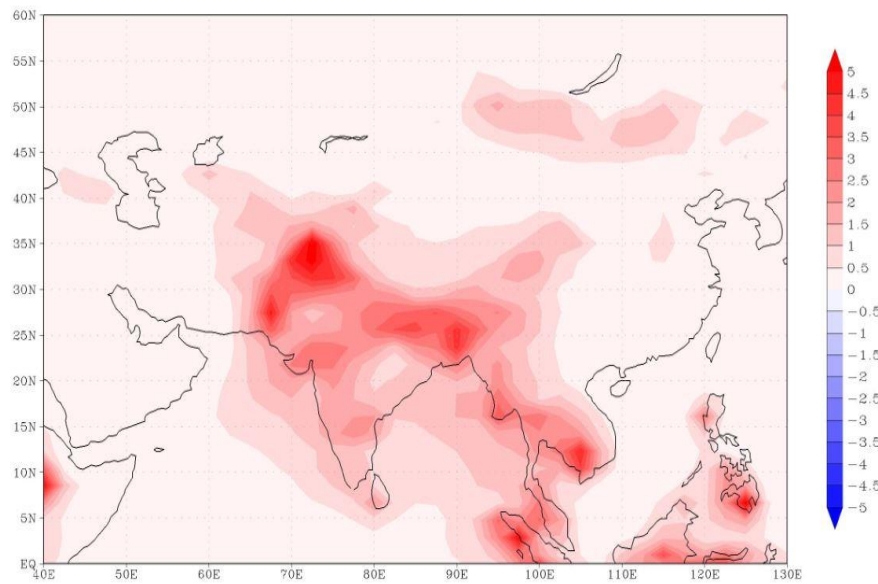


**Figure S3.** MOZART-4 model estimate of annual averaged  $\text{NH}_3/\text{NH}_4$  ratio ( $\times 10^9$  ppb) over Asia.

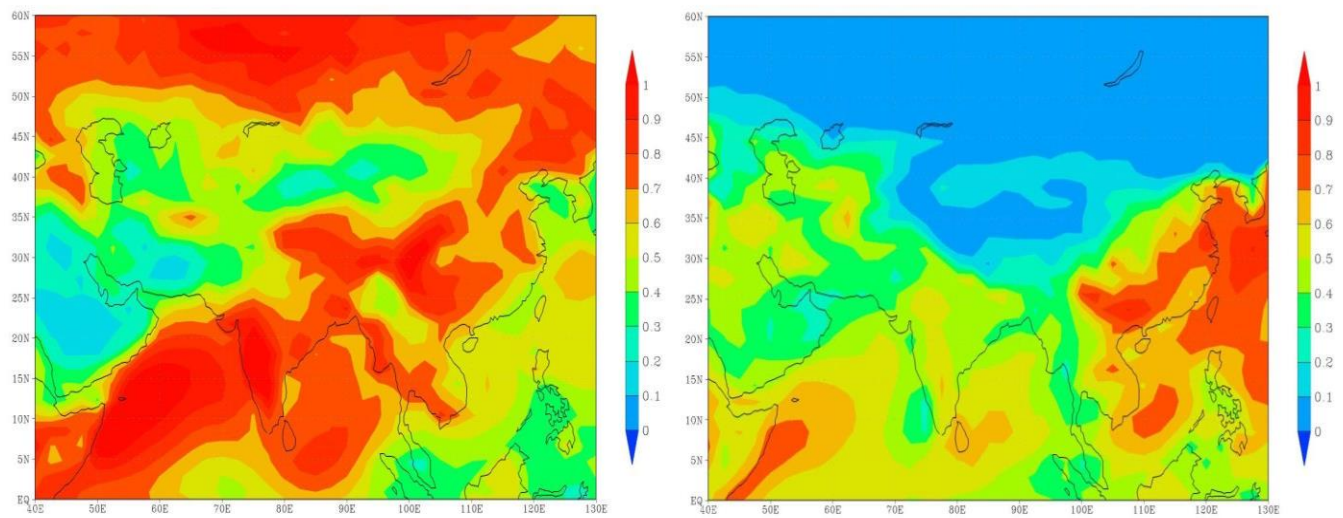


**Figure S4. MOZART-4 model estimate of dry deposition velocity (cm/s) during summer (JJA) season (left) and during winter (DJF) season (right).**

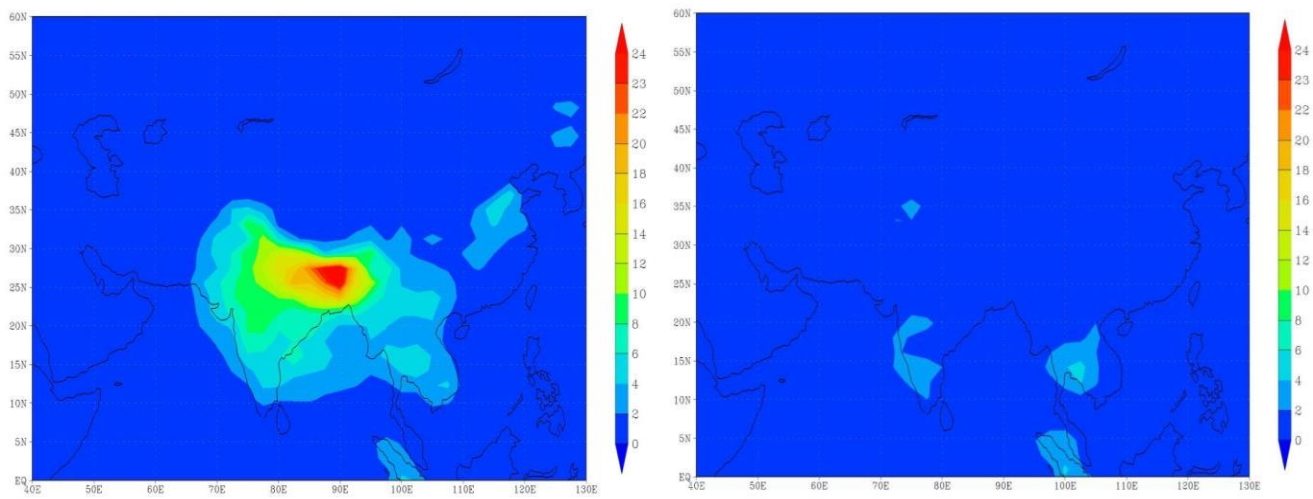


**Figure S5.** MOZART-4 model estimate of  $\text{NH}_3$  wet deposition flux ( $\times 10^{-9} \text{ kg m}^{-2} \text{ s}^{-1}$ ) during summer (JJA) season (left) and during winter (DJF) season (right).

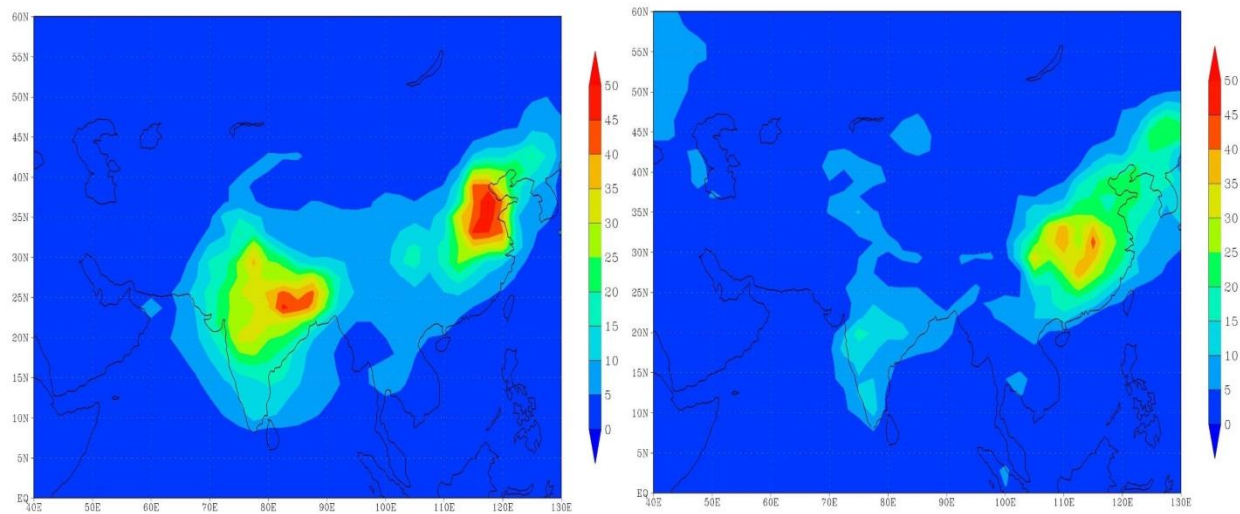


**Figure S6. MOZART-4 model estimate of  $\text{NH}_3\text{NO}_3$  wet deposition flux ( $\times 10^{-9} \text{ kg m}^{-2} \text{ s}^{-1}$ ) during summer (JJA) season (left) and during winter (DJF) season (right)**

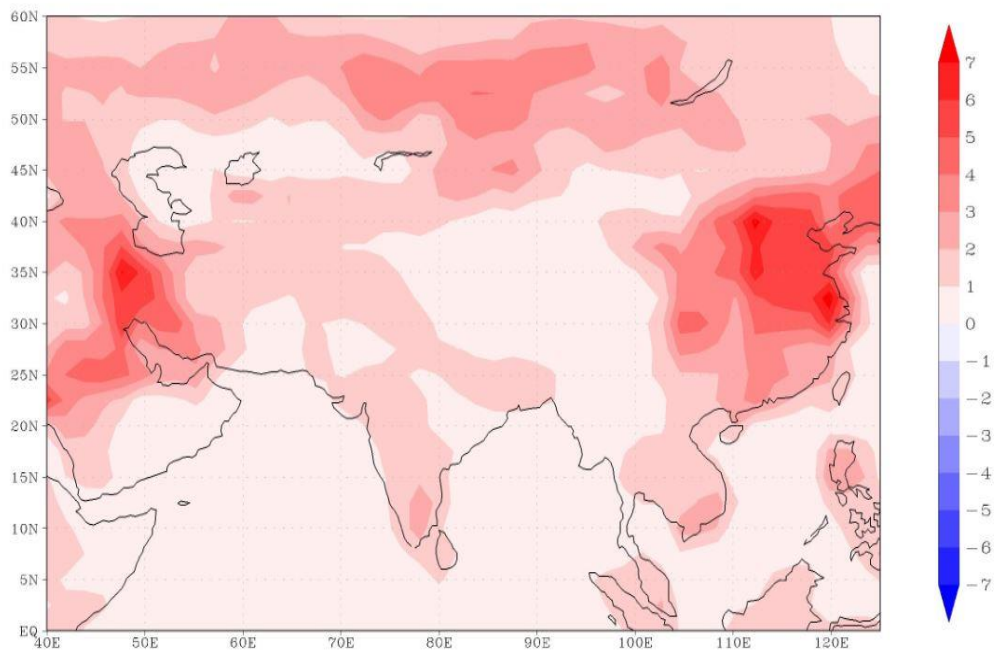


**Figure S7. MOZART-4 model estimate of annual averaged  $\text{NH}_3$  total emissions/ $\text{NH}_3$  total column ratio ( $\times 10^{-5} \text{ S}^{-1}$ ) over Asia**

